Report of Investigations No. 257

Using Airborne Geophysics to Identify Salinization in West Texas

by
Jeffrey G. Paine, Alan R. Dutton, and Martina U. Blüm

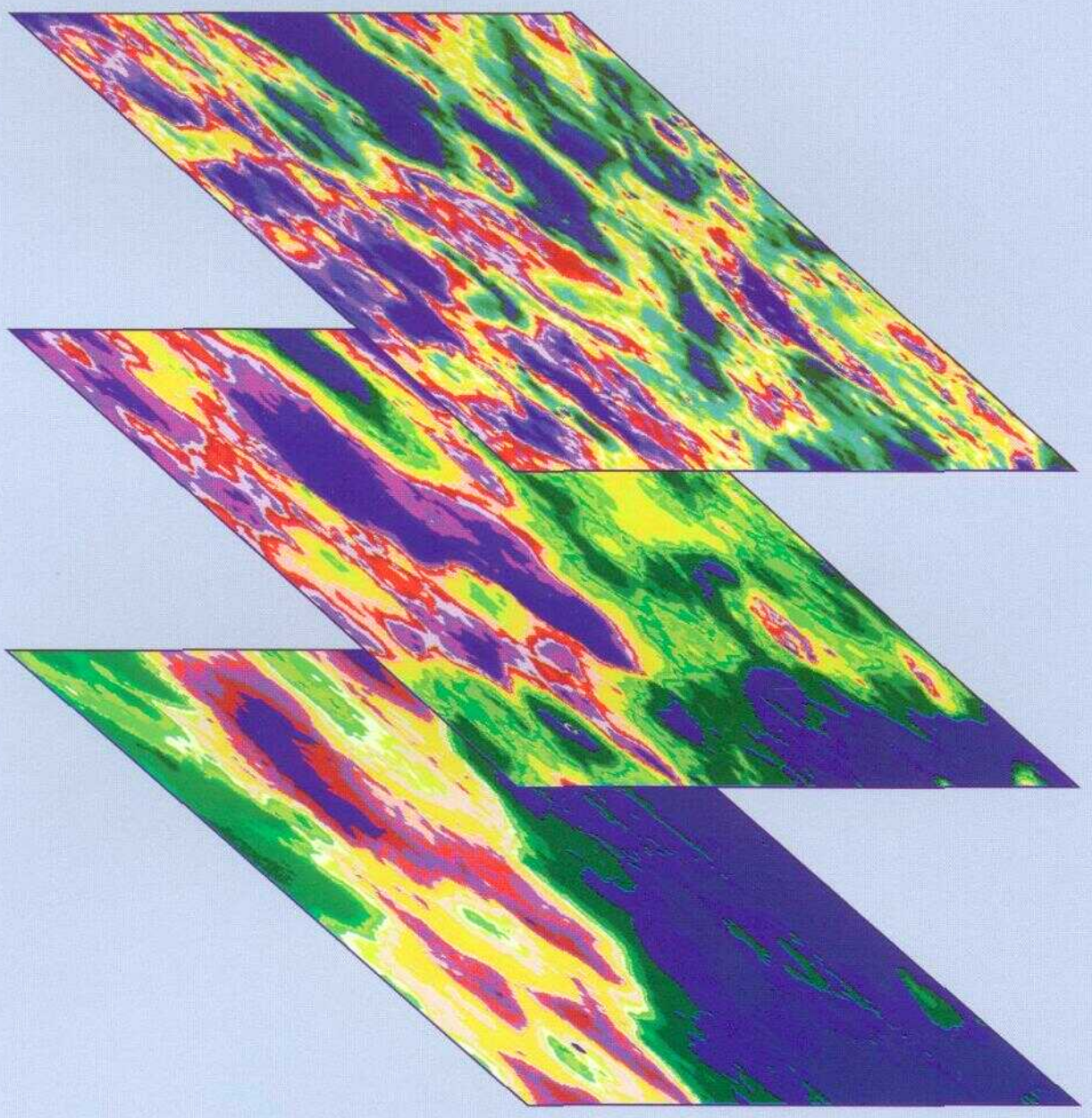

Bureau of Economic Geology
W. L. Fisher, Director *ad interim*
The University of Texas at Austin
Austin, Texas 78713-8924

1999

Report of Investigations No. 257

USING AIRBORNE GEOPHYSICS TO IDENTIFY SALINIZATION IN WEST TEXAS

by
Jeffrey G. Paine, Alan R. Dutton,
and Martina U. Blüm

Bureau of Economic Geology
W. L. Fisher, Director *ad interim*
The University of Texas at Austin
Austin, Texas 78713-8924

1999

CONTENTS

Figures

Tables

ABSTRACT

Salinization of soil and water is a chronic environmental and agricultural problem in arid regions. In this study of a 91-km^2 area in Runnels County, Texas, we integrated high-resolution airborne and ground-based geophysical surveys and chemical analyses of soil and water to identify near-surface salinization and determine its origin. Possible causes of salinization are migration of brine along natural conduits (faults, fractures, joints, and permeable stratigraphic units), infiltration from brine-disposal pits and leaking oil and gas wells, and evaporative concentration of shallow ground water.

An airborne geophysical survey of the Hatchel area, where more than 700 oil and gas wells have been drilled since the 1920's, measured magnetic-field intensity and ground conductivity at three electromagnetic frequencies to identify (1) conductivity anomalies caused by salinization and (2) magnetic-field anomalies caused by well casings and other ferrous objects. Water samples were analyzed to verify airborne data and distinguish salinity types. We combined airborne geophysical data with oil- and gas-well locations to identify 107 conductivity anomalies consistent with oil-field salinization.

Ground-based geophysical measurements, aerial-photograph interpretations, and record inspections of 54 anomalous sites revealed that at least 42 had oil-field salinization and that 22 might be wells that are leaking or have leaked in the past. We created a geophysical "profile" that captured 20 of the 22 potentially leaking wells identified during field investigations: a site that (1) has a magnetic anomaly or a known well location and (2) has anomalously high conductivity as measured by the high- and intermediate-frequency (56,000- and 7,200-Hz) airborne coils. These results suggest that airborne geophysics can be combined with well locations for identifying most potentially leaking wells without requiring ground investigations at every anomaly.

Used alone, airborne methods distinguish natural salinization from oil-field salinization but have difficulty discriminating among oil-field sources (pits, spills, and leaking wells). Used alone, ground-based surveys can map salinization extent and determine whether wells might be leaking, but unknown salinization is missed. In small areas where well locations are known, ground-based surveys can determine which wells might be leaking, and they are an inexpensive alternative to airborne surveys. Airborne methods are most effective in typical oil-field areas of tens to hundreds of square kilometers, where well locations are uncertain or multiple salinity sources are expected. Airborne data can be used to determine the extent and intensity of salinization, locate source areas, focus ground investigations, and estimate chloride mass in the ground.

Keywords: airborne geophysics, electromagnetic induction, oil-field pollution, salinization, water quality

INTRODUCTION

Infiltration of saline water into the shallow subsurface through natural geological conduits and oil-field sources can impact wildlife habitat, restrict or eliminate agricultural uses of land, and pollute aquifers and surface water (Dutton and others, 1989; Richter and others, 1990). Agricultural practices can exacerbate the problem by locally raising water tables and increasing dissolved mineral concentration by evaporation. Public concern about the environmental effects of salinization has led to an increasing interest in methods of determining whether oil-field brines have entered the subsurface, where they have migrated, and whether they are causing specific problems on the land surface, in water wells, or in surface water.

The purpose of this study was to evaluate the use of airborne and ground-based geophysics to identify and discern the sources of near-surface salinization. A high-resolution electromagnetic (EM) and magnetometer survey of a 91-km^2 study area (the Hatchel area) near Ballinger in Runnels County, Texas (fig. 1), was flown to locate areas having a geophysical signature consistent with that of a well leaking brine. The EM survey was employed to locate ground that is electrically conductive because of salinization. The magnetometer survey was employed to locate magnetic anomalies caused by well casings. Airborne geophysical signatures that might indicate a leaking well included a conductivity anomaly and either an associated magnetic anomaly or a known well location.

Ground-based investigations focused on representative sites identified by the airborne data. These investigations included detailed EM surveys and collection and chemical analyses of soil and water samples. Because ground conductivity is affected not only by pore-fluid chemistry but also by soil type, rock type, and moisture content, these factors were also considered. Once the data for a given site were analyzed, we interpreted the most likely cause of the conductivity anomaly at that site.

Geology and Soils

Rock and soil type can influence ground conductivity, but the effect of the host material on ground conductivity is generally much less than that caused by moisture content and ionic concentration in pore fluids. Clayey soils and rocks are generally more conductive than sandy units (McNeill, 1980a; Rhoades, 1981). Geologic units (Kier and others, 1976) at the surface or in the shallow subsurface include (1) Quaternary alluvium (Qal, fig. 2; table 1) that is generally sandy, relatively high in water content, and found in topographic lows along streams; (2) thin Pleistocene terrace deposits (Qu) that are composed of clay to gravel, are relatively dry and are mapped at higher elevations along the central part of the study area; and (3) outcrops of Permian Clear Fork Group strata (Pcf) and the Lueders Formation (Pl) containing units of sandstone, limestone, shale, and marl. Permian stratigraphic units dip west-northwestward into the Permian Basin. The Coleman Junction Formation, a limestone and shale formation of the Permian Wichita-Albany Group (Kier and others, 1976), is an artesian brine-bearing unit at depths of 200 to 300 m that is commonly cited as a principal source of near-surface brine (Richter and others, 1990). The Coleman Junction is beyond the exploration depth of airborne and ground-based geophysical instruments used in this study.

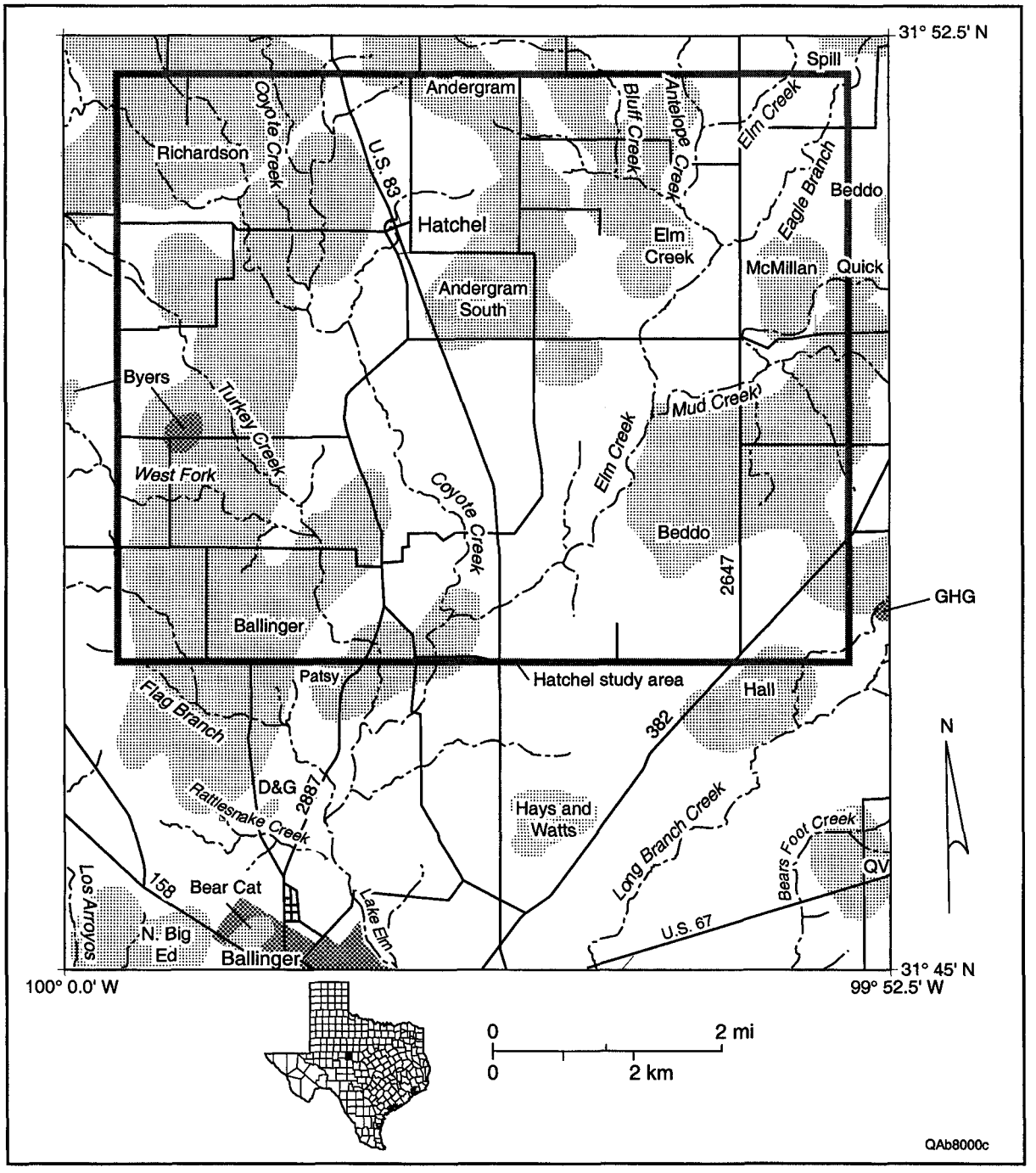

FIGURE 1. Map of the Hatchel, Texas, quadrangle, Runnels County. The airborne geophysical survey area is within the shaded rectangle. Shaded areas are oil and gas fields adapted from Abilene Geological Society (1992).

Soil type (fig. 3) can affect ground conductivities measured by high-frequency, shallow-penetrating conductivity instruments. Soils have been mapped in greater detail than have the geologic units in the study area (Wiedenfeld and others, 1970). In the lowlands, deep, loamy, relatively wet soils of the Spur-Colorado-Miles association are formed on Quaternary alluvium (figs. 2, 3). These soils generally contain less clay than do the upland soils, but they may have higher conductivity because they are thicker and wetter, and in many places they contain conductive pore

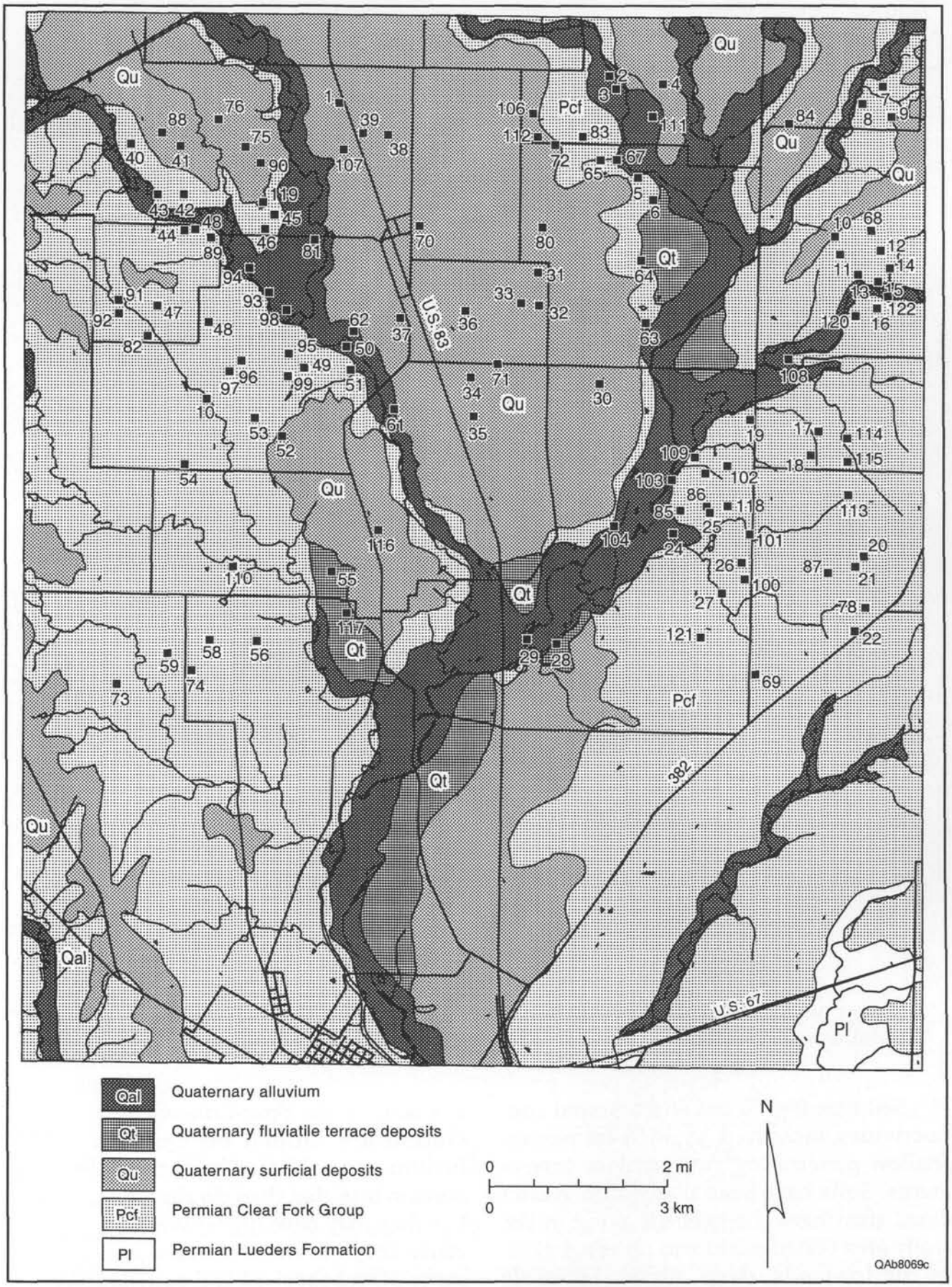

FIGURE 2. Generalized geologic map of the Hatchel quadrangle. Numbered sites are locations of local geophysical anomalies and ground-based geophysical surveys (app. A). Adapted from Kier and others (1976).

TABLE 1. Generalized stratigraphy of the Colorado River watershed. Modified from Brown and others (1972), American Association of Petroleum Geologists (1973), Eifler (1975), Lee (1986), and Richter and others (1990).

SYSTEM	SERIES	GROUP	FORMATION	LITHOLOGY
QUATERNARY	HOLOCENE			Alluvium
	PLEISTOCENE		Leona	Caliche and gravel
TERTIARY	PLIOCENE		Ogallala	Gravel, sand, and caliche
	MIOCENE			
CRETACEOUS	COMANCHEAN	Washita	Buda	Argillaceous limestone
		Fredericksburg	Edwards	Limestone and dolomite
			Comanche Peak	Limestone
			Walnut	Limestone and clay
		Trinity	Antlers	Sandstone and shale
TRIASSIC	UPPER TRIASSIC	Dockum		Sandstone and shale
PERMIAN	OCHOAN	Quartermaster		Sandstone and gypsiferous shale
		Whitehorse		
	GUADALUPIAN	Pease River	San Andres (Blaine)	Sandstone
			San Angelo	Sandstone, gypsum, and dolomite
	LEONARDIAN	Clear Fork	Choza	Sandstone and dolomitic limestone
			Vale	
			Arroyo	Shale and marly limestone
		Wichita-Albany	Lueders	Limestone and dolomite
			Talpa	Limestone and shale
			Grape Creek	
			Bead Mountain	
			Jagger Bend-Valera	
			Elm Creek	
	WOLFCAMPIAN		Admiral	
			Coleman Junction	
PENNSYLVANIAN	VIRGILIAN	Cisco		Limestone and shale
	MISSOURIAN	Canyon		
	DESMOINESIAN	Strawn		
	ATOKAN	Bend		Sandstone, shale, and limestone
	MORROWAN			
ORDOVICIAN	CANADIAN	Ellenburger		Dolomite
PRECAMBRIAN				Granite and gneiss

QA 11656c

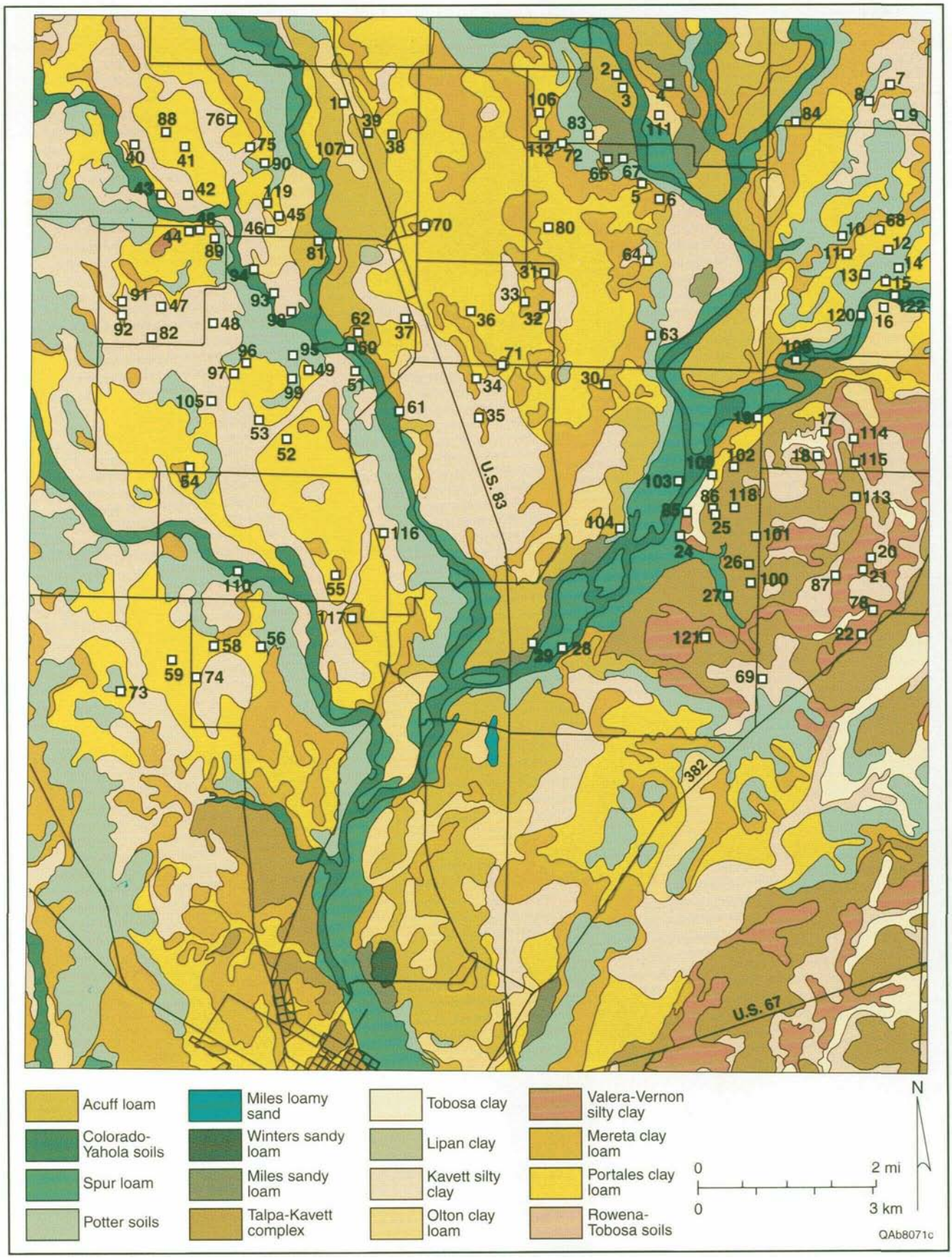

FIGURE 3. Soil map of the Hatchel quadrangle. Numbered sites are locations of local geophysical anomalies and ground-based geophysical surveys (app. A). Adapted from Wiedenfeld and others (1970).

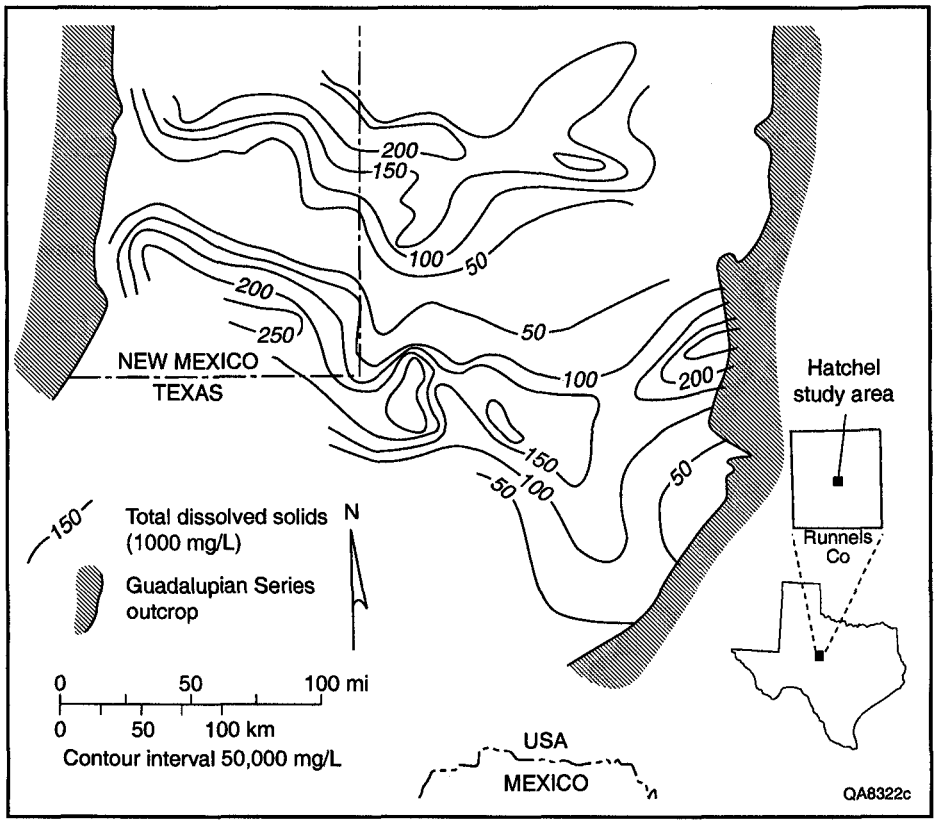

FIGURE 4. Total dissolved solids in brine from Guadalupian Series oil fields. Modified from McNeal (1965).

water. Soils on the uplands are generally the shallow, clayey to loamy, and relatively dry residual soils of the Portales-Potter-Mereta association that form on the Pleistocene terrace deposits and Permian Clear Fork Group strata (figs. 2, 3). Despite their relatively high clay content, these soils have low measured conductivity because of their thinness and low moisture content.

Hydrogeology

The Hatchel area lies on the east flank of the Southern Great Plains, which slopes gently southeastward from eastern New Mexico to Central Texas and at the south end of the Rolling Plains. The informally named Southern Great Plains regional ground-water flow system includes diverse hydrostratigraphic units in Ordovician to Neogene rocks (Jorgensen and others, 1988). Physiographic features of the Hatchel area include gently rolling, dissected uplands and valleys formed by the southward-draining Elm and Coyote Creeks and their tributaries.

The Upper Permian rocks that contain fresh ground water at shallow depths in the Hatchel area contain brine and hydrocarbons only tens of kilometers to the west (McNeal, 1965; Core Laboratories, 1972). Oil and gas fields occur at depths as shallow as 300 m in Permian formations to more than 1,800 m in Pennsylvanian and Ordovician rocks (table 1). Brine is prevalent throughout the Paleozoic section except where it is displaced by locally recharged meteoric water. For example, salinity of water in the Guadalupian Series, which overlies the Clear Fork Group (table 1), increases from 50,000 mg/L just west of the outcrop to more than 200,000 mg/L westward in the Permian Basin (fig. 4).

Regional and local topographic relief has large effects on ground-water flow

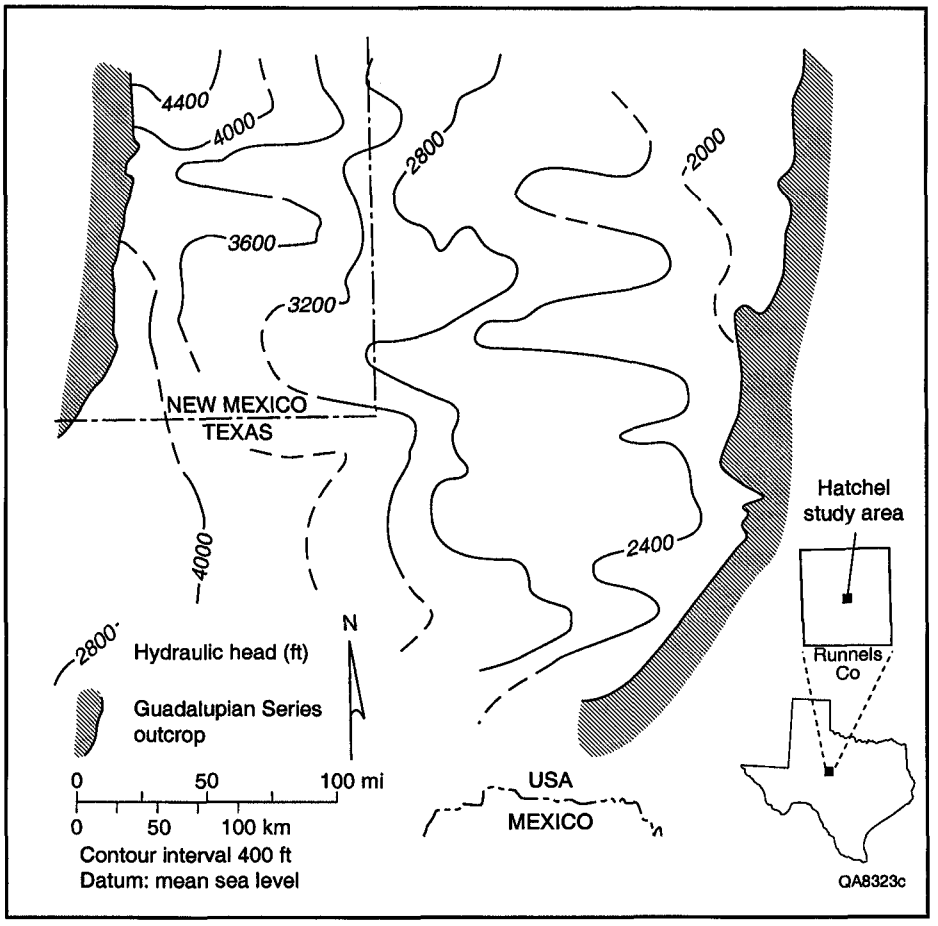

FIGURE 5. Potentiometric surface of brine in Guadalupian Series based on equivalent fresh-water hydraulic head. Modified from McNeal (1965).

(Tóth, 1962). Potentiometric surfaces in the Southern Great Plains regional flow system (Jorgensen and others, 1988) are inclined toward the east, indicating the potential for eastward flow of brine in Paleozoic rocks toward outcrops in the Hatchel area (fig. 5). Eastward fluid flow probably influenced migration of hydrocarbons into reservoirs across the east shelf of the Permian Basin. Richter and Kreitler (1986) showed that brine at shallow (~30 m) depths in the south part of the Rolling Plains is derived from deep parts of the regional flow system. Bein and Dutton (1993) mapped connate and meteoric water throughout the stratigraphic section across the Southern Great Plains and showed eastward movement of saline water into the Rolling Plains. Comparison of potentiometric surfaces of hydrostratigraphic units in Paleozoic rocks mapped by McNeal (1965) indicates that there is potential for upward movement of brine across confining layers if pathways such as fractures and unplugged boreholes exist. Potentiometric surfaces of brines beneath the valleys in the study area could be close to, and in some Wolfcampian formations (for example, Coleman Junction) higher than, ground surface elevations of 490 to 550 m.

Potentiometric surfaces of shallow ground water in different aquifer units most likely are inclined toward Elm and Coyote Creeks and their tributaries (fig. 1), reflecting topographic influence on recharge and discharge locations in the local ground-water flow system (Tóth, 1962). The upland areas are probably local re-

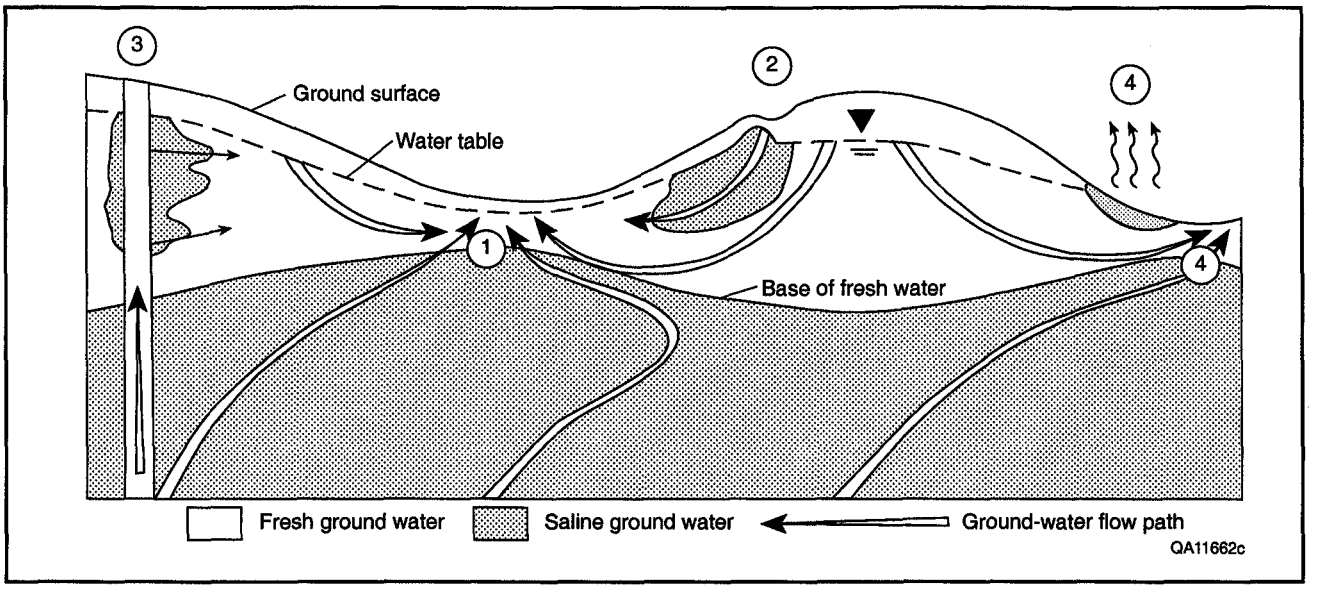

FIGURE 6. Conceptual model of West Texas salinity sources. Potential sources are (1) natural brine discharge through permeable stratigraphic units, fractures, and joints; (2) infiltration of saline water beneath brine-disposal pits; (3) upward flow of brine through inadequately plugged and leaky boreholes; and (4) evaporative concentration of shallow ground water. Adapted from Richter and others (1990).

charge zones, and ground-water discharge from local and regional flow systems is most likely focused in the valleys of Elm and Coyote Creeks.

Causes of Salinization

Salinization of soil and water is a common problem in the central and southwestern United States (Dutton and others, 1989; Richter and others, 1990). Potential causes of soil and water salinization in the Hatchel area include (1) natural discharge of subsurface brines through permeable units, fractures, or joints; (2) infiltration of produced brine beneath disposal pits; (3) upward movement of brine across confining beds through unplugged oil, gas, and deep water wells; and (4) evaporative concentration of ground water from shallow water tables that have risen in response to agricultural landscaping and consequently increased ground-water recharge (fig. 6).

Oil and gas wells provide potential paths for brine to move to the near-surface environment. If brine is associated with the produced oil or gas, it moves to the surface along with the hydrocarbons. In Texas, before the practice was banned in 1969 (Richter and others, 1990), produced brine was commonly discharged into unlined pits and left to evaporate or infiltrate the ground. Brine within nonproducing geologic units, such as the Coleman Junction Formation, can also reach the near-surface environment through deep water wells and improperly plugged oil and gas wells reaching deeper strata.

Although salinization from any of the natural, oil-field, or agricultural sources could cause similar increases in ground conductivity, each type may have a unique geophysical or chemical signature that would allow it to be distinguished. For example, ground conductivity that decreases with depth may indicate surface salinization associated with a brine-disposal pit or evaporative concentration. Conductivities that increase downward suggest deeper salinity sources, such as a

leaking well or natural flow path. Areal conductivity patterns and magnetic data from airborne surveys help further distinguish potentially leaking wells (point sources having magnetic anomalies) from natural conduits (curvilinear features having no magnetic anomalies).

Oil and Gas Activity

There are 18 named oil and gas fields that cover a substantial part of the Hatchel quadrangle (fig. 1). Railroad Commission of Texas (RRC) records indicate that there are at least 963 wells in the quadrangle and 718 in the Hatchel area (fig. 7) and that most of the exploration and production occurred before the no-pit order. Although these wells are distributed unevenly, few areas are unexplored. And because drilling, production, and plugging practices have improved over the decades that have passed since the discovery of oil and gas, areas of early activity are of greater environmental concern than are fields discovered recently.

Oil and gas production in the Hatchel area is largely from the Pennsylvanian Cisco, Canyon, and Strawn Groups (Fitzgerald, 1952; Gardner and Phifer, 1953; Abilene Geological Society, 1992). The oldest wells are found in McMillan and Beddo fields, which, discovered in the late 1920's, are located in the northeast and east parts of the study area (fig. 1). Most fields were discovered between the late 1940's and the early 1960's, including Ballinger (1947), Elm Creek (1950), Patsy (1951), Hays and Watts (1951), Spill (1952), Hall (1953), Richardson (1957), Byers (1957), Andergram (1958), and D&G fields (1963). Hatchel-area discoveries in the 1980's include QV field, Bear Cat field (1981), North Big Ed field (1982), Quick oil and gas field (1984), and GHG field (1985).

FIGURE 7. Oil- and gas-well locations in the Hatchel quadrangle. Well locations from Railroad Commission of Texas. Field locations shown in figure 1.

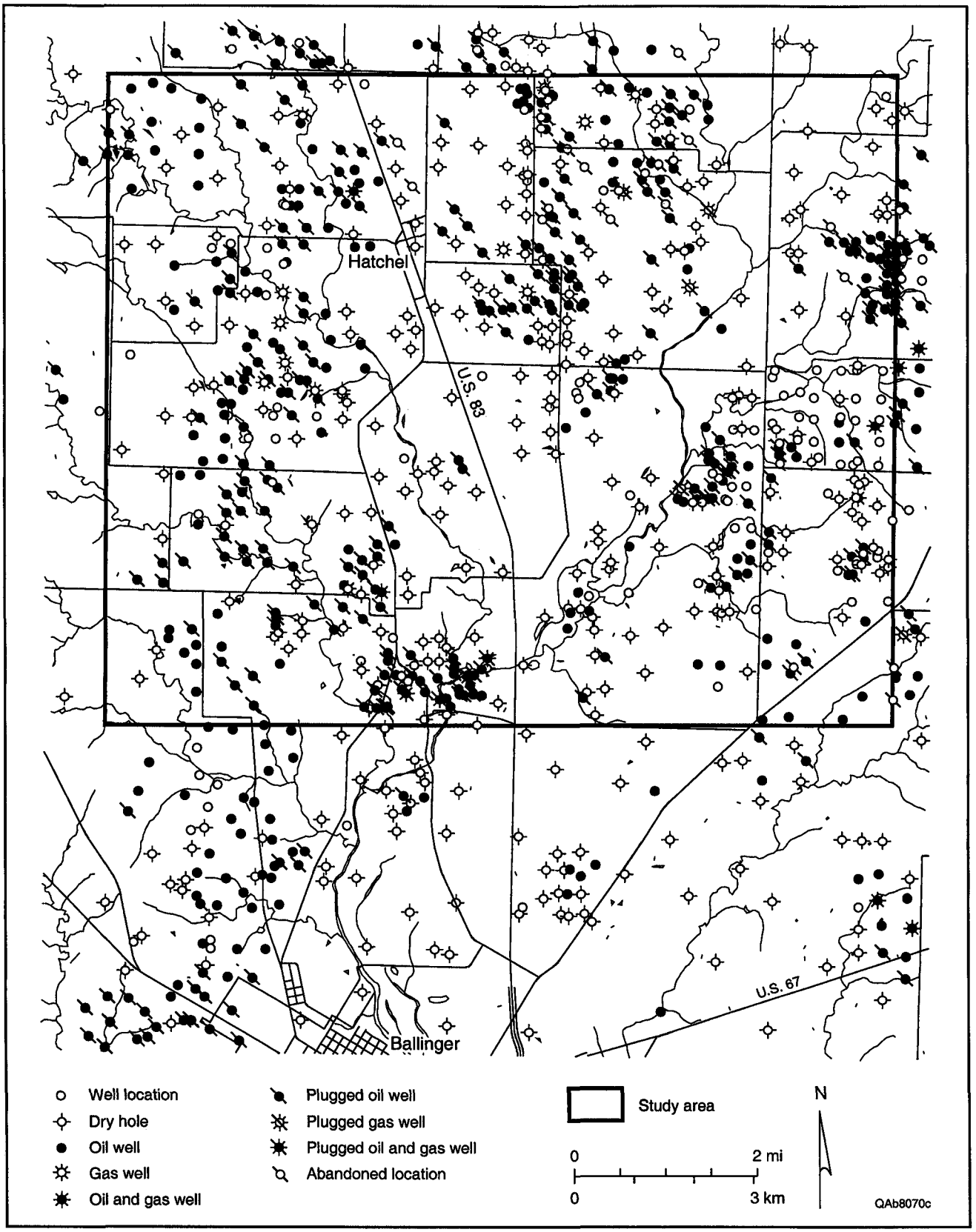
Hatchel
U.S. 83
U.S. 67
Ballinger
Well location
Dry hole
Oil well
Gas well
Oil and gas well
Plugged oil well
Plugged gas well
Plugged oil and gas well
Abandoned location
Study area
N
0
2 mi
0
3 km
QAb8070c

GEOPHYSICAL METHODS

We used electromagnetic induction (EM) methods (Parasnis, 1973; Frischknecht and others, 1991; West and Macnae, 1991) to measure apparent electrical conductivity of the ground with airborne and ground-based instruments. EM methods employ a changing primary magnetic field that is created around a transmitter coil to induce a current to flow within the ground, which in turn creates a secondary magnetic field that is sensed by the receiver coil. In general, the strength of the secondary field is proportional to the conductivity of the ground. We assume that the near-surface environment consists of horizontal layers of infinite lateral extent. Although not strictly true anywhere, near-surface layers have sufficient lateral extent in the Hatchel area to validate the assumption.

Airborne Geophysics

Geoterrex–Dighem, a geophysical service company based in Canada, surveyed the Hatchel study area using helicopter-based geophysical instruments in January 1996 (Garrie, 1996). Principal instruments mounted in the helicopter were the DIGHEM^V system that measures ground conductivity by using five EM coil pairs and that measures magnetic-field strength by using a Cesium vapor magnetometer. The EM coils and the magnetometer were slung beneath the helicopter (fig. 8) at nominal heights of 30 and 40 m, respectively. The helicopter maintained a height of 60 m and flew at an average speed of 108 km/hr (Garrie, 1996). Supporting instruments included a differential GPS navigation system having a locational accuracy to 5 m and a radar altimeter.

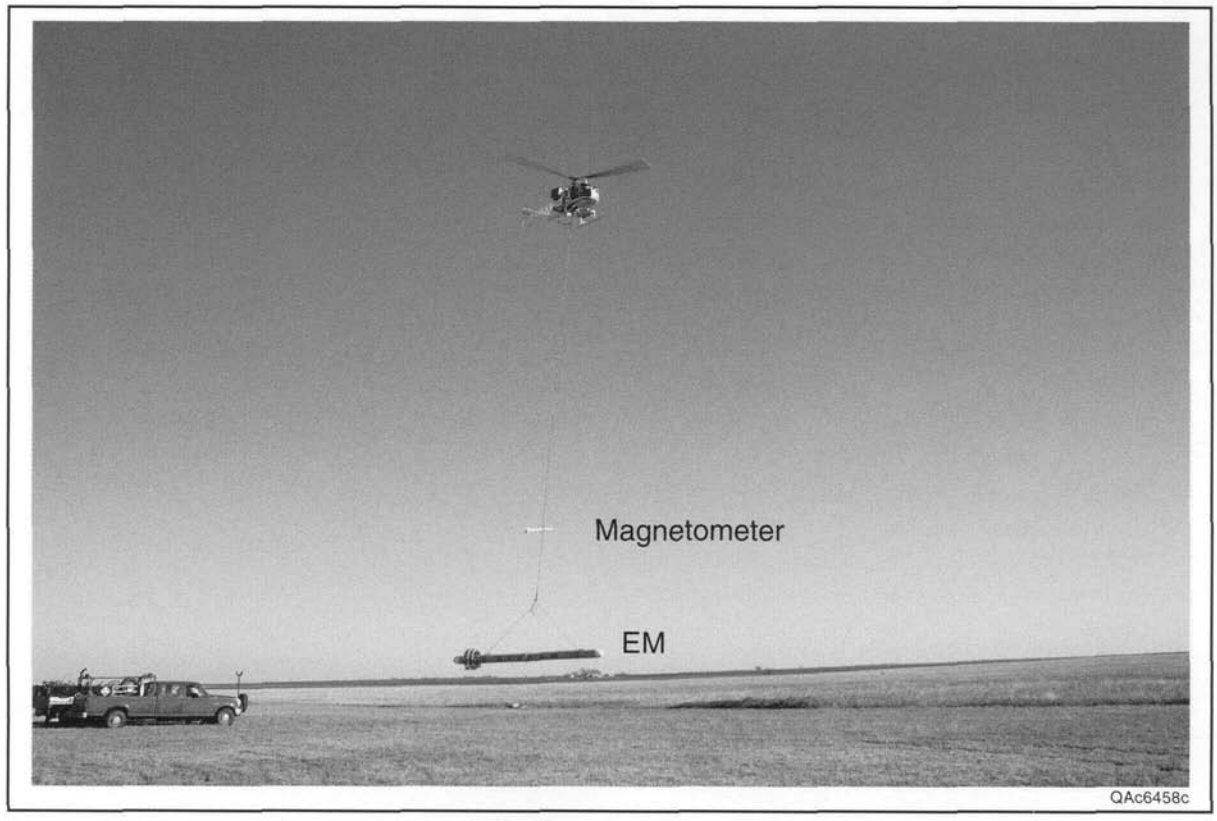

FIGURE 8. Photograph of helicopter lifting DIGHEM magnetometer and EM birds in preparation for airborne geophysical survey.

Flight lines for this high-resolution survey, oriented east-west and spaced 100 m apart, covered a total length of 940 km within the 91-km^2 Hatchel area (fig. 1). EM and magnetometer data were sampled at 0.1-s intervals, corresponding to a sample spacing of about 3 m along each flight line. EM coil separations of 6 to 8 m and a bird height of 30 m suggest a footprint a few tens of meters wide. EM and magnetometer data were processed by Geoterrex-Dighem (Garrie, 1996). Images of ground conductivity at three coil frequencies (900, 7,200, and 56,000 Hz in a vertical dipole orientation) and total and enhanced magnetic-field strength were imported into a geographic information system for spatial analysis that included comparisons with maps of soil type, geologic unit, and well location.

Ground-Based Geophysics

Bureau of Economic Geology (Bureau) staff investigated representative sites using ground-based EM instruments. Frequency-domain EM methods were used in a reconnaissance mode to confirm salinization and in multifrequency mode to delineate lateral and vertical extent of salinization. Time-domain EM (TDEM) soundings were used to estimate plume thickness and to examine changes in conductivity deeper than depths reached by other airborne and ground-based methods. RRC staff used a portable metal detector to locate well casings and guide conductivity survey placement at the selected sites (fig. 9).

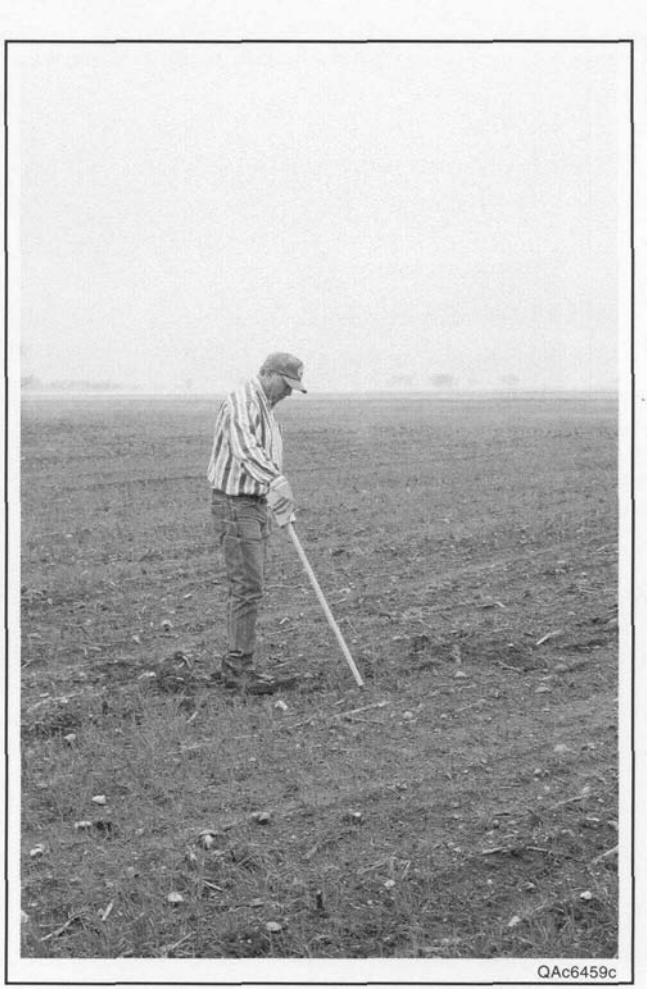

FIGURE 9. Photograph of RRC worker using a metal detector to locate an abandoned well.

Single- and Multiple-Frequency Conductivity Profiling

Reconnaissance conductivity profiles were completed at 28 sites (app. A) to locate highly conductive ground identified from the airborne data that may contain sites of salinization. In these surveys, a Geonics EM34-3 ground-conductivity meter (fig. 10) was used to measure apparent conductivity (McNeill, 1980b) along lines crossing the sites. The EM34-3 supports a 10-, 20-, or 40-m transmitter- and receiver-coil separation (fig. 11) and two principal coil orientations (horizontal and vertical dipole). A 10- or 20-m coil separation was used for reconnaissance surveys, having exploration depths of 6 or 12 m in the horizontal dipole orientation and 12 or 25 m in the vertical dipole orientation (fig. 11). The conductivity values represent a weighted average conductivity of the sensed soil volume beneath the transmitter and receiver coils. Although reconnaissance profiling can delineate salinized areas rapidly, it reveals little in-

FIGURE 10. Photograph of Bureau worker using Geonics EM34-3 ground-conductivity meter to perform reconnaissance EM survey across abandoned Gardner No. 1 well at site 33. Transmitter coil shown.

formation on conductivity changes with depth.

Multiple-frequency profiling, one of two ground-based methods used to examine conductivity variations with depth, was completed at 32 sites by using the EM34-3 (app. A). The exploration depth of the EM34-3 increases with increasing coil separation (decreasing frequency) for a given coil orientation (fig. 11). Consequently, conductivity measured at different coil separations and orientations can be used to infer conductivity changes with depth (McNeill, 1980b, c) to a maximum depth of about 30 m. We measured apparent conductivity (in mS/m) first at 10-m coil separation using horizontal and vertical dipole orientations. After we completed a line using the 10-m separation, the 20-m separation was selected, the instrument was recalibrated, and horizontal and vertical dipole data were collected along the same line. Finally, the 40-m separation was selected, the instrument was recalibrated, and apparent conductivity for both dipole orientations was measured.

EMIX34 Plus, a computer program published by Interpex, was used to process the data and produce simple models of lateral and vertical conductivity

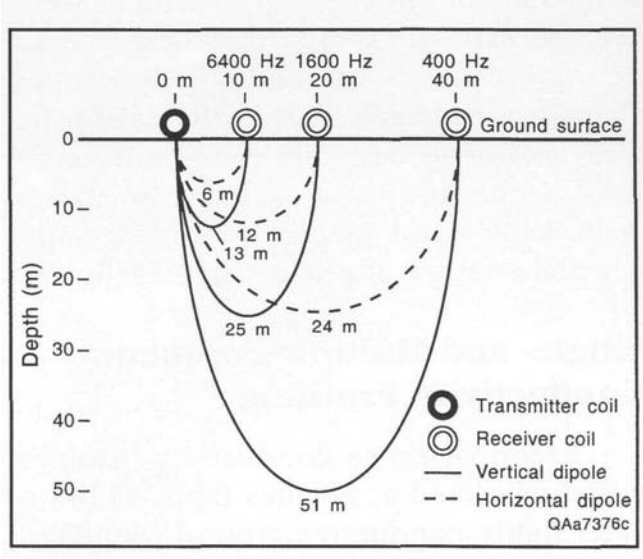

FIGURE 11. Exploration depth of various coil separations and orientations of the EM34-3.

changes. Horizontal and vertical dipole conductivities for each coil separation were entered in the program, and a starting conductivity model was entered, consisting of layer thicknesses and conductivities that qualitatively fit the observed data. The computer then displayed both the observed conductivities and those calculated from the model. The user then adjusted the model to better fit the observed data. After reasonable agreement was obtained, the program adjusted layer thicknesses and conductivities to obtain the best fit. The program then determined the range of model thicknesses and conductivities, producing an equivalent fit to the observed data.

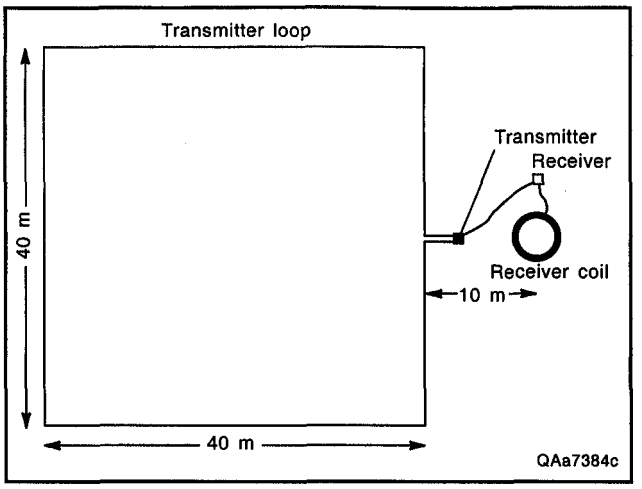

FIGURE 13. Instrument configuration of Protem TDEM sounding.

Time-Domain EM Soundings

We acquired time-domain, or transient, EM (TDEM) soundings (Kaufman and Keller, 1983; Spies and Frischknecht, 1991) using the Geonics PROTEM 47/S to produce vertical conductivity profiles to a maximum depth of 75 to 100 rn. Rather than changing coil frequencies and separations to vary exploration depth, TDEM instruments measure the decay of a secondary EM field (the "transient") produced by the collapse of a primary EM field (fig. 12). The secondary field strength is measured by the receiving coil at moments in time (or "gates") following transmitter-current termination. Secondary field strength at early time gives information about conductivity in the shallow subsurface; field strength at late time is governed by conductivity at depth. The computer program TEMIX, by Interpex, was used to construct vertical conductivity profiles that best fit the observed transient decay for each sounding.

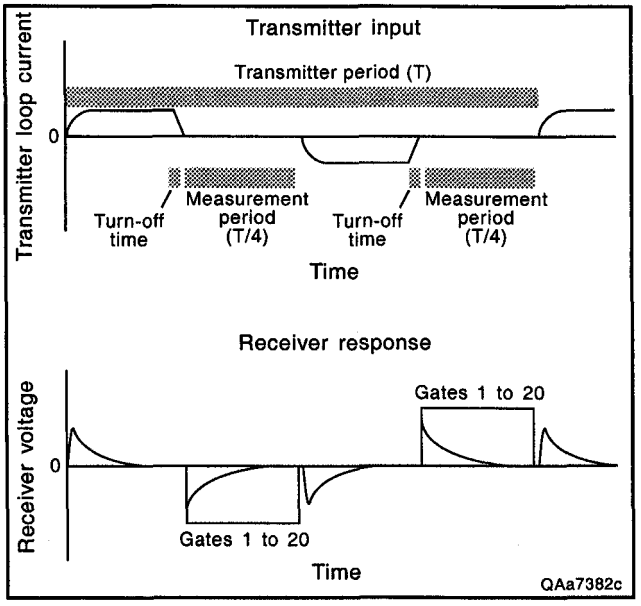

FIGURE 12. Protem 47/S transmitter input and receiver response. Adapted from Geonics Limited (1992).

Thirteen TDEM soundings were conducted at nine sites in April 1996 (app. A). We collected all time-domain soundings using a 40 x 40-m transmitter loop, with the receiver coil outside the transmitter loop (fig. 13). Whereas results of multiple-coil-separation soundings are given in the conductivity unit mS/m, results of TDEM soundings are customarily given in the resistivity unit ohm-m. These units are the inverse of each other and are converted by the equation

Conductivity (mS/m) = 1,000/Resistivity (ohm-m).

WATER AND SOIL SAMPLING

Ground-water, surface-water, and soil samples were collected to (1) evaluate how well the airborne geophysical data characterize ground-water and soil salinity and (2) identify sources of salinity in the Hatchel area. Data collected by the Bureau were merged with data collected by the Lower Colorado River Authority (LCRA) and the Colorado River Municipal Water District (CRMWD). Ground water was sampled from most of the accessible water wells, including 6 sampled by the Bureau and 19 by LCRA and CRMWD (figs. 14, 15). Sampled wells were in areas of high and low conductivity mapped by the airborne EM survey. Soil samples were paired with ground-water samples and chosen in areas of high and low conductivity shown on the 56,000-Hz ground-conductivity map. Surface water was sampled in January 1996 by LCRA and CRMWD and in April 1996 by the Bureau (fig. 15). In addition, water samples were collected at two abandoned oil wells being plugged by RRC and at an unplugged core hole.

Ground-water samples were taken by Bureau staff from abandoned and active wells. Where a well had no pump, we installed a temporary pump to purge the well bore and obtain a sample. Ground water was sampled by the LCRA and CRMWD from wells equipped with a pump or windmill. Three of the wells sampled by Bureau staff were hand-dug wells holding 475 to 2,480 L in storage. The others were drilled wells holding less than 40 L in storage.

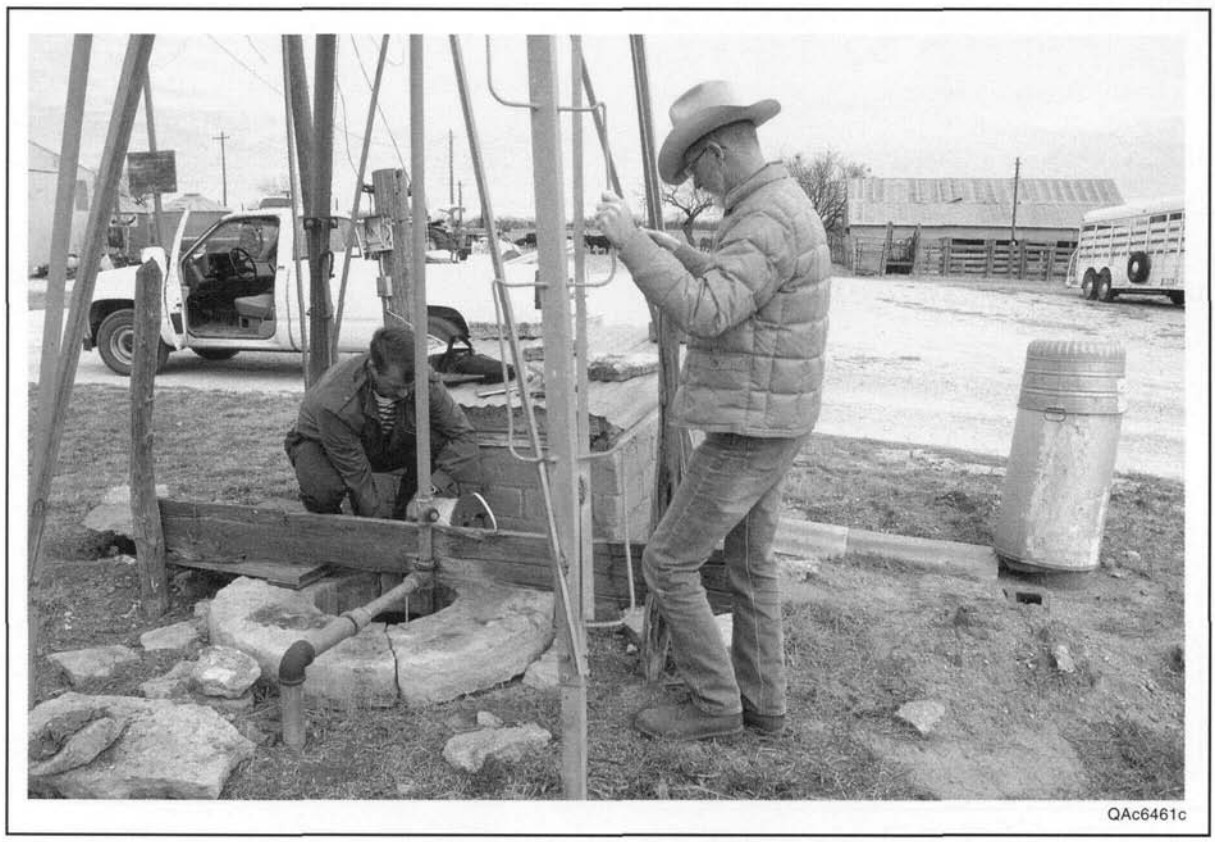

FIGURE 14. Photograph of LCRA and CRMWD staff sampling a water well during the airborne geophysical survey.

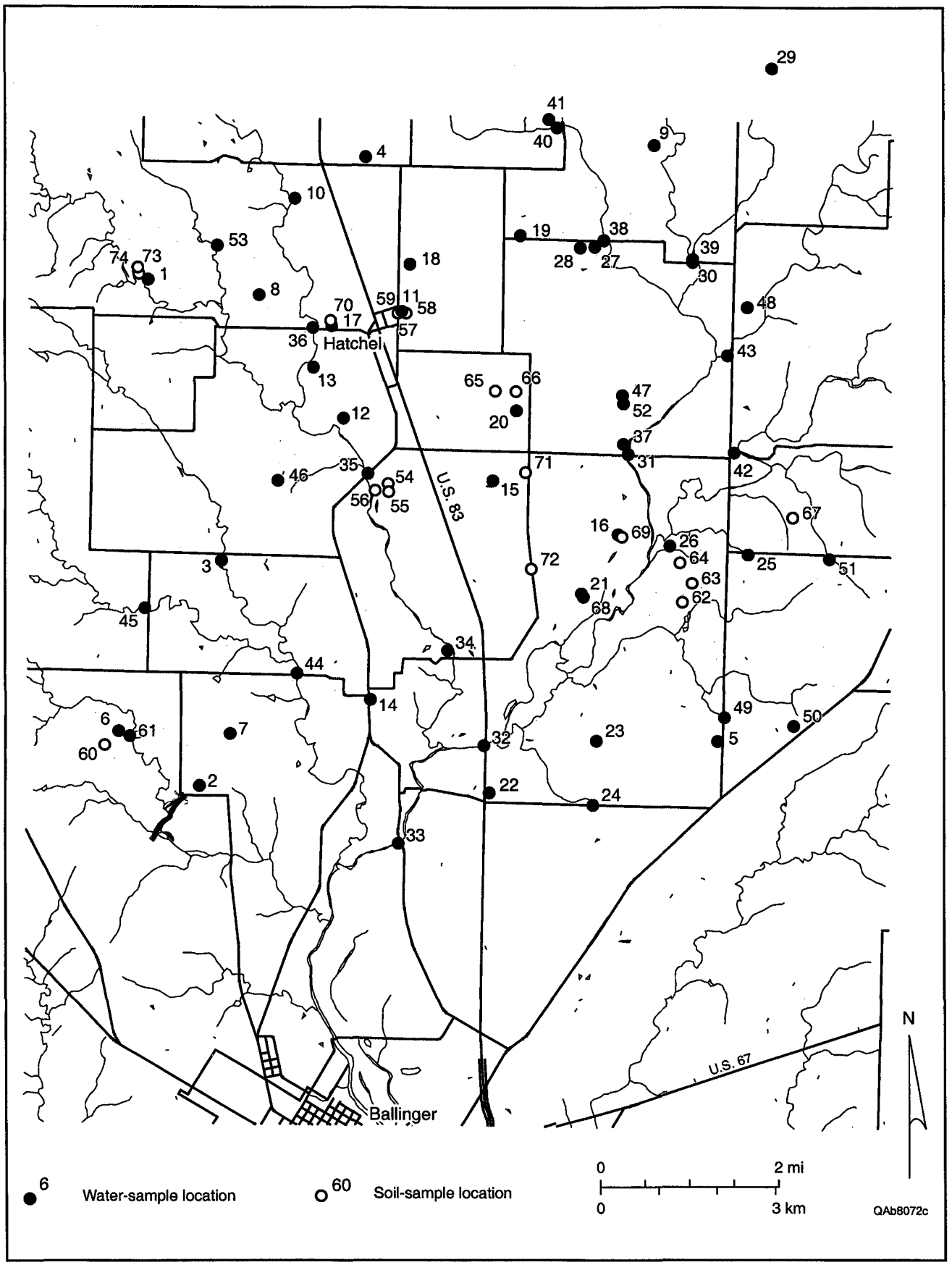

FIGURE 15. Location of water and soil samples collected by CRMWD, LCRA, and the Bureau (apps. B, C).

We collected water samples after the temperature, pH, and Eh had stabilized, which took less than 1 hr. During that time the water columns in the wells were drawn down as much as 80 percent at our 15- to 19-L/min pumping rate. Water sampling followed standard techniques (Brown and others, 1970; Wood, 1976), and samples were passed through a 0.45-µm filter and collected in bottles. We measured alkalinity by titration of unfiltered samples using H_2SO_4 within several hours of collection. Waters to be analyzed for cations were acidified in the field by means of 6N HNO_3; waters to be analyzed for anions were collected without treatment. Sample bottles were sealed and stored at 4°C before analysis. We measured cation concentrations using inductively coupled plasma-optical-emission spectroscopy. Fluoride, chloride, bromide, nitrate, and sulfate concentrations were measured by ion chromatography. Bicarbonate was determined by titration. TDS (total dissolved solids) of the CRMWD samples was determined by gravimetric analysis of a filtered sample. TDS of the Bureau samples was calculated as the sum of reported dissolved constituents (cations, anions, and dissolved silica).

Water from the abandoned oil wells was sampled at the wellhead. Fluid pressure allowed the wells to discharge through the valve used to control flow during plugging. The collected liquid contained black suspended solids (pipe scale) and some oil. The samples were prefiltered through glass wool and then drawn through an in-line 0.45-µm filter. Water temperature was measured in the stream flowing from the wellhead; pH was measured in the filtered sample. The sample from the core hole was drawn into the filter chamber through a 0.45-µm filter.

The four surface-water samples collected by the Bureau were drawn through a 0.45-µm filter and decanted into polyethylene bottles. Temperature was measured in the stream, and pH was measured on site.

Soil samples were collected with a hand auger, air dried, and milled. Electrical-conductivity and chloride measurements were performed on 1:1 extractions. Samples were shaken for 1 hr then centrifuged to obtain a particle-free liquid. Electrical conductivity, which indicates the concentration of soluble salts in an aqueous sample, was determined on the supernatant by means of a microconductivity cell and corrected to 25° C. Chloride concentrations were determined by argentometric titration or ion chromatography.

RESULTS

We analyzed airborne geophysical data to determine whether airborne methods can reliably delineate salinized areas, distinguish oil-field salinization from other causes, locate oil and gas wells and associated salinization, and guide ground investigations of salinization.

Airborne Geophysical Survey

One of the goals of the airborne geophysical survey was to identify areas where conductive ground coincided with a magnetic anomaly. This geophysical signature, insofar as a well casing produces a magnetic anomaly and salinization produces a conductivity anomaly, might indicate areas where saltwater has entered the ground through a brine-disposal pit or a leaking oil or gas well. Airborne-survey data, including maps of magnetic-field strength and ground conductivity, were analyzed to identify regional and local anomalies for field investigations.

Magnetic-Field Data

Total magnetic-field data from the Hatchel area show abundant local anomalies superimposed on the regional gradient of Earth's magnetic field (fig. 16). Magnetic-field strength increases along the regional gradient from the lowest value of 50,186 nanoTeslas (nT) in the southwest corner of the Hatchel area to the highest value of 50,382 nT in the northeast corner (Garrie, 1996). These results are consistent with regional maps of magnetic-field strength (Bennett and others, 1985).

Linear and oval magnetic anomalies are superimposed on the regional gradient (fig. 16). The anomalies are weak relative to the total field strength (as much as 30 nT, or about 0.06 percent) but are well above the 0.01-nT sensitivity of the magnetometer. The linear features, some of which extend completely across the study area, are generally 150 to 200 m wide. Their locations correspond to those of known pipelines. Two of the anomalies, the northwest-southeast-trending line in the southwest corner and the north-south-trending line on the east side that bends to the northeast, are both known pipelines that are mislocated on maps (fig. 16). Mapped pipelines are also in the study area that are not visible on the magnetic field map, perhaps because they are constructed of nonferrous material or oriented parallel to the flight lines.

Most of the oval anomalies are about 160 m across, although they range from 80 to 200 m. These are anomaly dimensions in an east-west direction (along the flight lines), where magnetometer measurements were acquired at 3-m intervals, rather than north-south (across the flight lines), where measurements were 100 m apart. Most of the oval magnetic anomalies coincide with known wells (fig. 16) and are interpreted to be magnetic-field perturbations caused by ferrous elements of the well (casing and pump jack). Other magnetic anomalies coincide with structures containing significant magnetically susceptible material, such as some homes, metal barns, and windmills.

Some oil and gas wells (known from RRC records and field investigations) are located where no magnetic anomalies are mapped. These wells were undetected because of either small magnetic anomalies located between flight lines or lack of well casing. Typical oval anomaly diameters of 80 to 200 m suggest that the 100-m flight-line spacing was a good compromise between anomaly detection and survey

cost. Line spacings of 200 m that were simulated during processing reduced the number of detected magnetic anomalies.

EM Data

Data for constructing ground-conductivity maps of the Hatchel area were obtained from EM coils operating at 56,000 (fig. 17), 7,200 (fig. 18), and 900 Hz (fig. 19) in a vertical dipole orientation. Because exploration depth depends on frequency and ground conductivity, deeper exploration depths were attained at lower coil frequencies and, for a given coil frequency, less conductive ground (fig. 20).

56,000-Hz vertical dipole data

Ground conductivities measured by the 56,000-Hz coils, the shallowest-exploration-depth frequency, showed good contrast between the lowest observed values of about 60 to the highest values of 730 mS/m (fig. 17). Maximum exploration depths range from 2.5 m over highly conductive ground to as much as 9 m over ground having the lowest observed conductivities (fig. 20). This shallow depth is most affected by soil type (clay soils are more conductive than sandy soils), moisture content (wet soils are more conductive than dry soils), and pore-water chemistry (saline water is more conductive than fresh water).

Highly conductive areas visible on the 56,000-Hz map include numerous small ovals that are generally 80 to 250 m across, curvilinear features that are a few hundred meters wide and hundreds of meters long, and large, irregular features covering many square kilometers (fig. 17).

Significant curvilinear features include (1) a zone about 200 m wide and more than 2 km long located along a bluff west of Bluff Creek in the north part of the study area, (2) a segment about 400 m wide along Coyote Creek that extends from the north edge to near the south edge of the Hatchel area, (3) a 200-m-wide zone along a bluff west of Elm Creek, and (4) a short segment of Elm Creek just downstream from its confluence with Eagle Branch (fig. 17). The curvilinear conductivity highs located at similar elevations along a bluff or hill slope probably mark ground-water seeps. Curvilinear features along the creeks most likely represent areas where higher salinity water flows in the creek or associated alluvium.

Ground investigations focused on the smaller, oval-shaped anomalies in the 56,000-Hz and lower frequency data. These anomalies are the ones most likely to be caused by oil-field salinization because of the limited lateral distance that saltwater plumes generally move from brine-disposal pits and leaking wells. Some anomalies in the 56,000-Hz data may also include small patches of conductive soil, springs, and stock tanks.

The most significant of the large, irregular areas of high conductivity are (1) the west third of the study area, (2) the area south of Hatchel and east of Coyote Creek, and (3) the area just east of Elm Creek and south of its confluence with Mud Creek (fig. 17). These features are too extensive to be caused by individual leaking wells, but some may indicate numerous and closely spaced saltwater sources. Most of these large features, probably not oil-field related, are instead areas where soils or shallow geologic units have more clay, have become wetter, or contain water that has a higher dissolved mineral content.

7,200-Hz vertical dipole data

Ground conductivity sensed by the 7,200-Hz airborne coils ranges from 60 to more than 700 mS/m, only slightly lower

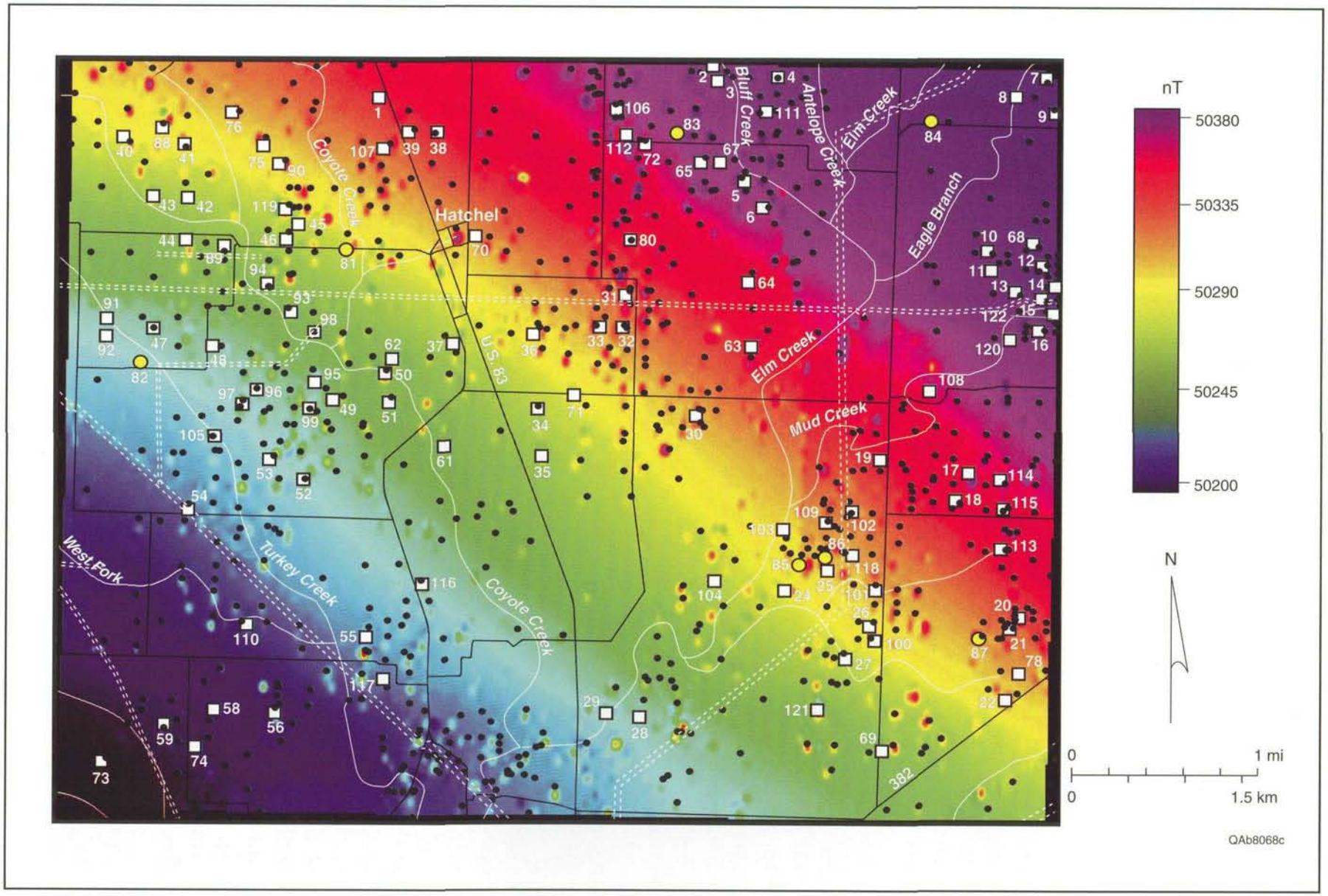

FIGURE 16. Map of enhanced total magnetic field strength. Black circles = oil- and gas-well locations, RRC. Dashed lines = pipeline locations, RRC. Numbered sites are locations of local geophysical anomalies and ground-based geophysical surveys (app. A).

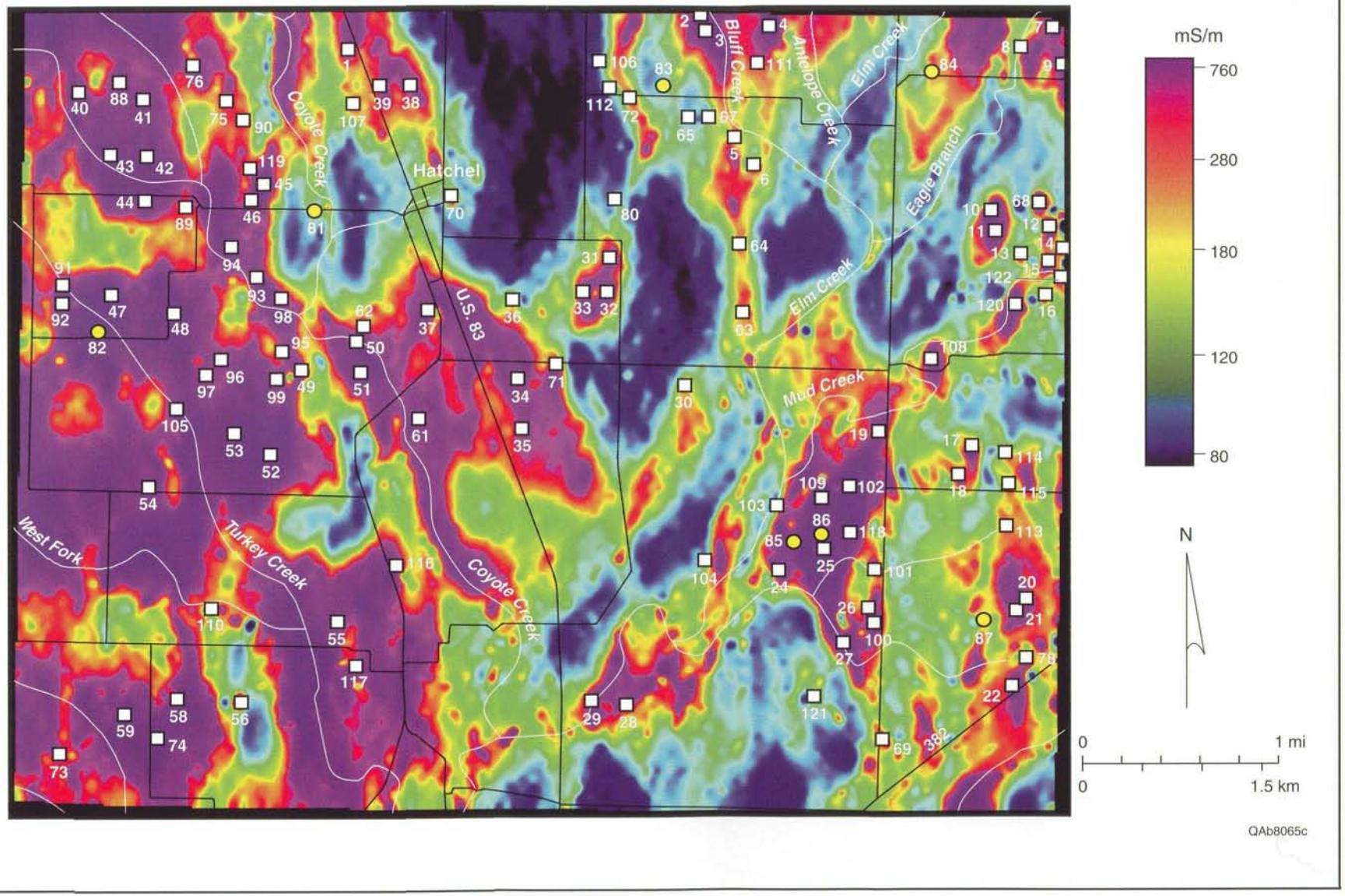

FIGURE 17. Map of shallow ground conductivity at 56,000 Hz (vertical dipole coil orientation). Numbered sites are locations of local geophysical anomalies and ground-based geophysical surveys (app. A).

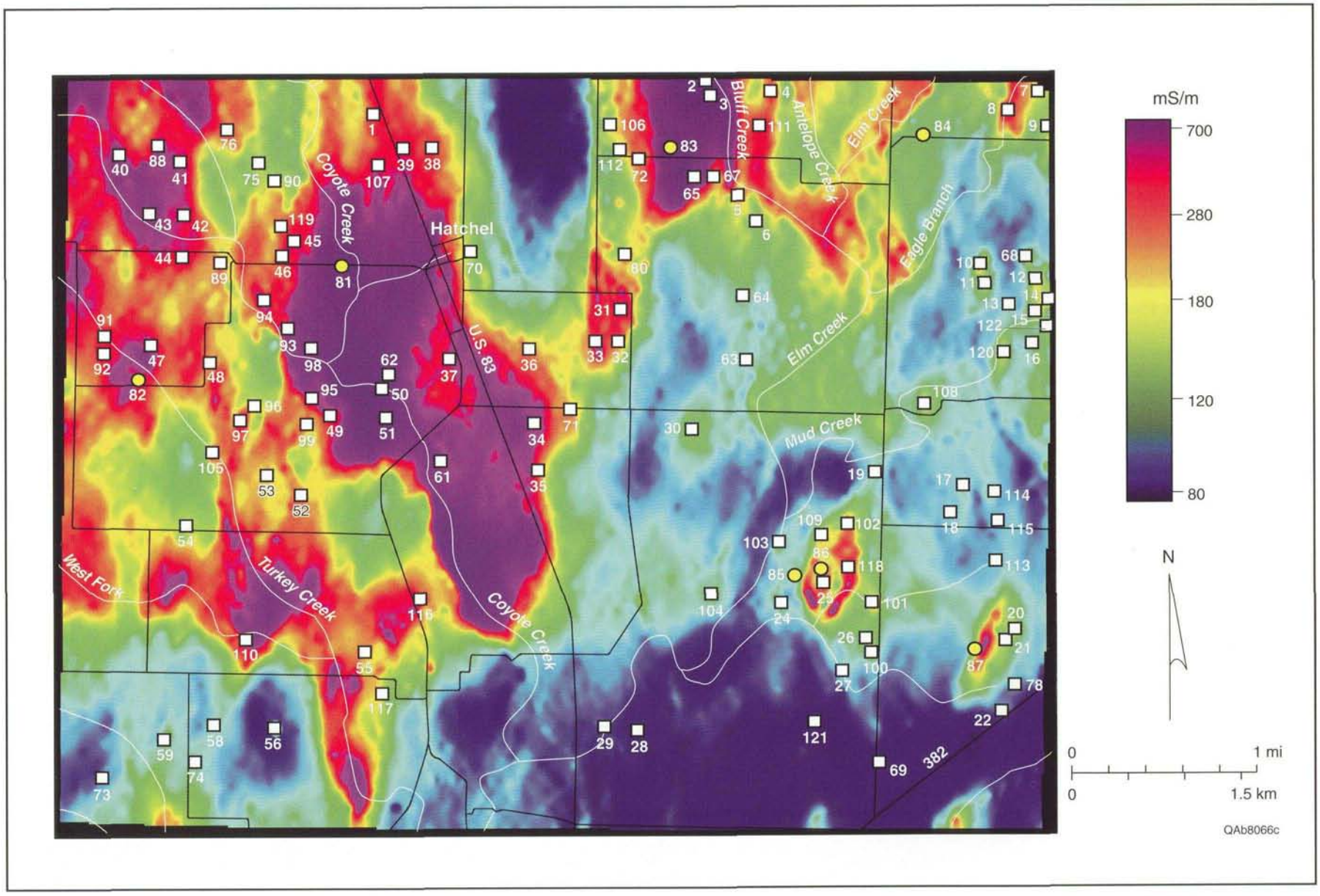

FIGURE 18. Map of moderately deep ground conductivity at 7,200 Hz (vertical dipole coil orientation). Numbered sites are locations of local geophysical anomalies and ground-based geophysical surveys (app. A).

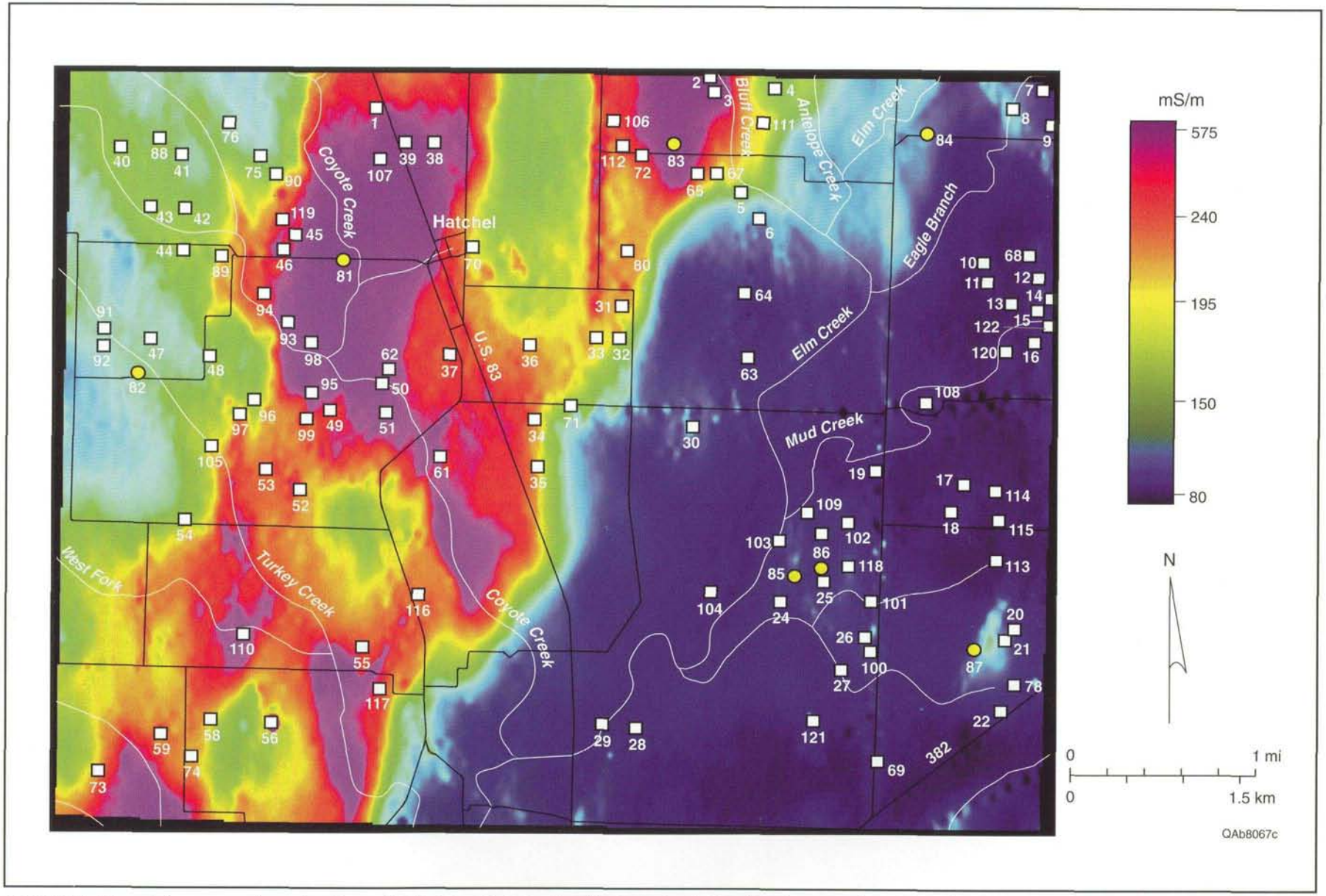

FIGURE 19. Map of deep ground conductivity at 900 Hz (vertical dipole coil orientation). Numbered sites are locations of local geophysical anomalies and ground-based geophysical surveys (app. A).

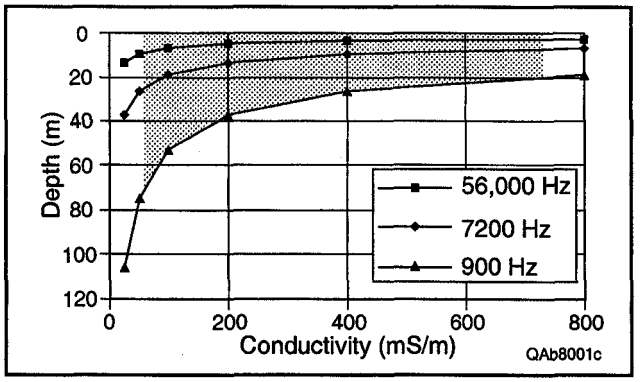

FIGURE 20. Changes in estimated exploration depth (skin depth) with ground conductivity for 900-, 7,200-, and 56,000-Hz airborne EM coils. Shaded area indicates conductivity range observed in the Hatchel area.

than the range observed for the higher frequency coils (fig. 18). The 7,200-Hz coils explore deeper than do the 56,000-Hz coils, ranging from 24 m for the least conductive ground to 7 m for the most conductive ground (fig. 20).

Highly conductive areas are more common on the 56,600-Hz map than on the 7,200-Hz map, suggesting that many of the conductivity anomalies visible on the 56,000-Hz map represent very shallow features. Local, oval-shaped anomalies that are ubiquitous on the high-frequency map are less common on the 7,200-Hz map. They are most common along the upper reaches of Mud Creek, east of Elm Creek and south of its confluence with Mud Creek, and east and northeast of Hatchel, and a few more are scattered across the study area (fig. 18). Large areas of anomalously high conductivity are found along and east of Coyote Creek, along and west of Bluff Creek upstream of its confluence with Elm Creek, and over the entire west-northwest section of the study area. The strongest large anomalies are along Coyote Creek and Bluff Creek. Linear and curvilinear features such as those evident on the 56,000-Hz map are absent at 7,200 Hz except along some roads. These are caused by power lines.

900-Hz vertical dipole data

Highly conductive ground measured by the 900-Hz airborne coils covers less area than that detected by the 7,200-Hz coils (fig. 19). Total range in conductivity is also lower for the 900-Hz coils, ranging between 60 and 400 mS/m. Maximum exploration depths are 68 m for the least conductive ground and 27 m for the most conductive ground (fig. 20).

Few local conductivity anomalies are visible in the 900-Hz data. The principal features are three areas of similar ground conductivity (fig. 19). The smallest is an area of low to moderate conductivity (100 to 150 mS/m) in the northwest part of the Hatchel area. This low-conductivity zone is bordered to the southeast by a 4- to 5-km-wide band of highly conductive (150 to 400 mS/m) ground trending north-northeast. Southeast of this zone is an extensive area of low conductivity (60 to 120 mS/m).

The north-northeasterly trend of the conductive band matches the strike of Permian geologic units (Kier and others, 1976). These units dip gently to the west-northwest into the Permian Basin. The 900-Hz coils, which are sensing the upper 30 to 40 m in this zone, are probably detecting a unit bearing saltwater. This unit, more conductive than units above and below it, shallows to the east-southeast. Probably too deep to be detected by the airborne instruments in the northwest corner of the study area, it has been removed by erosion in the southeast part of the area. We acquired more deeply exploring TDEM soundings to further investigate conductivity patterns evident at 900 Hz.

Regional Conductivity Patterns and Local Anomalies

Several natural and cultural effects can cause highly conductive ground.

Shapes of conductivity anomalies in map view and changes in conductivity with depth should allow us to distinguish natural conductivity anomalies (saline springs, clayey or wet soil, and saline geologic formations) from oil-field anomalies, but we might not be certain from airborne data alone whether a given oil-field anomaly represents a leaking well, a brine-disposal pit, or a spill. In an attempt to discover geophysical signatures for salinization and its various sources, we completed field investigations at sites representing the diversity that might be encountered in geophysical studies of oil-field salinization. These investigations included ground-based geophysical surveying and soil and water sampling. We also noted the soil type, geologic unit, and topographic setting for examining the potential effects of those properties on the geophysical signature.

Site Selection

We made ground-based geophysical measurements at 63 field sites chosen on the basis of airborne geophysical signatures (app. A). We examined regional conductivity patterns evident in the deep-exploring, 900-Hz conductivity images using TDEM soundings, and we examined local anomalies evident in the 56,000- and 7,200-Hz conductivity images using primarily single- and multiple-coil-separation conductivity profiling.

We identified 107 local geophysical anomalies (table 2; app. A) by visually inspecting the airborne magnetic and EM data. These anomalies were classified into five common airborne signature types: CMW, CM, CW, C, and MW. C denotes a conductivity anomaly detected by the 56,000-Hz coils, M denotes a magnetic anomaly, and W denotes a known well location. For example, type-CMW sites are those that have high-conductivity anomalies on the 56,000-Hz map, have magnetic anomalies, and have known wells nearby. Of the 107 local anomalies, 69 are type CMW and indicate possible salinization near known and detected wells. There are 15 CM sites, which might indicate salinization near tank batteries or near wells that are either mislocated or not inventoried. The 12 type-CW sites might indicate salinization at known wells undetected by the airborne magnetometer or at wells having no casing. The 11 type-C sites might be caused by salinization near an unknown well that went undetected by the airborne magnetometer. In addition to investigations at the conductivity anomalies, we visited two type-MW sites. These sites, which number in the hundreds, represent known wells having detected magnetic anomalies. Lack of an associated conductivity anomaly indicates no evidence of salinization.

Ground-based geophysical investigations consisted of (1) 43 reconnaissance conductivity profiles across 29 sites, (2) 60 conductivity profiles at multiple exploration depths at 32 sites, (3) 6 TDEM soundings at two local anomalies, and (4) 7 TDEM soundings at locations chosen on the basis of regional conductivity patterns.

Regional Conductivity Patterns

Conductivity patterns on the 900-Hz map differ fundamentally from those on maps showing conductivity at shallower depths (compare figs. 17 through 19), having a northeasterly trend resembling that on the regional geologic map (Kier and others, 1976). TDEM soundings detect vertical conductivity changes to maximum depths of 80 to 100 m, which are comparable to the 30- to 60-m exploration depth of the 900-Hz airborne coils (fig. 20) and greater than depths reached

TABLE 2. Summary statistics for airborne geophysical anomalies (figs. 17 through 19; app. A). Type-CMW sites are those that have a conductivity anomaly, a magnetic anomaly, and a known well. Type-CM sites have a conductivity anomaly and a magnetic anomaly, but no known well. Type-CW sites have a conductivity anomaly and a known well, but no magnetic anomaly. Type-C sites have a conductivity anomaly, but neither a known well nor a magnetic anomaly.

Conductivity anomalies mapped from airborne data	107	39 fit leaking-well profile[1]
CMW sites	69	29 fit profile
CM sites	15	5 fit profile
CW sites	12	5 fit profile
C only sites	11	0 fit profile
Conductivity anomalies, 56,000 Hz	99	
Conductivity anomalies, 7,200 Hz	56	
Conductivity anomalies, 56,000 and 7,200 Hz	48	
Conductivity anomalies, 56,000, 7,200, and 900 Hz	13	
Ground-based geophysical sites	63	
CMW	34	25 fit profile; 16 possible leaking wells
CM	6	4 fit profile; 1 possible leaking well
CW	7	5 fit profile; 3 possible leaking wells
C	7	
MW	2	
TDEM sounding-only sites	7	

Interpreted salinity source at 39 sites fitting an airborne profile of a potential leaking well[1]

Site	Anomaly type	Inferred salinity source
4	CMW (56,000+7,200)	Oil-field discharge at surface
5	CMW (56,000+weak 7,200)	Oil-field discharge at surface
8	CMW (56,000+7,200+weak 900)	Leaking well?
9	CM (56,000+weak 7,200)	Feedlot
10	CW (56,000+7,200)	Former leaking well
12	CW (56,000+7,200)	Oil-field discharge at surface
14	CMW (56,000+7,200)	Former leaking well
15	CMW (56,000+7,200)	Former leaking well
16	CW (56,000+weak 7,200)	Former leaking well?
19	CMW (56,000+weak 7,200)	Source not found
20	CMW (56,000+7,200+weak 900)	Leaking or former leaking wells?
22	CMW (56,000+weak 7,200+weak 900)	Oil-field discharge at surface
24	CM (56,000+weak 7,200)	Natural seep and metal debris
30	CMW (56,000+weak 7,200+weak 900)	Oil-field discharge at surface?
37	CW (56,000+weak 7,200)	Leaking well?
38	CW or C (weak 56,000+weak 7,200)	Source not found
40	CMW (56,000+weak 7,200)	Leaking well?
44	CM or CMW (56,000+7,200+weak 900)	Leaking well?
47	CMW (56,000+7,200)	Leaking well?
52	CMW (56,000+7,200)	Oil-field discharge at surface?
53	CMW (56,000+7,200+900)	Undetermined
56	CMW (56,000+7,200+900)	Leaking well?
59	CMW (56,000+weak 7,200+weak 900)	Oil-field discharge at surface
62	CM (56,000+weak 7,200)	Irrigation with creek water
64	CMW (56,000+weak 7,200)	Undetermined
68	CMW (56,000+7,200)	Leaking well or surface spill
71	CM (56,000+weak 7,200)	Oil-field discharge at surface
74	CMW (56,000+weak 7,200)	Oil-field discharge at surface
76	CMW (56,000+7,200)	Leaking well?

TABLE 2 (cont.)

80	CMW (56,000+7,200+900)	Former leaking well or surface spill
88	CMW (56,000+7,200+weak 900)	Leaking well?
94	CMW (56,000+7,200)	Oil-field discharge at surface; leaking well?
97	CMW (56,000+7,200+900)	Leaking well?
99	CMW (56,000+7,200+900)	Undetermined
105	CMW (56,000+7,200)	Leaking well?
110	CMW (56,000+7,200+900)	Leaking well?
116	CMW (56,000+7,200)	Leaking well?
118	CMW (56,000+7,200+weak 900)	Undetermined
119	CMW (56,000+7,200)	Undetermined

[1]Sites that fit a profile of a potentially leaking well are those that show conductivity anomalies measured by both the 56,000-Hz and 7,200-Hz airborne coils and have a known well location, a magnetic anomaly, or both.

by the EM34-3 (fig. 11). TDEM sounding sites (app. A; fig. 19) represented large areas having similar conductivities on the 900-Hz map. For sounding purposes, the Hatchel area was divided into a low-conductivity zone in the northwest part of the study area, a high-conductivity band trending north-northeast across the central part of the study area, and another low-conductivity zone in the east-southeast part of the study area.

Northwest low-conductivity zone

A triangular zone of relatively low conductivity on the 900-Hz map is located in the northwest part of the Hatchel area (fig. 19). Typical conductivities in this zone are 130 to 180 mS/m. Four TDEM soundings were acquired at two sites within this area: three at site 76 and one at site 82 near the upstream end of Turkey Creek.

Conductivity measured by the 900-Hz airborne coils is about 140 mS/m at site 76 (fig. 19). The deeper parts of the conductivity models for the site-76 TDEM soundings are similar (fig. 21), showing a 7.8-ohm-m (128 mS/m) layer extending from 10 m to 41 m below the surface that is underlain by a conductive (2.3-ohm-m or 430-mS/m) layer below 41-m depth. The 900-Hz coils, which sense to depths of 40 to 50 m in this area, measure conductivity that is close to that of the 10- to 41-m layer in the sounding models and are affected by only the upper part of the conductive layer beginning at 41 m and extending to an unknown depth. Ground-surface elevation at this site is 538 m above sea level; the top of the conductive layer is 497 m above sea level.

Mapped 900-Hz conductivity for the TDEM sounding at site 82 is about 150 mS/m (fig. 19). The conductivity model for sounding S82A (fig. 22) has deep layering similar to that at site 76: a relatively resistive (8.5-ohm-m or 118-mS/m) layer at depths of 15 to 37 m overlies a conductive (2.6-ohm-m or 384-mS/m) layer below 37-m depth. The conductive layer is modeled at a depth shallower than that of site 76, which accounts for the slight increase in conductivity sensed by the 900-Hz coils. With a ground-surface elevation of 530 m above sea level, the top of the conductive layer at site 82 is 493 m above sea level.

Relatively low conductivity sensed by the 900-Hz airborne coils largely reflects conductivities characteristic of a stratigraphic interval that extends to a depth of about 40 m in this area. The stratigraphic

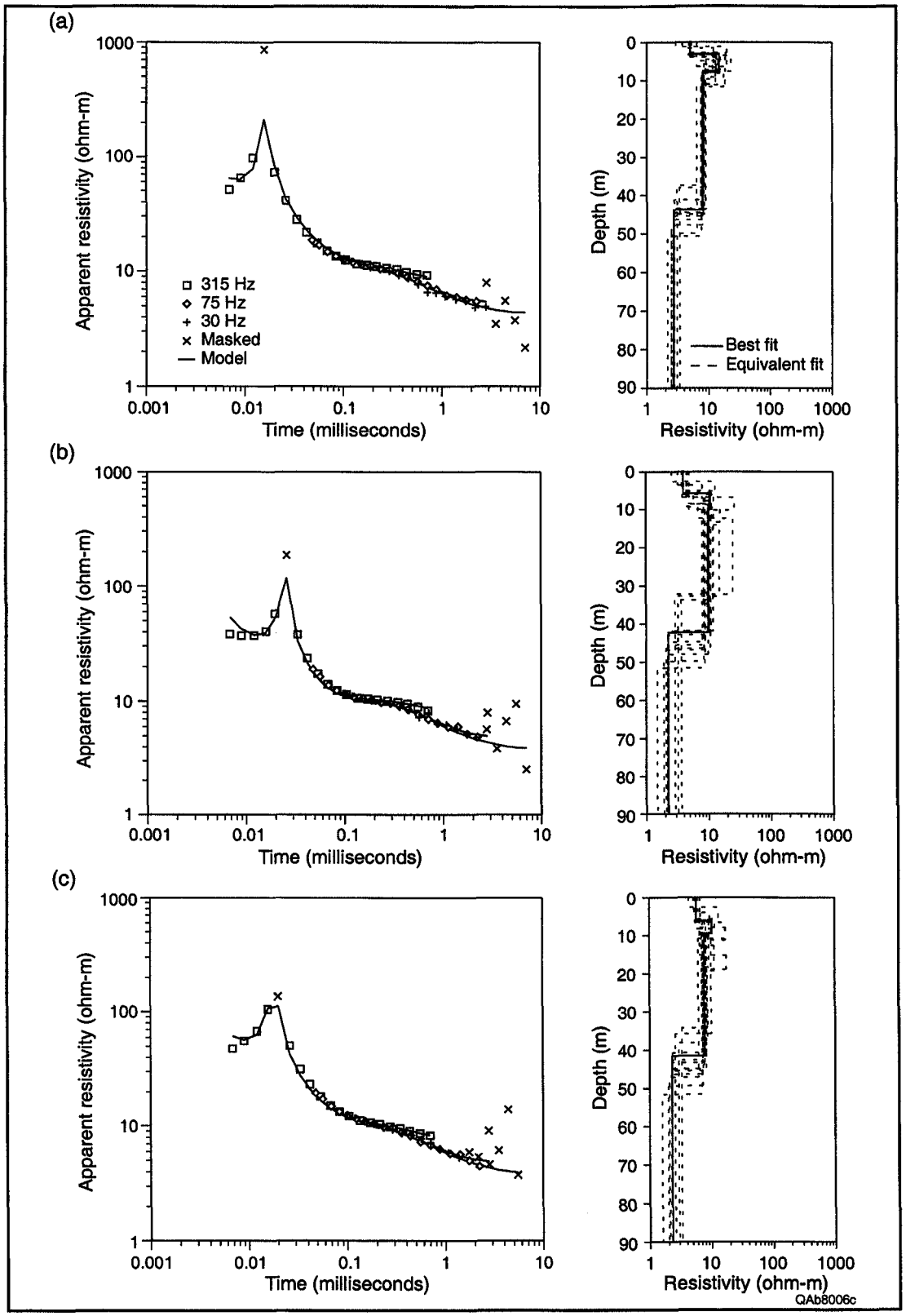

FIGURE 21. (left) Transient decay and (right) resistivity models at TDEM soundings (a) S76A, (b) S76B, and (c) S76C at site 76 (figs. 17 through 19; app. A). Symbols in the decay curve at left represent field measurements; the solid line through the data points at left represents the calculated decay of the resistivity model at right. The resistivity model at right that has the solid line represents the model fitting the field data best; the dashed lines at right represent models fitting the field data to within 10 percent of the fit provided by the best model.

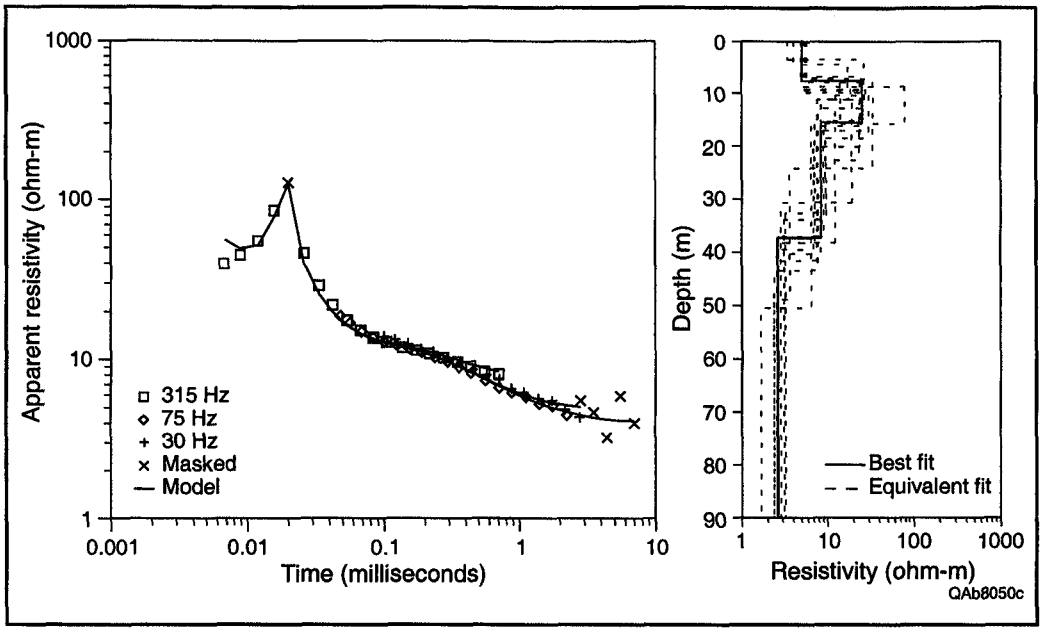

FIGURE 22. (left) Transient decay and (right) resistivity models at IDEM sounding S82A at site 82 (figs. 17 through 19; app. A).

interval does not contain large volumes of saltwater. TDEM soundings detected a more conductive stratigraphic interval deeper than about 40 m that is likely to contain saltwater. This zone follows the regional geologic trend of west-northwestward deepening into the Permian Basin.

Central conductive zone

The central conductive zone, as depicted on the 900-Hz airborne map (fig. 19), trends north-northeastward from the southwest corner of the Hatchel area. Conductivities are high, ranging from 175 to 350 mS/m. At these conductivities, exploration depth at 900 Hz is 30 to 40 m (fig. 20). Two TDEM soundings were located within the most conductive parts of this trend: site 81, located in a cultivated field west of Hatchel, and site 83, near Bluff Creek at the north edge of the study area (fig. 19).

At site 81, conductivity measured by the 900-Hz airborne coils is about 340 mS/m. TDEM sounding S81A indicated the presence of a conductive (2.7-ohm-m or 365-mS/m) layer at a depth of 11 m that extends to 61 m (fig. 23). This thick layer encompasses most of the effective exploration depth of the 900-Hz airborne coils and matches the measured conductivity well. A more resistive (8.2-ohm-m or 123-mS/m) layer lies below 61-m depth. The top of the model's 50-m-thick conductive layer is 509 m above sea level.

The conductivity profile that best fits the TDEM data at site 83 also indicates a conductive layer close to the land surface (fig. 24). Conductivity measured by the 900-Hz airborne coils is about 300 mS/m, slightly lower than at site 81 (fig. 19). The conductive layer detected by the sounding is also slightly less conductive (3.2 ohm-m or 313 mS/m) than the conductive layer at site 81 and again matches the airborne measurements. The conductive layer extends from 10 to 71 m below the surface and is underlain by a resistive (13.5-ohm-m or 74-mS/m) layer. The top of the conductive layer is 514 m above sea level.

The main differences between conductivity models constructed for TDEM soundings in this zone and those in the northwest low-conductivity zone are that (1) the conductive layer is detected at shallower depths and (2) the base of the

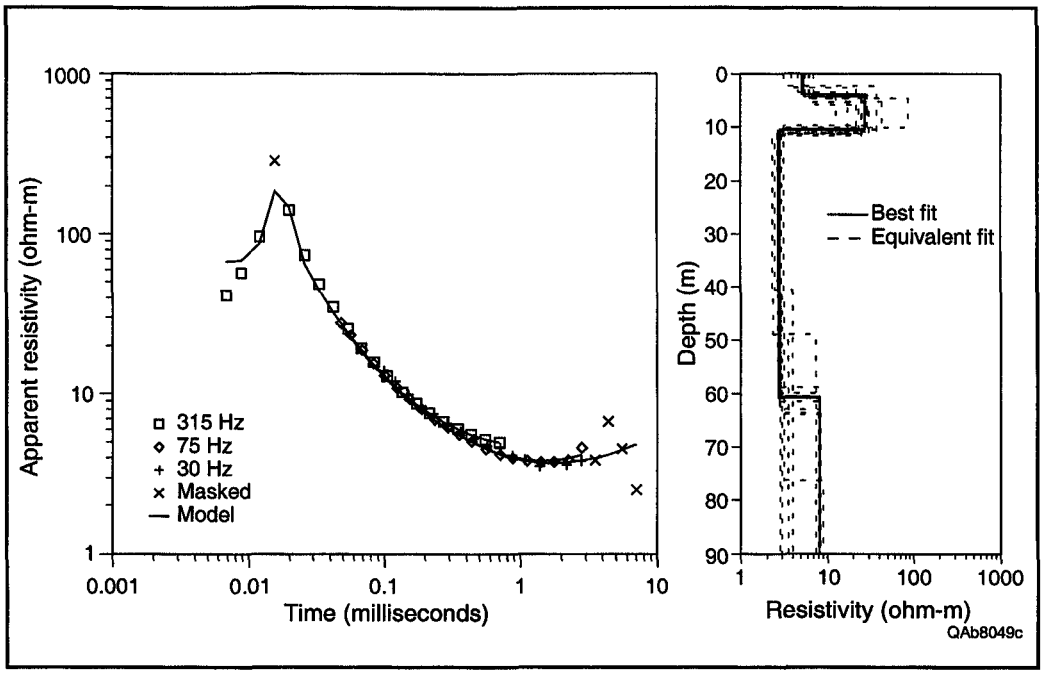

FIGURE 23. (left) Transient decay and (right) resistivity models at IDEM sounding S81A at site 81 (figs. 17 through 19; app. A).

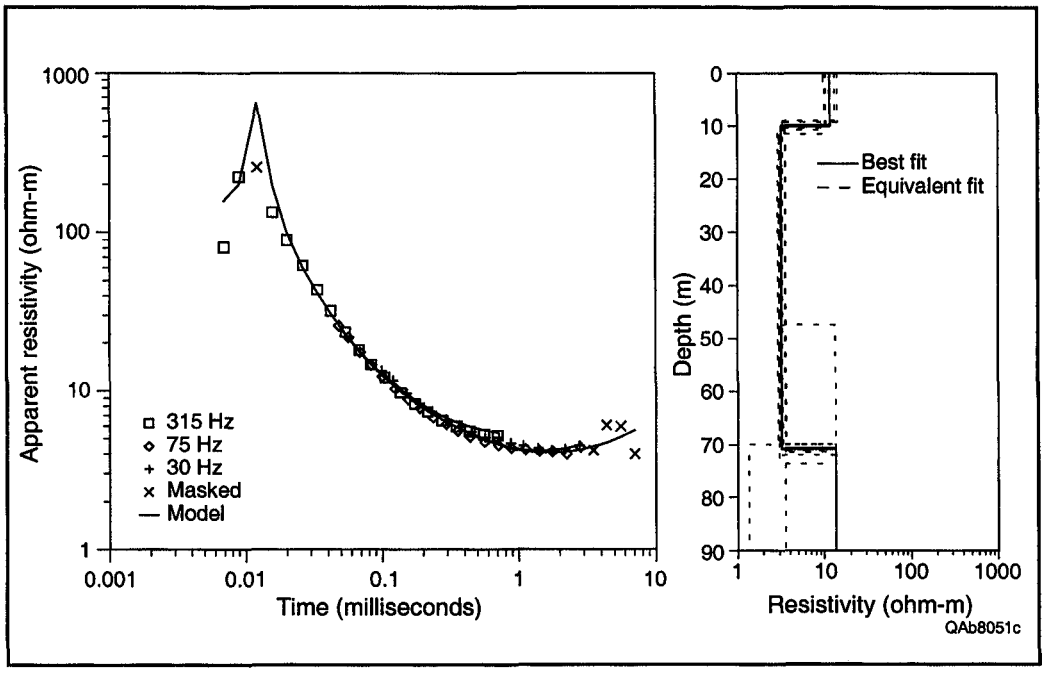

FIGURE 24. (left) Transient decay and (right) resistivity models at TDEM sounding S83A at site 83 (figs. 17 through 19; app. A).

conductive layer is detected. Soundings in the central conductive zone are consistent with the interpretation that the conductive layer is a saltwater-bearing geologic interval that is shallowing east-southeastward away from the Permian Basin. This unit is 50 to 60 m thick, and its top approaches the land surface on the southeast margin of the central conductive zone.

East-southeast low-conductivity zone

This zone is the largest of the three regional zones, covering the east-southeast

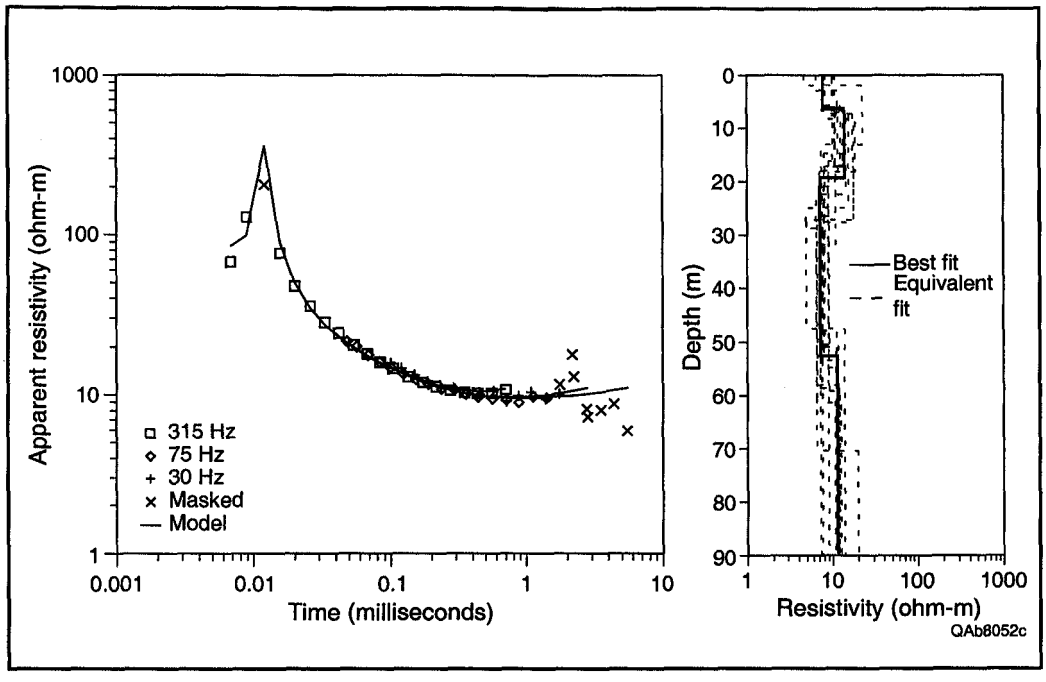

FIGURE 25. (left) Transient decay and (right) resistivity models at TDEM sounding S84A at site 84 (figs. 17 through 19; app. A).

part of the Hatchel area. Ground conductivities measured by the 900-Hz airborne coils are lowest here, ranging from 60 to 150 mS/m (fig. 19). Consequently, maximum exploration depths are greatest (45 m in 150-mS/m terrain and 70 m in 60-mS/m terrain, fig. 20).

Seven TDEM soundings were acquired at five sites in this zone. At site 84 in the northeast corner of the study area (fig. 19), conductivity measured by the 900-Hz airborne coils is 120 mS/m. A conductivity model constructed for sounding S84A (fig. 25) includes a layer having similar conductivity (7.4 ohm-m or 136 mS/m) between 19- and 52-m depth, an interval that covers most of the exploration depth range of the 900-Hz airborne coils. No highly conductive layer was detected in the sounding.

Soundings at sites 85 and 86 (figs. 26, 27) are located at the base (S85A) and the top (S86A) of a hill in Beddo field overlooking Elm Creek (fig. 19). Because sounding S85A was acquired at lower elevation, it explores to elevations lower than that of S86A. Conductivity measured using the 900-Hz airborne coils is 100 mS/m, which falls between those of two relatively resistive layers modeled for the sounding (fig. 26). The more resistive (86.8-ohm-m or 12-mS/m) layer lies between the depths of 5 and 20 m and is underlain by a 7.5-ohm-m (133-mS/m) layer below 20 m. The 900-Hz airborne coils sense both of these layers. No highly conductive layer was detected in either TDEM sounding.

Of the five sounding sites in this low-conductivity zone, conductivities measured by the 900-Hz airborne coils are the lowest (about 80 mS/m) at site 17 (fig. 19). The deeper parts of three soundings acquired as part of a local anomaly investigation are similar (fig. 28). Representative sounding S17B (fig. 28b) shows the presence of a relatively resistive (12.4-ohm-m or 81-mS/m) layer between the depths of 11 and 39 m that corresponds well with observed 900-Hz airborne coil measurements. No highly conductive layer other than the surface layer was detected. The conductive layer at the surface is related to salinization at a pit.

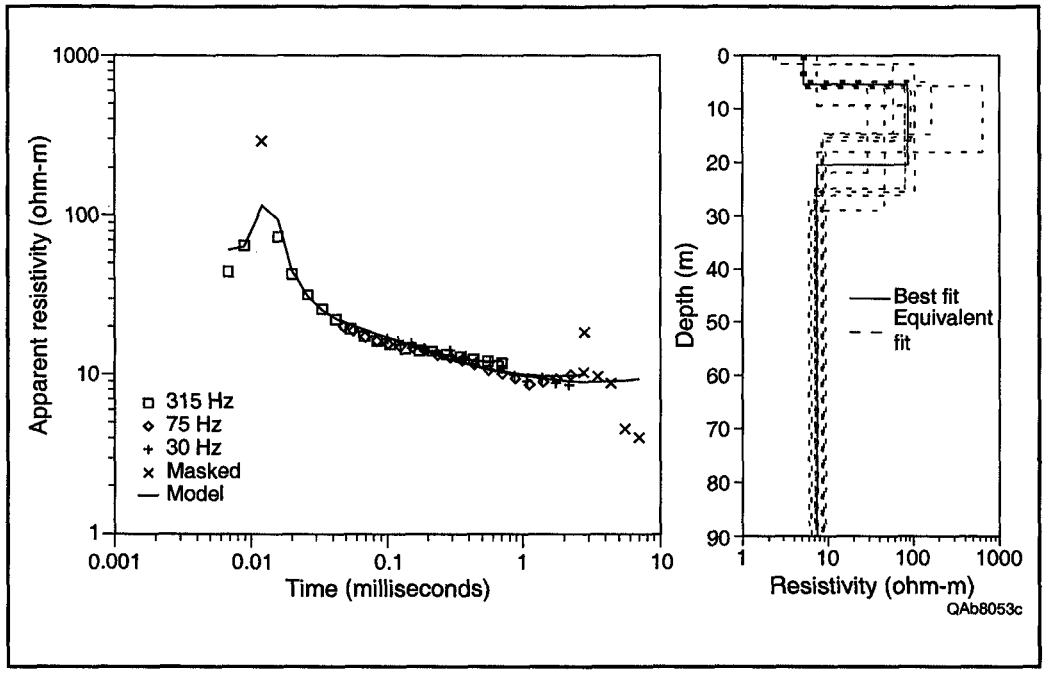

FIGURE 26. (left) Transient decay and (right) resistivity models at TDEM sounding S85A at site 85 (figs. 17 through 19; app. A).

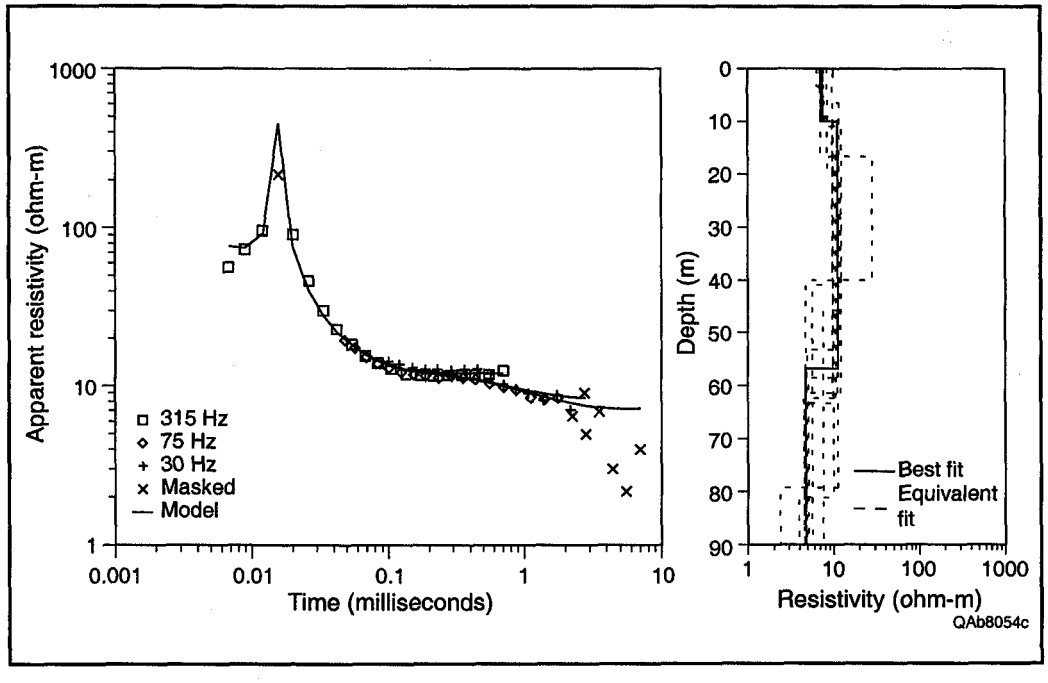

FIGURE 27. (left) Transient decay and (right) resistivity models at TDEM sounding S86A at site 86 (figs. 17 through 19; app. A).

Site 87 is located in the southeast corner of the Hatchel area, where conductivity measured by the 900-Hz airborne coils is about 100 mS/m (fig. 19). The conductivity model constructed for sounding S87A (fig. 29) indicates three relatively conductive layers within the depth range sensed by the airborne coils. The most conductive (6.2 ohm-m or 161 mS/m) of the three layers extends from 14- to 24-m depth and is underlain by a more resistive (17.5-ohm-m or 57-mS/m) layer between 24- and 42-m depth. Below 42 m is a layer of intermediate resistivity (9.4 ohm-m or

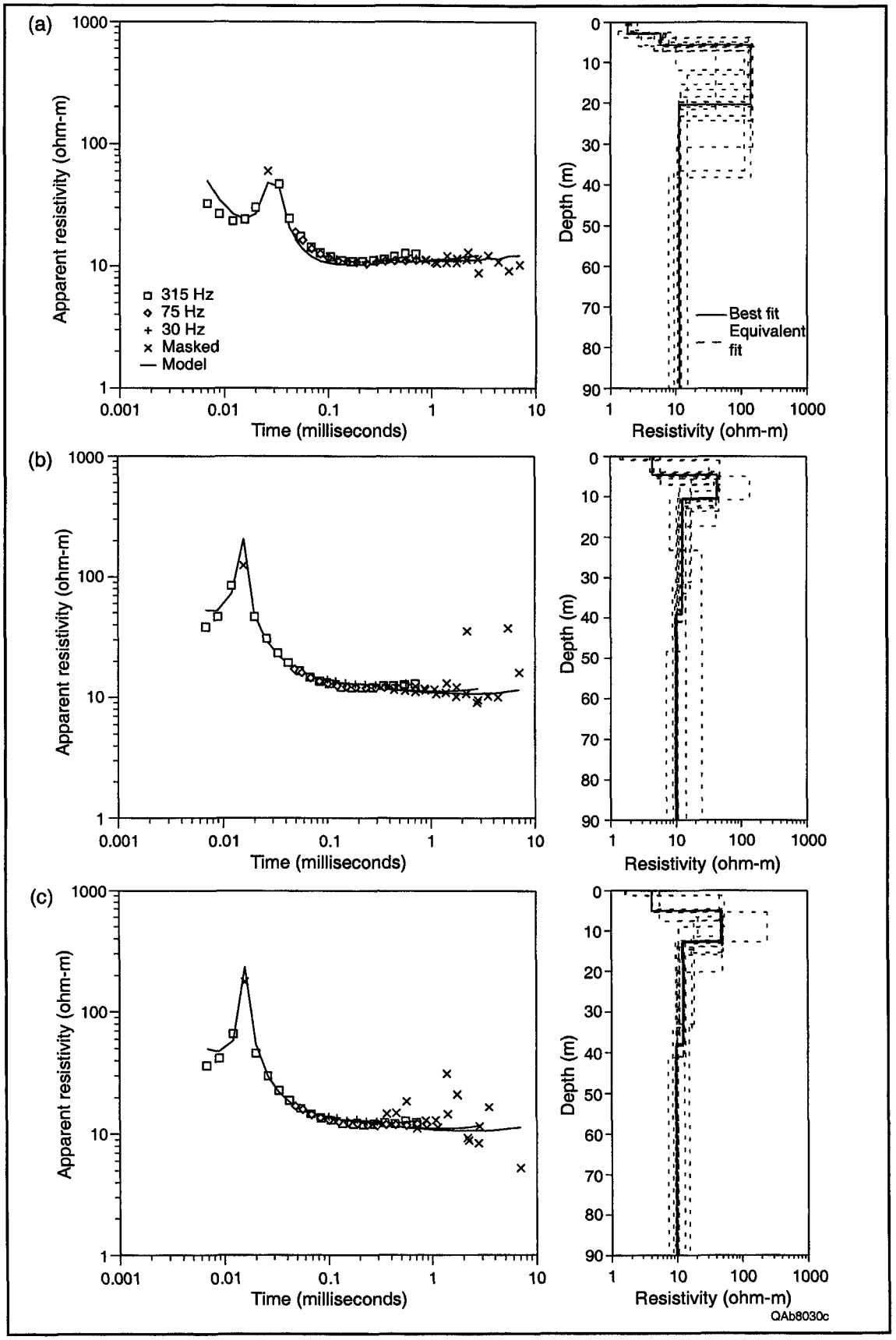

FIGURE 28. (left) Transient decay and (right) resistivity models at time domain soundings (a) 17A, (b)17B, and (c) 17C at site 17 (figs. 17 through 19; app. A).

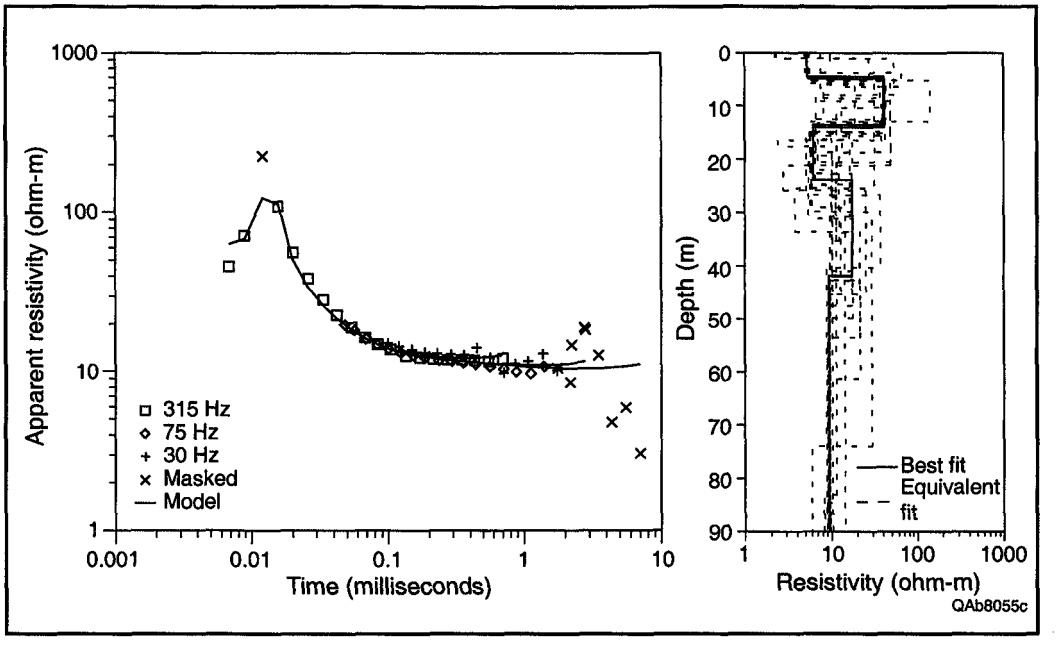

FIGURE 29. (left) Transient decay and (right) resistivity models at TDEM sounding S87A at site 87 (figs. 17 through 19; app. A).

107 mS/m). These three layers have a combined resistivity similar to that measured by the airborne coils. No highly conductive interval was detected.

The highly conductive, saltwater-bearing geologic unit that was detected at progressively shallower depths to the east and southeast across the northwest low-conductivity zone and the central conductive zone is absent in the southeast zone. Considering the flatness of the study area and the west-northwestward dip of Permian strata, part of the unit probably reaches the surface and has been eroded, has discharged saltwater, or has been infiltrated by fresher water. Exploration depths of the airborne and ground-based instruments were insufficient to reach the Coleman Junction Formation, a known brine-bearing interval beneath the Hatchel area.

Known Wells Having Conductivity and Magnetic Anomalies

Type-CMW sites, where a conductivity anomaly (C), a magnetic anomaly (M), and a known well location (W) coincide, were the most common of the 107 local conductivity anomalies identified from the airborne geophysical data (table 2; app. A). We investigated 34 of these sites using ground-based geophysical methods, four of which are detailed next. The remaining sites are summarized in table 2 and appendix A.

Site 76

Site 76, located in the northwest part of the Hatchel area, is an anomalously conductive area on the shallow (56,000-Hz) and moderately deep (7,200-Hz) airborne conductivity maps, but not on the 900-Hz map (figs. 17 through 19). The conductivity anomaly measures about 120 m east-west and 200 m north-south on the 56,000-Hz map and coincides with a magnetic anomaly that is similar in size (fig. 16). The site encompasses the abandoned Vancil No. 1 well (fig. 30), which was drilled and completed in 1966 and plugged in 1975. Thin Quaternary surficial deposits cover Permian Clear Fork strata (fig. 2); soil is mapped as Portales clay loam (fig. 3).

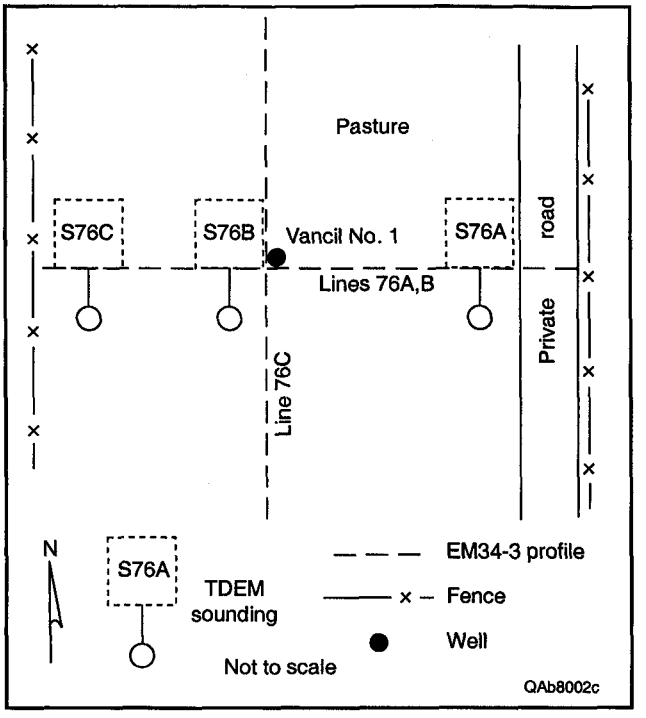

FIGURE 30. Sketch map of site 76 (figs. 17 through 19; app. A). One reconnaissance conductivity profile (76A), two multiple-coil-separation profiles (76B and 76C), and three TDEM soundings (S76A, S76B, and S76C) were acquired near the abandoned Vancil No. 1 well.

Ground investigations consisted of a reconnaissance conductivity profile, two multiple-coil-separation conductivity profiles, and three TDEM soundings. The reconnaissance profile revealed that elevated ground conductivity extends about 130 m across the site from east to west for the 20-m coil separation. This distance is similar to that measured from the airborne survey maps. High conductivities for the horizontal dipole mode (>100 mS/m) are found near the well, with highest values located 20 m west of the well.

Multiple-coil-separation profiles (fig. 31) were acquired along an east-west line and a north-south line across the well to determine vertical and lateral ground-conductivity patterns. Horizontal dipole measurements show well-defined conductivity peaks (fig. 31a, b); vertical dipole measurements show characteristic reductions in apparent conductivity over the most conductive ground (McNeill, 1980b). Highest ground conductivities measured in the horizontal dipole configuration on line 76B, the east-west line, are found for the 10- and 20-m coil separations (fig. 31a), indicating that the upper 6 to 12 m is more conductive than the 12- to 24-m depth range.

The highest conductivity for the 10-m coil separation on line 76B is 10 m west of the abandoned well. For the 20-m separation, the peak is 10 m farther west. Highest conductivities for the 40-m separation, although lower than those for the shorter separations, cover a broader area and are also centered about 20 m west of the well (downslope). East and west of the peak, conductivities increase with coil separation from 50 to 60 mS/m at 10-m separation, to 70 to 80 mS/m at 20 mS/m, to 80 to 90 mS/m at 40-m separation. This increase suggests that, away from the peak, conductivity increases with depth within the upper 20 m.

Similar trends are visible on the north-south line 76C (fig. 31b). Peaks at each of the three separations have similar conductivities (~100 mS/m) and are all centered within 5 m of the well. Peaks drop off more quickly north of the well (upslope) for the 10- and 20-m coil separations than they do south of the well.

Horizontal dipole data were used to construct two-layer conductivity models along lines 76B and 76C (fig. 32). On line 76B, a low-conductivity layer (23 to 90 mS/m) overlies a layer having higher conductivities (144 to 211 mS/m) on the east and west flanks of the abandoned well (fig. 32a). The surficial low-conductivity layer thins from about 4 m at each end of the line to less than 1 m in thickness near the well. At the well, the low-conductivity layer is replaced by a layer 2 to 4 m thick that is more conduc-

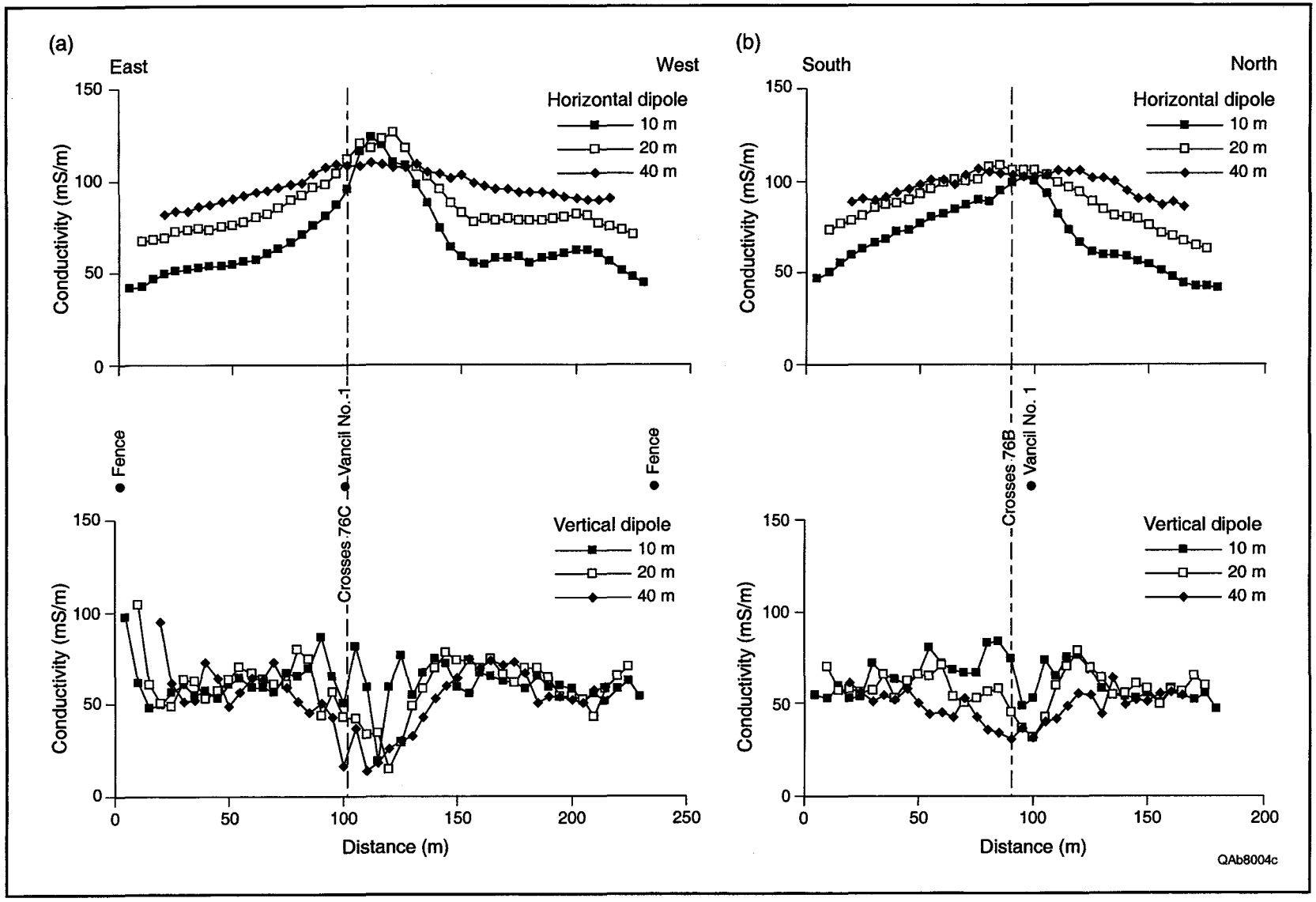

FIGURE 31. Apparent ground conductivity at site 76, measured using multiple coil separations (10, 20, and 40 m) and (upper plot) horizontal dipole and (lower plot) vertical dipole orientations. (a) Line 76B crosses the abandoned Vancil No. 1 well from east to west. (b) Line 76C crosses the well from south to north.

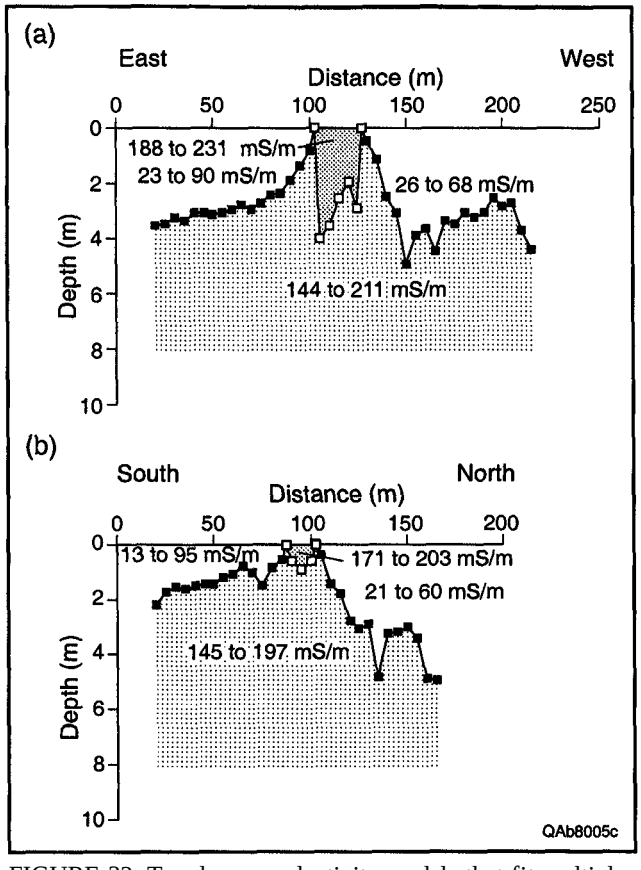

FIGURE 32. Two-layer conductivity models that fit multiple-coil-separation data for (a) east-west line 76B and (b) north-south line 76C at site 76. Vancil No. 1 well is located at 100 m on line 76B and at 90 m on line 76C.

tive than the layer below it. Two-layer models constructed along north-south line 76C (fig. 32b) are similar: a poorly conductive surface layer overlies a more conductive layer and is a few meters thick away from the well, is thinner toward the well, and is replaced at the well by a layer that is 1 to 2 m thick and that is more conductive than the underlying layer.

We located TDEM soundings at three sites along line 76B (fig. 30) to examine deeper variations in ground conductivity. Transients show decreasing apparent resistivity with time (fig. 21), suggesting that conductivity increases with depth. Four-layer conductivity models provide good fits to the observed transients. These models (fig. 21) confirm that resistivity decreases (or conductivity increases) in general with depth, and they differ significantly only in the upper 10 m.

A thin surface layer that is more conductive than are underlying units thickens from less than 5 m at the most upslope sounding (S76A, fig. 21a) to 7 or 8 m at the soundings closest to the well (S76B, fig. 21b) and downslope from the well (S76C, fig. 21c). This conductive surface layer, correlating with the lower conductive layer detected on the multiple-coil-separation profiles, probably represents salinization adjacent to the well.

Despite a lack of surface evidence of saltwater leakage (no barren zone or salt water at the surface), this well is probably leaking or has leaked recently. Evidence suggesting a recent or ongoing leak includes conductivity anomalies visible on 56,000- and 7,200-Hz airborne conductivity maps, conductivity peaks centered near the abandoned well for the 10-, 20-, and 40-m coil separations, a modeled conductive layer that shallows near the well, and the presence of a near-surface high-conductivity zone downslope of the well. The most likely cause of elevated ground conductivity near the well is the presence of saltwater. Background conductivity levels are reached within about 50 m of the well, suggesting that little saltwater has migrated farther than that distance.

Site 34

Site 34 is located south-southeast of Hatchel (fig. 17) on a cultivated and terraced field. Portales clay-loam soil grades westward into thinner Mereta clay-loam soil across the site (fig. 3). Caliche fragments are present at the surface where the clay loam is thinnest. These soils formed on thin Quaternary surficial deposits that overlie Clear Fork Group rocks (fig. 2). The site includes the location of the

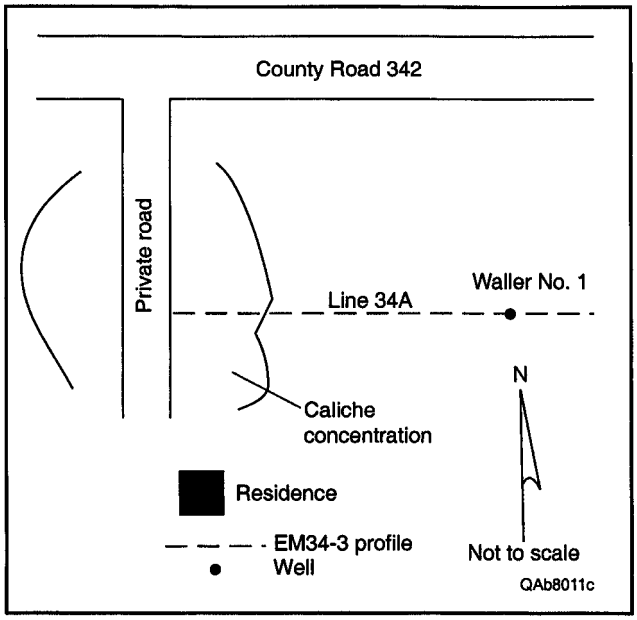

FIGURE 33. Sketch map of site 34 (figs. 17 through 19; app. A). Reconnaissance conductivity profile 34A crosses the Waller No. 1 dry hole.

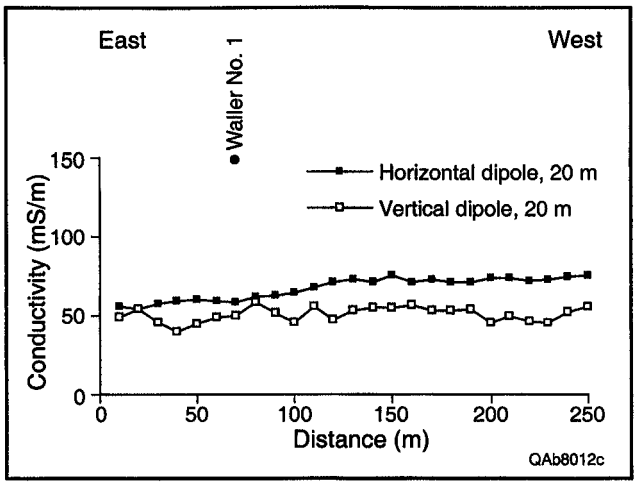

FIGURE 34. Apparent ground conductivity at site 34, measured using 20-m coil separation and horizontal and vertical dipole orientations. Line 34A crosses the abandoned Waller No. 1 well from east to west.

Waller No. 1 well, a dry hole that was drilled and plugged in 1977 (fig. 33).

This site has a weak magnetic anomaly (fig. 16) and anomalously high conductivity on the 56,000-Hz map (fig. 17). Conductivity is high on the 7,200- and 900-Hz maps, but no higher than that of adjacent areas (figs. 18, 19). A reconnaissance east-west conductivity profile (fig. 33) shows relatively low ground conductivity in both dipole orientations (fig. 34). There is no conductivity peak at the well, but ground conductivity in the horizontal dipole mode gradually increases from near 55 mS/m at the east end of line 34A to 75 mS/m at the west end of the line. This gradual westward increase is also indicated on the 7,200- and 900-Hz conductivity maps (figs. 18, 19).

Absence of high ground conductivities near the well suggests that it is not leaking. The gradual westward increase in ground conductivity coincides with a westward decrease in elevation, an observation that supports an interpretation of increasing conductivity related to a reduction in depth of saline ground water.

Site 43

Site 43 is located in the northwest part of the Hatchel area near a tributary to Coyote Creek. The airborne survey reveals a shallow conductivity anomaly (fig. 17) that coincides with a magnetic anomaly (fig. 16) near a known well. The conductivity anomaly does not appear on the 7,200- or 900-Hz maps (figs. 18, 19).

The site lies in rangeland that straddles alluvial deposits of the Coyote Creek tributary and Clear Fork Group strata (fig. 2). Soil is classified as moderately deep Portales clay loam (fig. 3). A reconnaissance conductivity profile (line 43A, fig. 35) was acquired across an elongate barren area. The landowner reports that this barren area occasionally flows saltwater that runs off into the tributary and that there is an abandoned well located near the barren area. Aerial photographs taken in 1940 show road access to the site and a disturbed area. A buried well was not located by RRC staff during a metal-detector survey of the barren area.

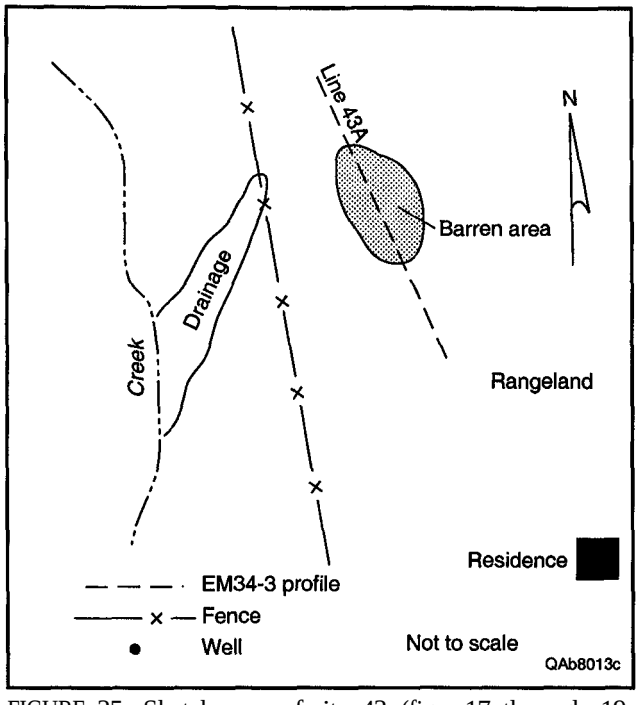

FIGURE 35. Sketch map of site 43 (figs. 17 through 19; app. A). Reconnaissance conductivity profile 43A crosses a barren area on rangeland.

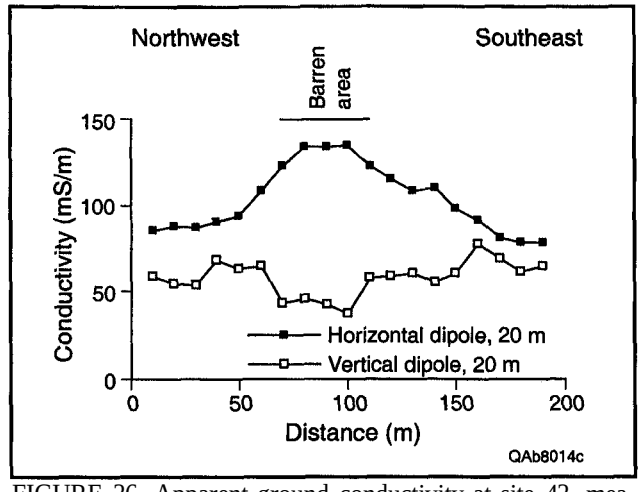

FIGURE 36. Apparent ground conductivity at site 43, measured using 20-m coil separation and horizontal and vertical dipole orientations. Line 43A crosses the barren area from northwest to southeast.

Line 43A shows a distinct horizontal dipole conductivity peak centered on the barren area (fig. 36). The peak, which is nearly 150 m wide, has conductivities as high as 135 mS/m. These values are significantly higher than background conductivities of 70 to 80 mS/m. Vertical dipole data show characteristic lowering of apparent conductivity beneath the barren area.

Two possible interpretations of the geophysical data at this site are that (1) an abandoned well at or near the barren area is leaking or has leaked brine into the shallow subsurface or (2) a natural saline spring periodically discharges. The broad conductivity peak on the ground-based data, the presence of a conductivity anomaly on the shallow airborne data, surface evidence of brine leakage, aerial photographic evidence of oil-field activity, and landowner reports of an abandoned well suggest that a potentially leaking well is at the site.

Site 51

Site 51 is south of Hatchel (fig. 17) on an alluvial terrace west of Coyote Creek. The active Cederholm B No. 2 well was drilled and completed on the terrace in 1994. Deep, clayey Rowena and Tobosa soils grade eastward into deep Spur loam on the floodplain west of Coyote Creek (fig. 3). Clear Fork Group strata underlie the thick alluvial and eolian deposits (fig. 2).

There is a magnetic anomaly at the well site (fig. 16). Conductivities at the site are high on the 56,000-, 7,200-, and 900-Hz maps (figs. 17 through 19) but are higher than at adjacent areas only on the 56,000-Hz map. Conductivities for the 900-Hz data are uniform at the site, whereas the 7,200-Hz map shows conductivity increasing eastward.

Reconnaissance profile 51A extends northeastward from higher to lower floodplain elevations (fig. 37). This profile crosses a barren area adjacent to the well that was disturbed during drilling and completion activities. Horizontal dipole ground conductivities are relatively high at this site but show no peak at either the barren area or the well (fig. 38). Conduc-

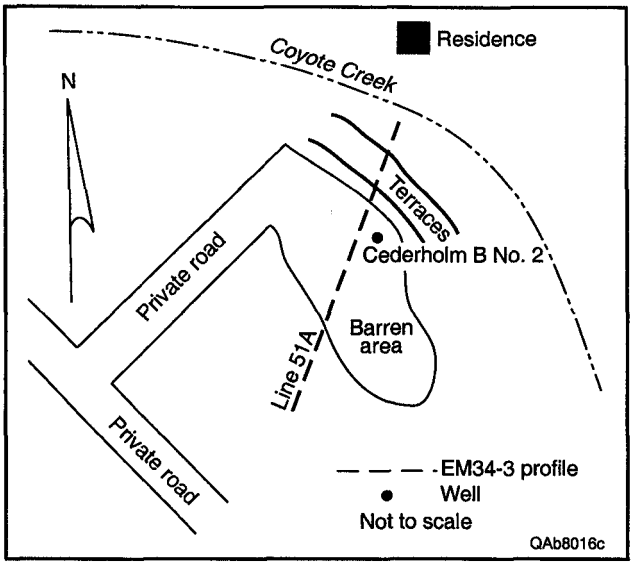

FIGURE 37. Sketch map of site 51 (figs. 17 through 19; app. A). Reconnaissance conductivity profile 51A crosses the Cederholm B No. 2 well and an adjacent barren area.

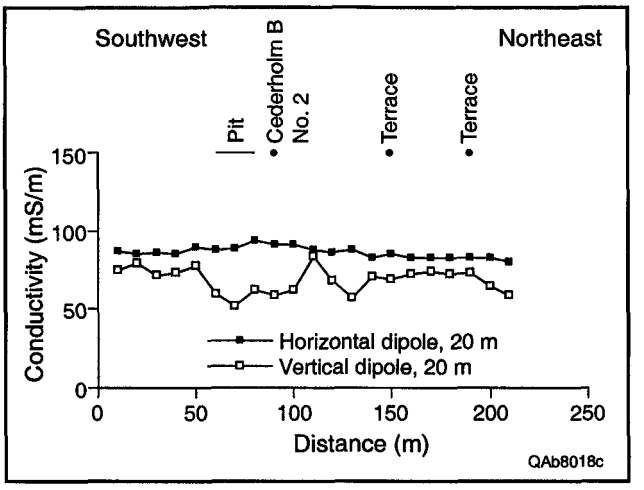

FIGURE 38. Apparent ground conductivity at site 51, measured using 20-m coil separation and horizontal and vertical dipole orientations. Line 51A crosses the well from southwest to northeast.

tivities decrease slightly from the upslope, southwest end of the line to the downslope, northeast end. This trend is similar to that observed in the 7,200-Hz data (fig. 18).

Ground-based geophysical measurements suggest that this well is not leaking. The slight and gradual decrease in conductivity along line 51A toward Coyote Creek is best explained as an effect of decreasing clay content from the thick Rowena and Tobosa clay and clay-loam soils at the southwest end of the line to the thick, loamy Spur soils lower on the Coyote Creek floodplain at the northeast end of the line.

Conductivity and Magnetic Anomalies

Type-CM sites are those where a conductivity anomaly (C) and a magnetic anomaly (M) coincide, but there is no mapped well. These sites are important because they might indicate unknown or mislocated oil or gas wells that are leaking brine. Ground-based geophysical methods were employed at 6 of the 15 CM sites identified to determine the cause of the airborne signatures. Two sites are discussed next in detail; the remaining sites are summarized in table 2 and appendix A.

Site 17

This site, located on the east side of the Hatchel area along a tributary of Mud Creek, is defined by a large conductivity anomaly on the 56,000-Hz map and a weak anomaly on the 7,200-Hz map (figs. 17, 18). The conductivity anomaly is elongate northwest-southeast and measures about 200 × 400 m. There is a coincident magnetic anomaly (fig. 16), but conductivity on the 900-Hz map is not anomalously high (fig. 19).

Aerial photographs and site visits reveal that the conductivity anomaly extends northwestward from a former brine-disposal pit northwest of the active Williams No. 1 well. Northwest of the pit (downslope toward the creek) is a barren area (figs. 39, 40). Soils are classified as the moderately deep Valera-Vernon silty clay, the shallow Kavett silty clay, or the moderately deep Tobosa clay (fig. 3).

FIGURE 39. Photograph of vegetation-kill area adjacent to abandoned brine-disposal pit, site 17.

These soils all overlie Clear Fork Group limestone (fig. 2).

Ground-based investigations consisted of two reconnaissance profiles, two multiple-coil-separation profiles, and three TDEM soundings (fig. 40). The reconnaissance profiles confirm the presence of a conductivity peak centered on the pit and adjacent barren zone. Horizontal dipole conductivities increase from background levels of 50 to 60 mS/m at distances of 100 m northwest of the pit to 150 mS/m. The total width of the conductive zone, greater than 140 m northwest-southeast, is about 200 m northeast-southwest.

Multiple-coil-separation profiles 17C (fig. 41a) and 17D (fig. 41b) show that, as coil separation (and, thus, exploration depth) increases, ground conductivity decreases for the horizontal dipole mode. Conductivity reaches a peak of 220 mS/m at the 10-m coil separation, 160 mS/m at the 20-m separation, and 110 mS/m at the 40-m separation. Peak conductivities on line 17D, which crosses the pit and the barren area from southeast to northwest, are offset to the northwest (downslope) of the pit. Ground conductivity away from the peaks on both lines shows little variation with increasing coil separation.

Decreasing ground conductivities accompany increasing coil separation, implying that conductivity decreases with depth near the pit. Three TDEM soundings support this observation. These soundings have transients that are generally similar (fig. 28), differing the most at early times (or shallow depths). Deeper than 10 to 20 m below the surface, resistivities are about 10 ohm-m. Nearer the surface, thin conductive layers overlie a more resistive layer. The conductive layers are thickest (7 m) and least resistive at

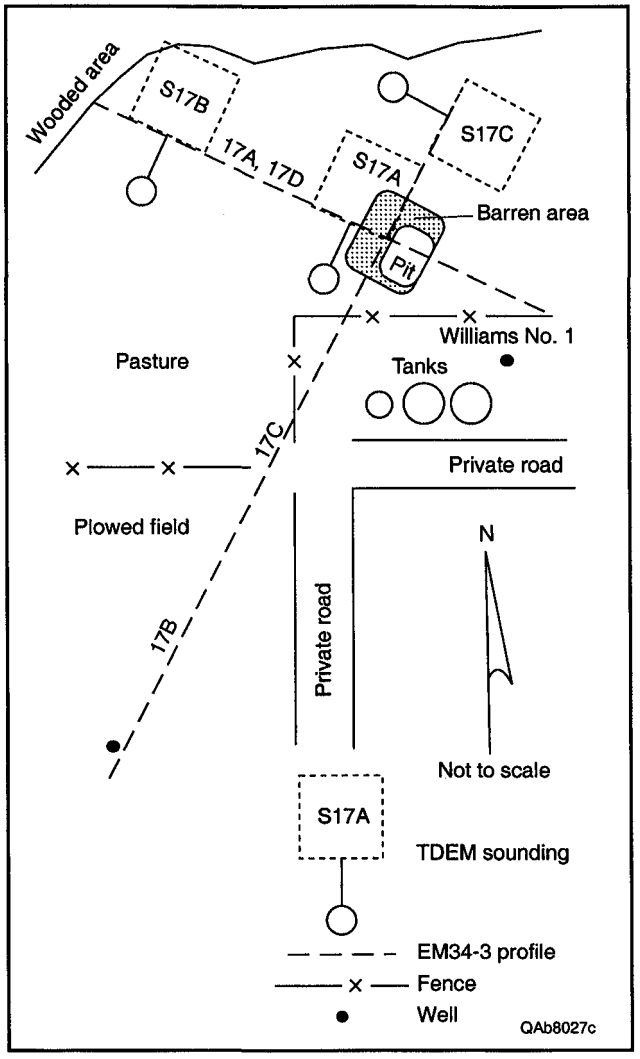

FIGURE 40. Sketch map of site 17 (figs. 17 through 19; app. A). Two reconnaissance conductivity profiles (17A and 17B), two multiple-coil-separation profiles (17C and 17D), and three TDEM soundings (S17A, S17B, and S17C) were acquired near the surface pit.

S17A (fig. 28a), which was acquired closest to the pit and barren area. Thicknesses of the surface conductive layer decrease to about 5 m, and resistivities increase at soundings S17B (fig. 28b) and S17C (fig. 28c), which are farther from the pit.

Airborne data, ground surveys, and visual observations support the interpretation that the shallow subsurface is salinized at site 17 and saltwater has migrated northwestward (downslope). Infiltration depths are probably 5 to 7 m. Decreasing conductivities with depth imply a surface source. The presence of a pit having an adjacent barren area that coincides with a ground-conductivity peak suggests that saltwater was discharged to the pit and subsequently infiltrated the shallow subsurface.

Site 71

Site 71 is located near an abandoned residence southeast of Hatchel. An anomaly is visible on the shallow (56,000-Hz) conductivity map (fig. 17) and the magnetic-field map (fig. 16). Maps of ground conductivity at deeper levels show slightly anomalous values at 7,200 Hz (fig. 18) and background values at 900 Hz (fig. 19). No wells are mapped nearby. Thin Mereta clay loam and thicker Portales clay loam cover the area (fig. 3), which is cultivated in places. These soils are formed on thin Quaternary deposits that cover Clear Fork Group strata.

Two reconnaissance conductivity profiles cross the site east-west (line 71A) and north-south (line 71C) (fig. 42). Line 71A shows low, background conductivities (<50 mS/m) on the grassland at the east end of the line, a horizontal dipole conductivity peak of about 125 mS/m in the middle of the cultivated field, and a return to background conductivity values westward (fig. 43a). Northward from the county road on line 71C (fig. 43b), horizontal dipole conductivities increase to a peak of 125 mS/m and decline northward to background values of 50 to 60 mS/m. Peak conductivity on both lines was found in a barren area. A metal-detector search by RRC staff at the barren area (fig. 9) failed to locate a well but did locate numerous scattered metallic objects.

On geophysical evidence alone, one might conclude that there is a buried well near the barren area. Aerial photographs show that oil-field tanks were installed at this site between 1940 and 1970 and have

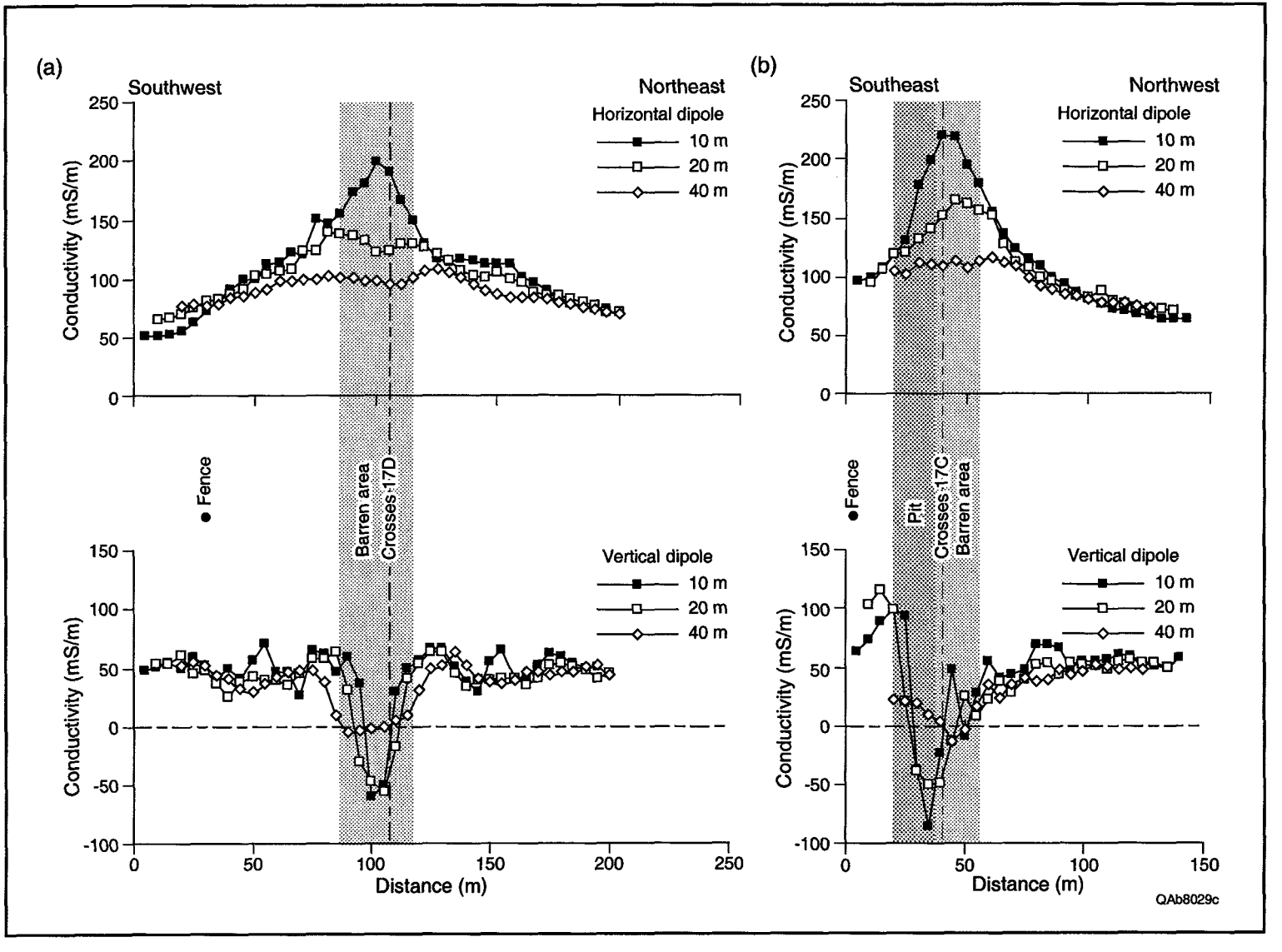

FIGURE 41. Apparent ground conductivity at site 17, measured using multiple coil separations (10, 20, and 40 m) and (upper plot) horizontal dipole and (lower plot) vertical dipole orientations. (a) Line 17C crosses barren area adjacent to pit from southwest to northeast. (b) Line 17D crosses pit and barren area from southeast to northwest.

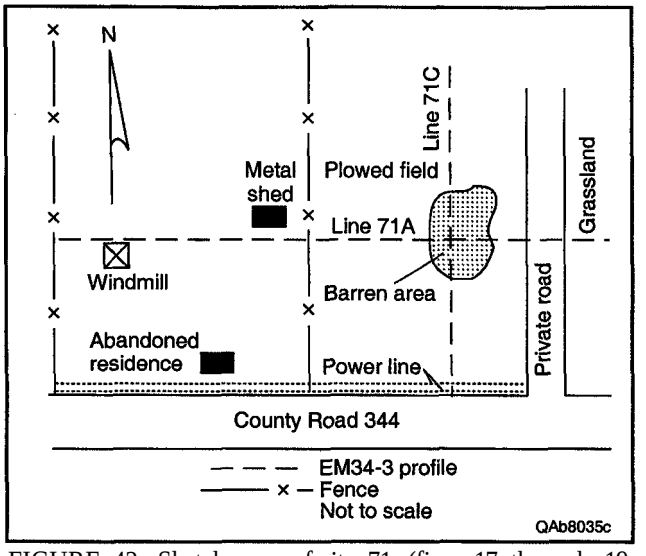

FIGURE 42. Sketch map of site 71 (figs. 17 through 19; app. A). Reconnaissance conductivity profiles 71A and 71C cross a barren area in a cultivated field near an abandoned residence.

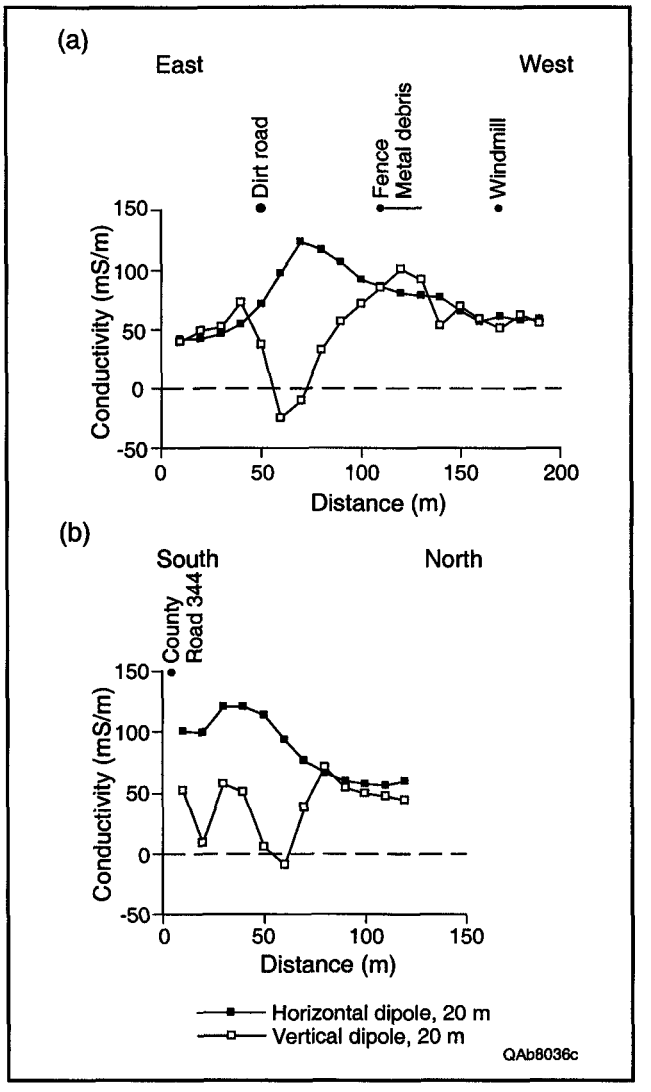

FIGURE 43. Apparent ground conductivity at site 71, measured using 20-m coil separation and horizontal and vertical dipole orientations. (a) Line 71A crosses an abandoned oil-field facility, residence, and windmill from east to west. (b) Line 71B crosses the abandoned oil-field facility from south to north.

been removed. No evidence of a well was found, either on aerial photographs or during site visits. Salinization at the site probably arose from spills or leakage from the tanks while they were operating.

Known Wells Having Conductivity Anomalies

Type-CW sites are those where a conductivity anomaly (C) and a known well (W) coincide, but there is no magnetic anomaly. These sites are important because the airborne signature combined with the knowledge that there is a well at the site could be interpreted as presence of an uncased well that might leak. Ground-based conductivity profiles were acquired at 7 of the 12 CW sites identified to determine the cause of the airborne signatures. Three of these sites are discussed next.

Site 12

Located in the northeast part of the Hatchel area, site 12 has two known wells with no associated magnetic anomaly (fig. 16) and high conductivity anomalies on the 56,000- and 7,200-Hz airborne maps (figs. 17, 18). No 900-Hz anomaly is apparent (fig. 19). Soils are classified as Portales clay loam and Potter clay loam (fig. 3), consisting of thin clay loam overlying pedogenic carbonate. The soils have formed on Permian Clear Fork Group rocks (fig. 2).

Two reconnaissance geophysical profiles were acquired at site 12 (fig. 44). Line 12A extends east-west across the

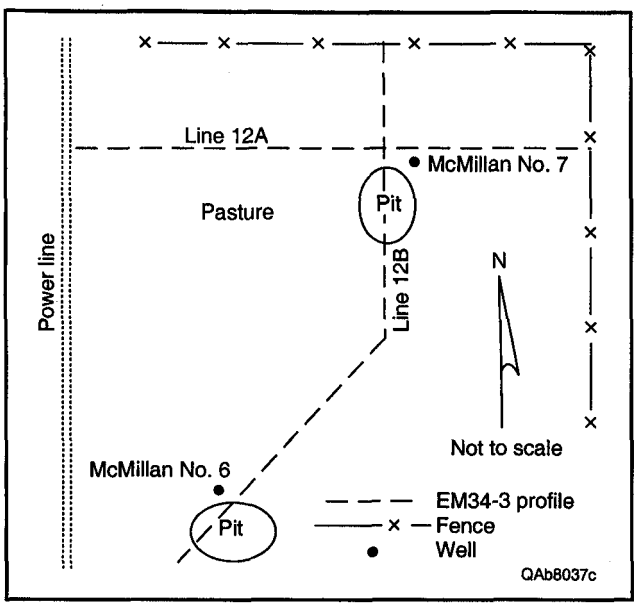

FIGURE 44. Sketch map of site 12 (figs. 17 through 19; app. A). Two reconnaissance conductivity profiles (12A and 12B) cross the abandoned McMillan No. 6 and No. 7 wells and adjacent surface pits.

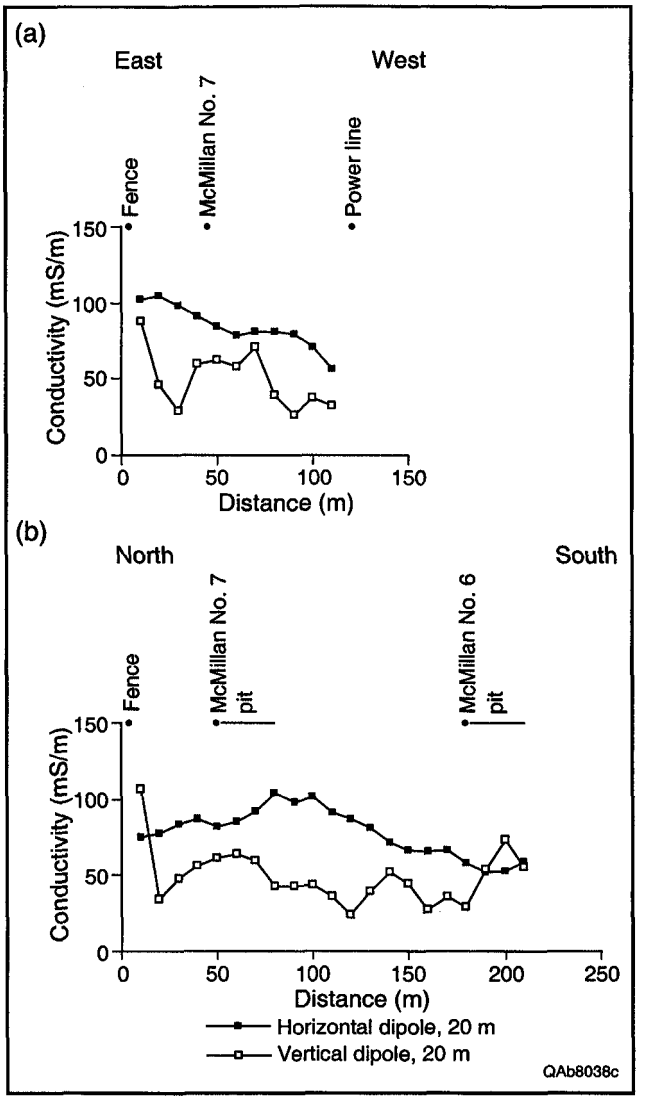

FIGURE 45. Apparent ground conductivity at site 12, measured using 20-m coil separation and horizontal and vertical dipole orientations. (a) line 12A crosses abandoned McMillan No. 7 well from east to west. (b) Line 12B crosses McMillan No. 7 and No. 6 wells from north to south.

abandoned McMillan No. 7 well. Line 12B extends north-south across the No. 7 well and an adjacent brine-disposal pit, then turns southwestward to cross the abandoned McMillan No. 6 well and its disposal pit. RRC records indicate that the No. 6 well was drilled in 1934 and plugged in 1942 and that the No. 7 well was drilled in 1935.

No conductivity peaks were found centered on either of the two wells at site 12 (fig. 45). For the horizontal dipole data at 20-m coil separation, the highest conductivities were just above 100 mS/m in two areas: 30 m east of well No. 7 on line 12A (fig. 45a) and 35 to 45 m south of the No. 7 well on line 12B (fig. 45b). The broad conductive zone south of well No. 7 extends 90 m downslope (south) of the well. Highest conductivities in this zone are adjacent to the No. 7 well pit. Horizontal dipole ground conductivities near the McMillan No. 6 well are relatively low (50 to 60 mS/m) both near the well and across the adjacent pit (fig. 45b).

Neither well has surface evidence of leakage. Well No. 6, which RRC records show to have been plugged, has no ground-based geophysical evidence of leakage and is probably not leaking. Elevated conductivities near well No. 7, which are visible in both airborne and ground-based geophysical data, suggest that the ground is salinized near this well. The presence of a conductivity peak adjacent to the pit rather than at the well implies that salt-

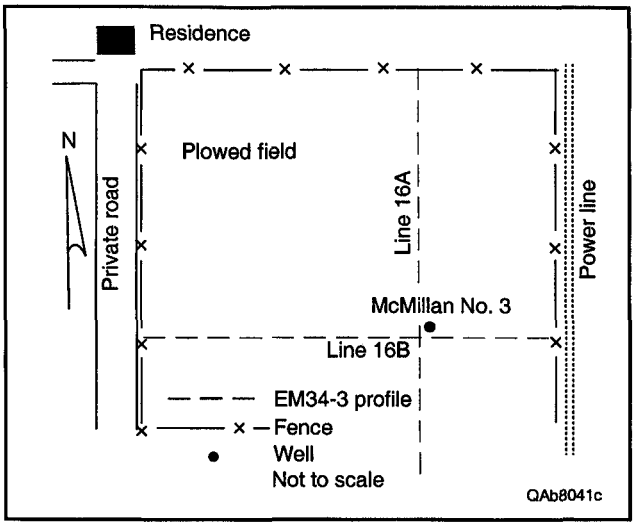

FIGURE 46. Sketch map of site 16 (figs. 17 through 19; app. A). Reconnaissance conductivity profiles 16A and 16B pass near the abandoned McMillan No. 3 well in a cultivated field south of Mud Creek.

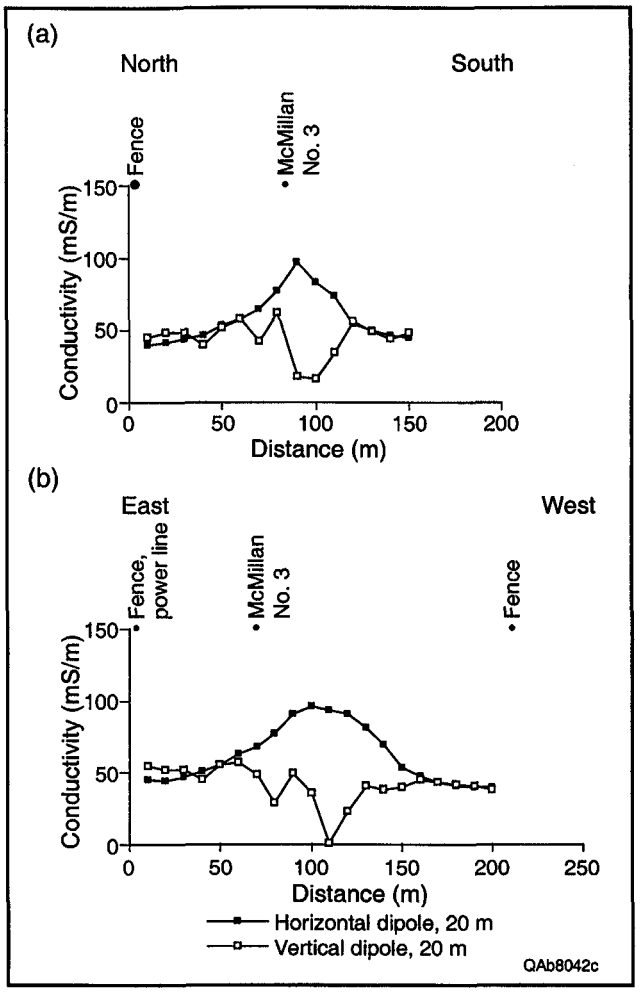

FIGURE 47. Apparent ground conductivity at site 16, measured using 20-m coil separation and horizontal and vertical dipole orientations. Lines (a) 16A and (b) 16B cross the abandoned McMillan No. 3 well.

water discharged into the pit is the likely source of elevated conductivities.

Site 16

Site 16 contains an abandoned well in a cultivated field south of Mud Creek. The site is associated with a shallow anomaly on the 56,000-Hz map (fig. 17) that weakens on the 7,200-Hz map (fig. 18) and is absent on the 900-Hz map (fig. 19). There is no magnetic anomaly. Ground investigations revealed the presence of concrete blocks and well debris associated with the McMillan No. 3 well, which was drilled in 1928 and abandoned in 1930. Deep Olton clay-loam soil covers the site and overlies Clear Fork Group strata.

Two conductivity profiles pass near the abandoned well (fig. 46). A horizontal dipole conductivity peak more than 100 m wide is present on north-south line 16A (fig. 47a). The peak, which reaches conductivities of 100 mS/m, is centered within a few meters of well No. 3. The east-west line 16B reveals a slightly broader peak of similar magnitude, but the highest values are centered 20 to 50 m west (downslope) of the well (fig. 47b). Background conductivities of 40 to 50 mS/m are reached within 160 m west of the well.

The airborne conductivity and magnetic signature suggest an uncased well that might be leaking. Well casing was detected during the ground surveys despite the lack of a magnetic anomaly in the airborne survey. Saltwater is in the shallow surface near the well that was detected by both the airborne and ground-based instruments. Conductivity profiles suggest that either (1) the well is leaking saltwater that is migrating to the west

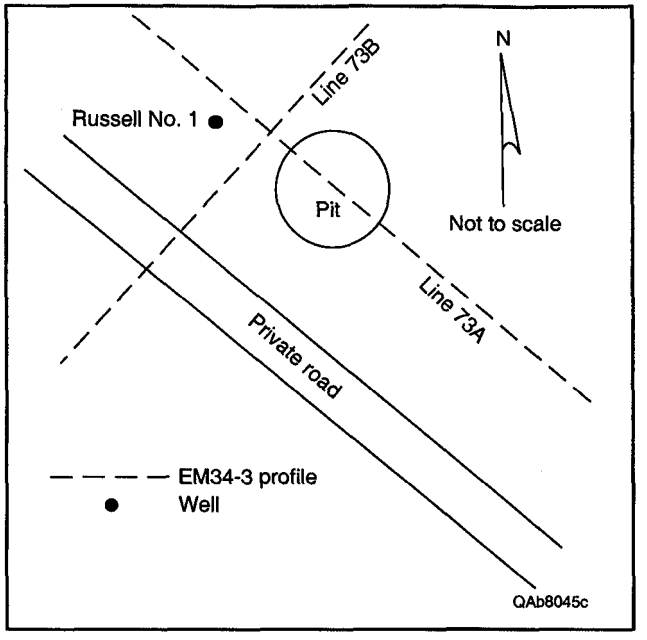

FIGURE 48. Sketch map of site 73 (figs. 17 through 19; app. A). Reconnaissance conductivity profiles 73A and 73B pass near the abandoned Russell No. 1 well and an adjacent pit.

(downslope) or (2) the pit was located west of the well and brine that was discharged into it has infiltrated the subsurface. RRC reentered and plugged this well in 1997 after the airborne and ground-based investigations. Saltwater flow was encountered during reentry.

Site 73

This site surrounds the Russell No. 1 well, which was drilled and abandoned in 1928. The site, located west of Flag Creek in the southwest corner of the Hatchel area, has thin Potter clay-loam soil over Clear Fork Group strata. Conductivities are high and slightly anomalous on the 56,000-Hz airborne map (fig. 17). The deeper maps neither indicate anomalously high conductivities (figs. 18, 19) nor evidence a magnetic anomaly (fig. 16). A metal-detector survey by RRC staff located the well.

Two conductivity profiles were acquired across the site (fig. 48). Line 73A reveals a conductivity peak in the horizontal dipole mode that is 110 m wide (fig. 49a). Conductivities increase from background values of 50 mS/m to nearly 100 mS/m. The peak is centered at a pit 10 to 20 m southeast (downslope) of the well. Line 73B, which passes between the well and the pit (fig. 48), measured conductivities as high as 80 mS/m near the well and pit (fig. 49b).

The location of peak conductivities at the pit rather than the well and the absence of anomalous conductivity on the

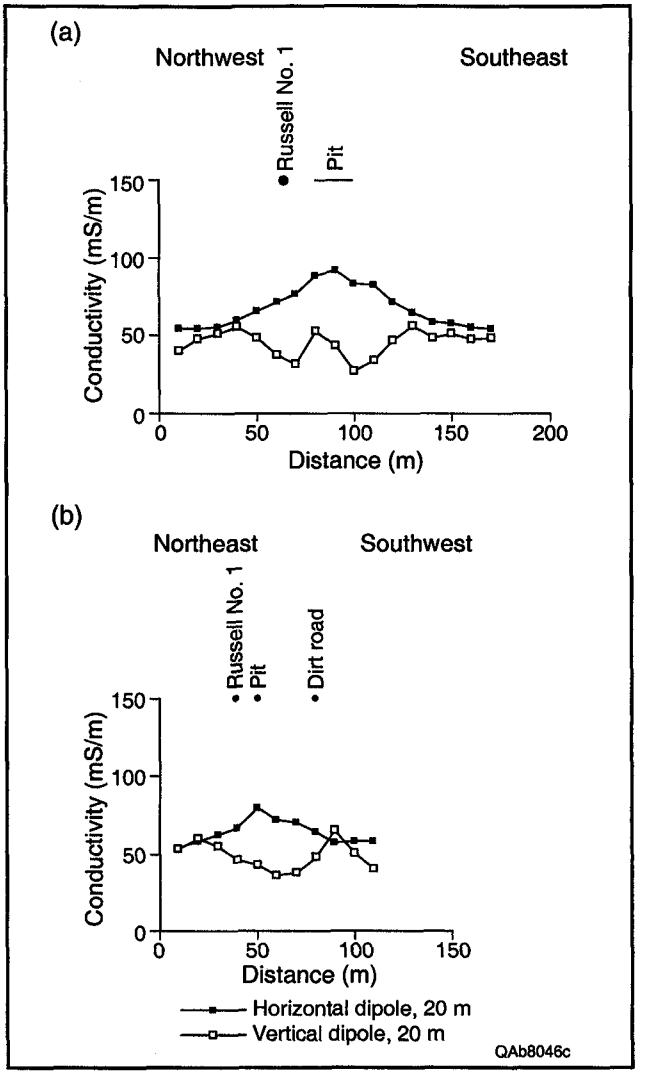

FIGURE 49. Apparent ground conductivity at site 73, measured using 20-m coil separation and horizontal and vertical dipole orientations. (a) Line 73A crosses the abandoned Russell No. 1 well and pit from northwest to southeast. (b) Line 73B crosses the well and pit from northeast to southwest.

FIGURE 50. Photograph of abandoned Early A No. 2 well leaking saltwater at site 67.

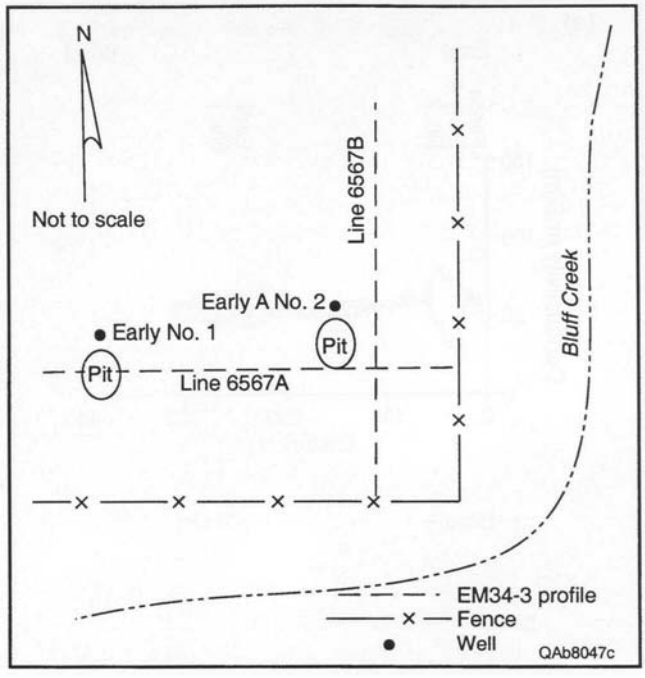

FIGURE 51. Sketch map of sites 65 and 67 (figs. 17 through 19; app. A). Reconnaissance conductivity profiles 6567A and 6567B pass near the leaking Early No. 1 and Early A No. 2 wells in a cultivated field upslope of Bluff Creek.

7,200- and 900-Hz maps support an interpretation that this well is not leaking. Despite the passage of more than 70 yr since abandonment in 1928, the salinization appears to be related to saltwater discharge into the pit during drilling or operation.

Other Local Anomalies

In the course of field investigation, a few other site types were examined. For example, there are numerous type-C sites where conductivity anomalies (C) visible on the airborne maps do not coincide with magnetic anomalies (M) or well locations (W). There are also many type-MW sites, where magnetic anomalies associated with known wells have no coincident conductivity anomaly. Most of the wells in the study area are in this category, suggesting no evidence of extensive salinization at these wells.

Sites 65 and 67

These are adjacent type-MW sites in the northeast part of the Hatchel area (fig. 17). Site 65 consists of a magnetic anomaly associated with the Early No. 1 well, a recently abandoned oil well that was drilled in 1982. Site 67 is a separate magnetic anomaly encircling the Early A No. 2 well, another recently abandoned oil well also drilled in 1982. Both wells recently began leaking brine at the surface (fig. 50) and were plugged in 1996 during this study. These wells are in a cultivated field on deep Miles sandy-loam soil just upslope from Bluff Creek (fig. 51). The soil grades downward into Clear Fork Group strata and Quaternary alluvium.

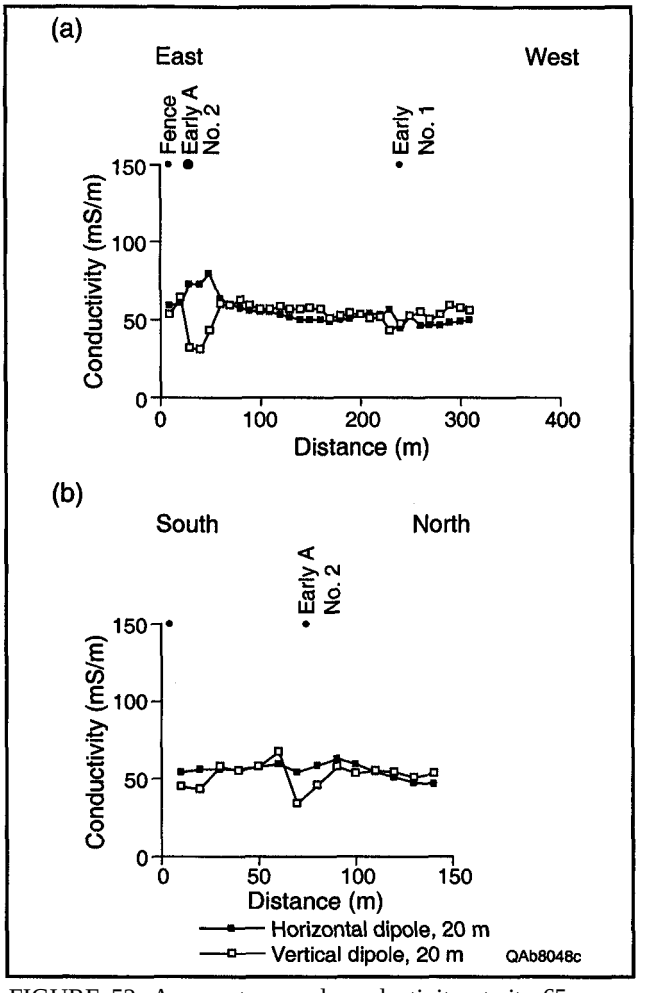

FIGURE 52. Apparent ground conductivity at site 65, measured using 20-m coil separation and horizontal and vertical dipole orientations. (a) Line 6567A crosses the abandoned and leaking wells from east to west. (b) Line 6567B crosses Early A No. 2 from south to north.

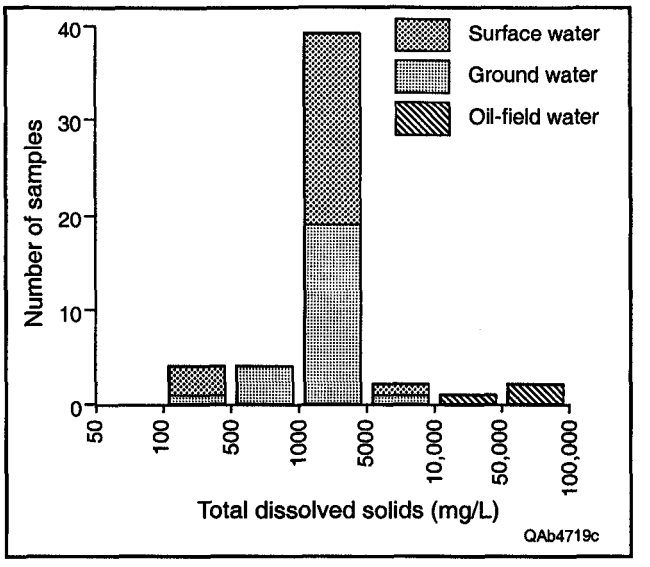

FIGURE 53. Histogram of TDS in ground-, surface-, and oil-field-water samples in the Hatchel area (app. B). Mean values of surface and ground waters are similar.

The airborne survey shows no conductivity anomaly at either site. On the 56,000-Hz map, conductivities are generally low and decrease eastward toward the creek (fig. 17). On the deeper, 7,200- and 900-Hz maps, conductivities are high and they increase toward the creek, although they show no anomalies at the wells (figs. 18, 19).

Ground-based measurements verify the absence of significant conductivity anomalies. Line 6567A, which passes near both wells (fig. 51), shows a gradual increase in conductivity (horizontal dipole mode) eastward and a modest increase in conductivity near the Early A No. 2 well (fig. 52a). There is no evidence of any increase in conductivity near the No. 1 well. The modest peak near the No. 2 well is about 50 m across and reaches peak values of 80 mS/m. Line 6567B, passing near the No. 2 well along a north-south line, shows only a small ground-conductivity increase near the well (fig. 52b).

These wells were leaking, but airborne and ground-based geophysical data show that little salinization occurred before the wells were plugged. Leakage began recently and has occurred at low rates through the top of the surface casing.

Chemical Composition of Water Samples

Water Salinity

Total dissolved solids (TDS) in ground-water samples (app. B) range from 480 to 7,620 mg/L (fig. 53). TDS, or salinity, of water generally follows a logarithmically normal distribution. The best

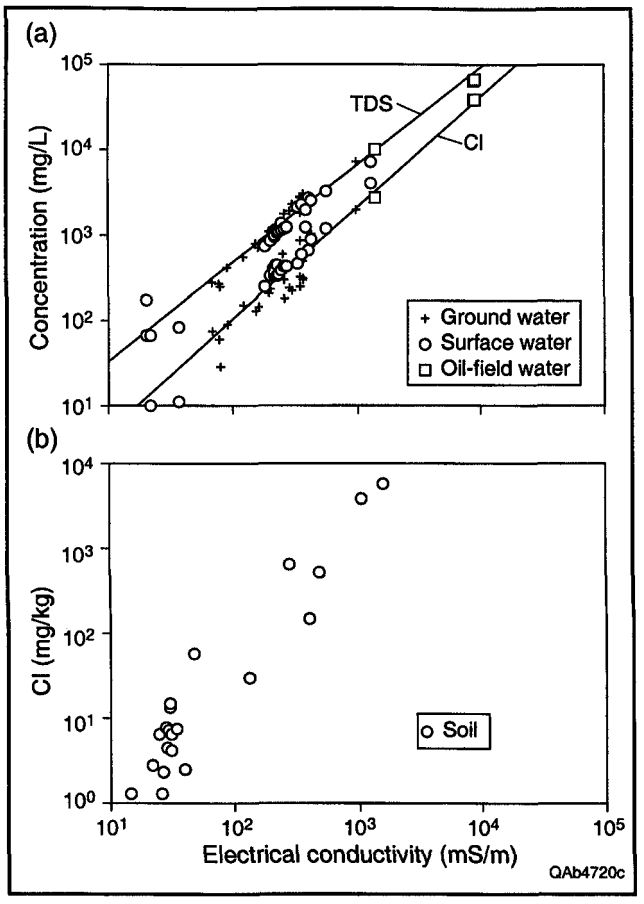

FIGURE 54. Relation between electrical conductivity and (a) TDS and Cl content of water samples and (b) Cl content of soil samples having linear least-squares regression lines (apps. B, C). Electrical conductivity is a good predictor of Cl and TDS.

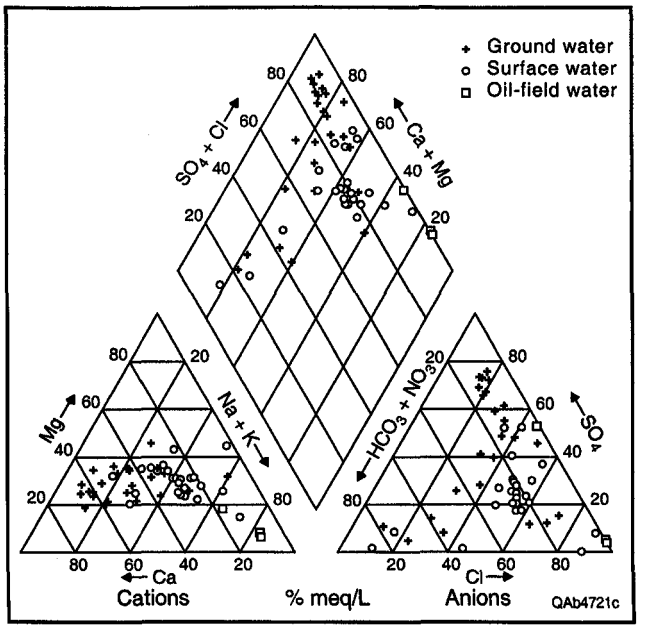

FIGURE 55. Chemical composition of hydrochemical facies in ground-, surface-, and oil-field-water samples in the Hatchel area (app. B).

estimate of average TDS, 1,746 mg/L, is based on the logarithm of TDS values. TDS does not significantly differ with well depth. Surface-water samples have nearly the same range and mean in TDS (fig. 53; app. B).

The three oil-field samples have markedly higher salinity (app. B) than surface on ground water. TDS of the two samples from abandoned oil wells (sample sites 27 and 28, fig. 15) was about 66,000 mg/L. Water collected from the seeping core hole on Elm Creek (sample site 26, fig. 15) had a TDS of more than 10,200 mg/L.

TDS of water samples (fig. 54a) and chloride content of soil (fig. 54b; app. C) correlate with electrical conductivity measured on the samples.

Chemical Composition

Ground water and surface water in the Hatchel area have similar chemical compositions that include calcium-bicarbonate, calcium-sulfate, mixed-cation—mixed-anion, and sodium-chloride hydrochemical facies (Back, 1966) (fig. 55). In this area, we can assume that the calcium-bicarbonate hydrochemical facies is derived from the reaction of ground water flowing through limestone and that the calcium-sulfate type results from ground water encountering gypsum. The Permian formations are dominated by limestone, gypsum, and shale. A change from calcium- to sodium-dominated cations can take place along a flow path because of ion exchange or because of mixing with sodium-chloride water. The water samples in which no single cation or anion dominates most likely reflect mixtures of water of different

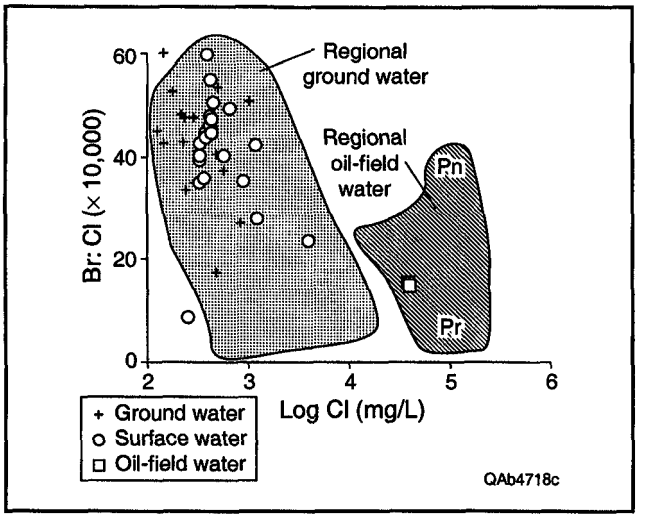

FIGURE 56. Relationship between Br:Cl ratio and Cl concentration in water samples collected during this study (pluses, circles, and squares), compared with regional data presented by Richter and others (1990). Ground- and surface-water samples collected in the Hatchel area resemble ground water elsewhere in the region. The oil-field water sampled in this study resembles the Permian (Pr) more closely than it does the Pennsylvanian (Pn) end member of oil-field brine defined by Richter and others (1990).

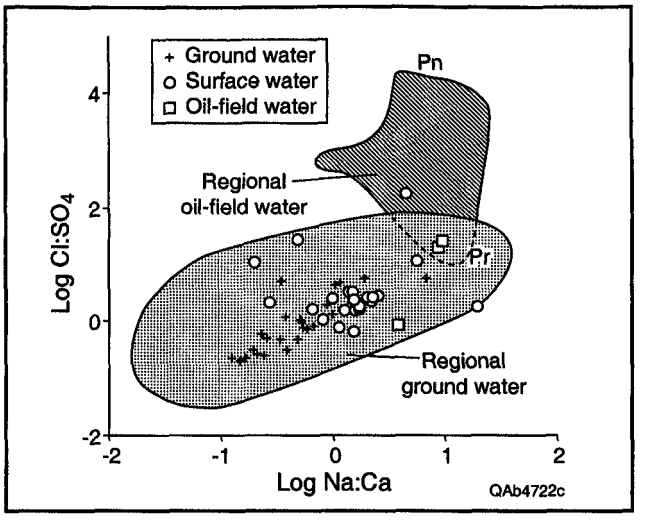

FIGURE 57. Relationship between $Cl:SO_4$ ratios and Na:Ca ratios in water samples collected during this study (pluses, circles, and squares), compared with regional data presented by Richter and others (1990). Ground- and surface-water samples collected in the Hatchel area are similar to ground water elsewhere in the region. The oil-field water sampled in this study resembles the Permian (Pr) more closely than it does the Pennsylvanian (Pn) end member of oil-field brine defined by Richter and others (1990). Some surface-water samples have a high Na and Cl content similar to that of the Permian brine end member.

hydrochemical facies, movement of water from one lithology to another, or samples taken at intermediate positions along a flow path.

Samples from the two abandoned oil wells (samples 27, 28; fig. 15; app. B) have a sodium-chloride hydrochemical facies typical of oil-field waters. The diluted water from the unplugged core hole has higher proportions of calcium and sulfate (fig. 55).

Comparison with Regional Trends

Dutton and others (1989) and Richter and others (1990) studied salinity sources affecting ground-water quality in and near the Hatchel area. The ground- and surface-water samples collected for this study do not differ from ground water described in the earlier regional study. For example, the ratio of bromide:chloride (Br:Cl) of the new samples overlaps that of the older ground- and surface-water samples (fig. 56). The new samples also overlap the regional samples on a cross plot of the chloride:sulfate ($Cl:SO_4$) ratio and the sodium:calcium (Na:Ca) ratio (fig. 57). Dutton and others (1989) and Richter and others (1990) identified these graphical techniques as particularly effective in distinguishing among different sources of water. Note that the surface and ground water lie along a well-defined trend on the $Cl:SO_4$ versus Na:Ca graph (fig. 57). The trend "points" toward the Permian formation end member of oil-field water defined by Dutton and others (1989) and Richter and others (1990). The new oil-field samples plot at that Permian formation end member (figs. 56, 57).

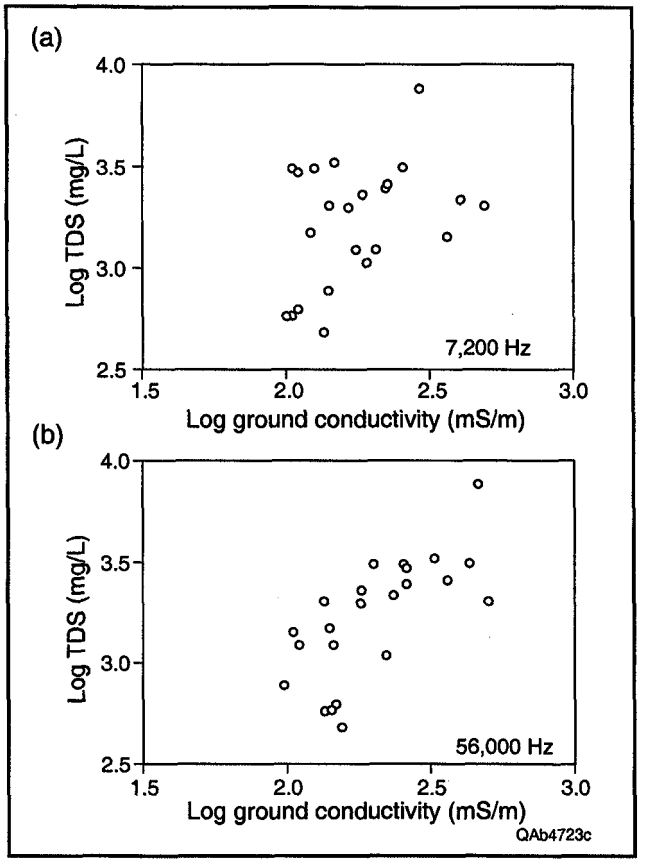

FIGURE 58. Comparison of TDS of ground-water samples and ground conductivity measured by (a) 7,200- and (b) 56,000-Hz surveys.

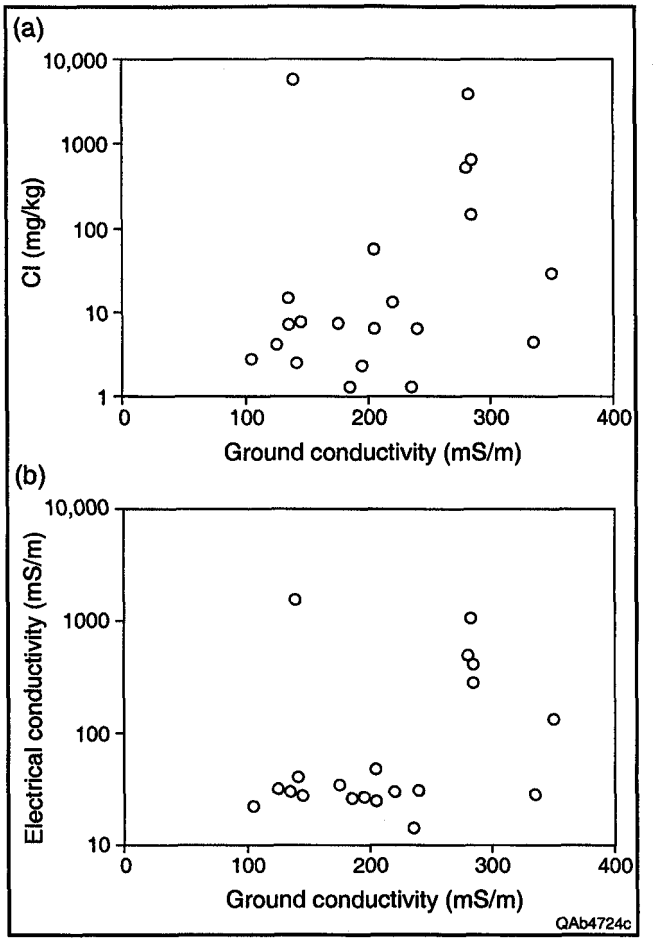

FIGURE 59. Comparison of measurement of ground conductivity by airborne geophysical survey (56,000 Hz) and measurement of (a) Cl content and (b) electrical conductivity of soil samples.

Comparison of Soil and Water Salinity with Measured Conductivity

Although the sample size is small, ground conductivity measured by the 56,000- and 7,200-Hz airborne coils generally increases with increasing ground-water TDS (fig. 58; app. B). The 56,000-Hz ground-conductivity survey does not correspond well to chloride content or electrical conductivity measured in soil samples (fig. 59; app. C). There are several reasons for this poor correlation, including the difficulty in preparing soil samples for electrical conductivity measurements, the difference between the electrical conductivity of a large soil volume sensed by the airborne coils and a very small volume of soil measured in the laboratory, and the effect of in situ soil moisture on measured conductivity (Paine and others, 1998b).

DISCUSSION

High-resolution airborne geophysical measurements, when combined with detailed ground-based geophysical surveys, water soil sampling and chemical analyses, information on soil type, and rock type and oil- and gas-well distribution, provide an excellent opportunity for understanding ground-conductivity changes and their causes. Specifically these data from the Hatchel area allow us to distinguish oil-field and non-oil-field causes of salinization, assess the merits of ground-based and airborne geophysical methods in the study of salinization, determine the usefulness of the method in discriminating among causes of oil-field salinization, and develop a geophysical profile of a potentially leaking well.

Effectiveness of Airborne Geophysics

As the ground surveys at anomalies detected by the airborne survey show, the effectiveness of the airborne geophysical method depends on the objective. If the goal is to identify areas of salinization, then the airborne method is obviously successful. It measures ground conductivity accurately, locates anomalies with adequate precision, determines the lateral extent and intensity of salinization, and illustrates lateral and vertical conductivity changes adequately to determine whether salinization is likely due to natural or oil-field causes. If the goal is to locate oil and gas wells with an airborne magnetometer, this study demonstrates that wells can be detected this way, but that some magnetic anomalies are small enough to be missed if the line spacing is too coarse. If the goal is to distinguish leaking wells from other oil-field-salinity sources, then the results are mixed. The airborne method increases the likelihood of locating leaking wells, but it cannot distinguish leaking wells from brine pits in all cases and cannot distinguish leaking wells from those that were once leaking and subsequently were plugged.

An understanding of the airborne conductivity data, combined with a knowledge of oil-field history, qualitative plume-migration rates, and land use, allows us to distinguish conductivity anomalies related to agricultural practices, soil and rock types, and soil moisture from those that are oil-field related. We can infer that most oil-field salinization will be manifested as point sources showing limited lateral migration (typically tens to hundreds of meters). Conversely, long, curvilinear conductivity anomalies that follow topography are likely to be related to agricultural practices, natural hillside seeps, or water-saturated alluvium near flowing creeks. Large conductivity anomalies covering several square kilometers are most likely related to changes in soil or rock type. The airborne method is quite successful in identifying these broad source types.

Ground investigations are required to help researchers using the airborne method to distinguish among common oil-field-salinity sources. Airborne signatures of leaking tank batteries, brine-disposal pits, and leaking wells are similar, requiring follow-up work to verify the likely source type. In the Hatchel area, where more than 700 known wells have been drilled, 107 conductivity anomalies were identified in the airborne data that are consistent with oil-field salinization. Ground-based surveys suggest that most are indeed sites with oil-field-related salinization (42 of the 54 conductivity anomalies visited), but fewer are attributable to po-

tentially leaking wells (22 of 54 anomalies visited).

Most (99) of the conductivity anomalies were identified on the 56,000-Hz conductivity map, which is the map that shows the shallowest exploration depth (fig. 17; table 2). Many of these anomalies appear to be related to surface sources such as brine pits or tank batteries. As exploration depth increases, fewer sites have anomalous conductivities. Only 56 of the 107 sites show anomalous conductivities on the 7,200-Hz map, only 48 show anomalous conductivities on both the 7,200- and 56,000-Hz maps, and only 13 show anomalous conductivities at all three frequencies (table 2). Ground surveys indicate that anomalies visible on both the 56,000- and 7,200-Hz maps were more likely to be potentially leaking wells than anomalies visible only on the 56,000-Hz map.

Geophysical Profile of a Leaking Well

Ground investigation of airborne geophysical signatures allows development of a profile of a well that may be leaking saltwater. Sites that have a suspicious airborne signature are those that (1) have either a magnetic anomaly or a known well location and (2) have anomalously high ground conductivity on both the shallow-exploring 56,000-Hz airborne coils and the deep-exploring 7,200-Hz coils (table 2; app. A). The suspicious site might have a conductivity high on maps produced from the deeply penetrating 900-Hz coils.

In the Hatchel area, 39 of the 107 sites fit the airborne profile of a potentially leaking well (table 2). Ground surveys at 34 of these sites show that at least 29 of them have significant oil-field salinization and that 20 might be actively or formerly leaking wells. The 20 profile-matching, potentially leaking wells are CMW (16), CM (1), or CW (3) sites. Of the four surveyed sites having conductivity and magnetic anomalies but no known well (a potentially leaking unknown well), one was a potentially leaking well, one was a feedlot, one was metal debris at a seep, and one was a tank or pit.

Ground investigations reduce the number of anomalous sites to a list of wells that might be leaking or might have had significant leaks in the past. These investigations should include precise location of the well and reconnaissance ground-conductivity profiles that cross the well site and any other potential saltwater sources, such as pits or tank batteries. If a well has been leaking brine into the shallow subsurface, measured ground conductivities should increase by a factor of two or three from background levels to maximum levels recorded within a few meters of the well. Wells that have begun to leak recently may show only a small anomaly at the shallowest investigation depths; conversely, wells that have been leaking longer will have the highest conductivity peaks and the broadest areas of influence. Further information on the lateral extent and depth of salinization can be obtained by using more sophisticated geophysical surveys, such as those employing multiple coil separations and TDEM soundings.

Utility of Airborne and Ground-Based Geophysics

Airborne geophysics measured magnetic-field strength and ground conductivity that allowed us to focus our ground investigations. The airborne magnetometer located many, but not all, wells in the study area; it also located some wells that were absent from, or mislocated

on, RRC maps. The magnetic data serve best as a reconnaissance tool in areas where well locations are unknown or inaccurate. Typical measured magnetic anomaly widths of 80 to 200 m suggest that, as flight-line spacing lengthens beyond the 100 m used in this study, progressively more well-related magnetic anomalies will be missed. The 100-m spacing was a compromise between survey cost, which is roughly proportional to line length flown, and the percentage of wells detected. Closer flight lines are required to detect all wells that have casings. Wells having no casings cannot be detected by using airborne or ground-based magnetometers.

Airborne EM instruments mapped the lateral and vertical conductivity distribution to depths of a few tens of meters. The conductivity data acquired at multiple frequencies allowed us to discriminate between near-surface causes of elevated conductivity, such as brine-disposal pits, and deeper causes, such as brine-bearing geologic formations. Used alone, each coil frequency had limitations. Data collected by the 56,000-Hz airborne coils showed the most detail, but some of the anomalies had non-oil-field causes. Conversely, the deep data collected by the 900-Hz coils showed conductivity changes that are probably related to the subsurface distribution of geologic units. Distinct anomalies were not, however, always visible near wells that ground surveys suggest are leaking (table 2; app. A). The single most useful coil frequency was 7,200 Hz, which was insensitive to most shallow conductivity anomalies related to soils, soil moisture, brine pits, and surface-water bodies, as well as deeper natural patterns.

When data from each of the coil frequencies are combined, they provide a powerful method of visualizing lateral and vertical conductivity changes. Patterns evident at individual frequencies allow us to distinguish source types and map salinization extent and intensity, whereas differing exploration depths among the frequencies allow us to distinguish surface salinity sources from subsurface ones. By combining lateral and vertical conductivity information, we can estimate chloride mass within saltwater plumes (Paine and others, 1998a).

Ground-based geophysical surveys complement the airborne data, forming a critical component in the understanding of ground-conductivity changes in general and in the search for potentially leaking wells in particular. Metal-detector searches of suspected well sites that were chosen from the airborne geophysical signature allowed precise location of abandoned wells. Reconnaissance conductivity profiles across these well sites allowed us to determine whether the conductivity anomaly was likely to be related to saltwater from a leaking well or to saltwater that entered the subsurface through a nearby pit or surface spill. Multiple-coil-separation surveys and TDEM soundings enabled us to delineate the lateral and vertical extent of salinization. The TDEM soundings also extended the maximum exploration depth of the airborne survey, located a subsurface saltwater-bearing unit, and helped us better understand conductivity patterns visible on the deeper, 900-Hz conductivity maps.

Without the ground-based geophysical surveys, it is possible to determine salinization extent and intensity and distinguish oil-field from natural salinization, but it is difficult to distinguish among the various oil-field sources. Without the airborne data, ground-based surveys can help determine whether known wells might be leaking and may be used as a relatively inexpensive method of testing whether a well is leaking saltwater into

the shallow subsurface. With ground-based geophysics alone, however, unknown wells and unsuspected salinization area would most likely be missed and site-specific conductivity, soil, and water data would lack a broader context.

No matter how successful the airborne method is judged to be, its application is hindered by cost. Mobilization costs preclude its use in small areas of a few tens of square kilometers or less, where ground-based methods are more appropriate. Furthermore, short flight-line spacings required to locate small conductivity and magnetic anomalies make the method uneconomical in excessively large areas. A realistic upper limit might be a typical oil-field size of a few tens to a few hundreds of square kilometers. Areas larger than a given oil field would involve surveying non-oil-field land for oil-field salinization. In addition to survey cost, the airborne data commonly require follow-up, ground-based investigations to distinguish likely leaking wells from other oil-field sources.

In summary, ground-based surveying of known wells is a relatively inexpensive means of determining wells that should be plugged in small areas (a few tens of square kilometers or less). Over large areas (oil-field size) where well locations are uncertain or the extent of salinization is unknown, an airborne survey should be considered because it identifies salinized ground, determines the lateral and vertical extent and intensity of salinization, distinguishes natural from oil-field salinity sources, and focuses ground investigations.

CONCLUSIONS

Analysis of airborne and ground-based geophysical data and soil- and water-quality data in the Hatchel area of West Texas shows that

- airborne methods accurately portray location, size, and magnitude of conductivity and magnetic-field anomalies;
- airborne instruments can generally be used to distinguish oil-field from natural and agricultural sources of salinization, particularly if well locations are known;
- salinization causes include upward migration of brine along natural pathways, seepage of saltwater into the subsurface at brine-disposal pits, brine discharge at abandoned wells and coreholes that are either unplugged or not plugged in compliance with present standards, and evaporative concentration of chloride in shallow ground water;
- airborne geophysical data alone can be used to identify wells that have evidence of salinization, but ground investigations are required to reliably distinguish surface spills and pit discharge from wells that are potentially leaking saltwater;
- persistence of salinization in arid, near-surface environments makes formerly leaking wells geophysically indistinguishable from leaking wells;
- airborne instruments are best used in relatively large areas where it is likely that there are multiple unknown sources and it is impor-

tant to determine salinization extent and intensity, source areas, or volume of infiltrated saline water;

- ground-based instruments are best used in surveying small areas having few sources, determining whether specific known wells might be leaking, and verifying airborne geophysical data;
- chemical analyses of soil and water can help differentiate between natural, agricultural, and oil-field causes of salinization; and
- ground-water salinity correlates better than soil salinity with measured ground conductivity.

ACKNOWLEDGMENTS

This project was funded by the Railroad Commission of Texas (RRC) under Contracts IAC 94-0443 and IAC 96-0034, Jeffrey G. Paine, Principal Investigator. The Lower Colorado River Authority (LCRA) contributed financially to the project. Interpretations and conclusions presented in this report are not necessarily those of the RRC, LCRA, or the Colorado River Municipal Water District (CRMWD).

Airborne geophysical data were acquired and processed by David Miles, Megan Sheffer, Mark Nicholas, and Douglas Game of Geoterrex-Dighem. Staff from LCRA and CRMWD sampled surface and ground water during the airborne survey and provided chemical analyses.

Jose Mayorga and Randall Ross of RRC, Geoff Saunders of LCRA, Okla Thornton of CRMWD, and Brace Smith of the U.S. Geological Survey made many suggestions that helped us complete the project. Isack Ramirez and Robert Luxton of the San Angelo District RRC office provided invaluable assistance in searching well records, locating wells, contacting landowners, and facilitating project progress.

Bureau staff Thomas A. Tremblay and Erica R. Boghici conducted GIS analyses of data; Steven Tweedy collected and analyzed soil and water samples; and Ianthe Nelson researched the history of oil and gas exploration in the Hatchel area. The report was reviewed by James C. Gibeaut, Rebecca C. Smyth, James L. Simmons, and Jay A. Raney. Jamie H. Coggin drafted the figures, did the typesetting, and designed the cover and layout under the direction of Joel L. Lardon, Graphics Manager. Susan Lloyd did the word processing, and Lana Dieterich edited the report.

REFERENCES

Abilene Geological Society, 1992, The stratigraphic distribution of hydrocarbon production from 19 counties in the Abilene area: Abilene, Texas, variously paginated.

American Association of Petroleum Geologists, 1973, Geological highway map of Texas: U.S. geological highway map of Texas: U.S. Geological Highway Map Series, Map No. 7, scale 1:500,000.

Back, W., 1966, Hydrochemical facies and ground-water flow patterns in the northern part of the Atlantic coastal plain: U.S. Geological Survey Professional Paper 498-A, 42 p.

Bein, Amos, and Dutton, A. R., 1993, Origin, distribution, and movement of brine in the Permian Basin (U.S.A.): a model for displacement of connate brine: Geological Society of America Bulletin, v. 105, no. 6, p. 695–707.

Bennett, J. E., Collins, C. L., and Colby, R. J., 1985, Aeromagnetic map of Texas: Bendix Field Engineering Corporation, scale 1:750,000.

Brown, E., Skougstad, M. W., and Fishman, M. J., 1970, Methods for collection and analysis of water samples for dissolved minerals and gases: U.S. Geological Survey

Techniques of Water-Resources Investigations, book 5, chapter Al, 160 p.

Brown, L. E., Jr., Goodson, J. L, and Harwood, Peggy, 1972, Abilene sheet: The University of Texas at Austin, Bureau of Economic Geology, Geologic Atlas of Texas, scale 1:250,000.

Core Laboratories, Inc., 1972, A survey of the subsurface saline water of Texas: Texas Water Development Board Report 157, v. 1, 12 p. + illustrations.

Dutton, A. R., Richter, B. C, and Kreitler, C. W., 1989, Brine discharge and salinization, Concho River watershed, West Texas: Ground Water, v. 27, no. 3, p. 375–383.

Eifler, G. K., Jr., 1975, San Angelo sheet: The University of Texas at Austin, Bureau of Economic Geology, Geologic Atlas of Texas: scale 1:250,000.

Fitzgerald, N. D., 1952, The Beddo field, Runnels County, Texas: Abilene Geological Society Contributions, p. 7–8.

Frischknecht, F. C., Labson, V. F., Spies, B. R., and Anderson, W. L., 1991, Profiling using small sources, *in* Nabighian, M. N., ed., Electromagnetic methods in applied geophysics—applications, part A and part B: Tulsa, Oklahoma, Society of Exploration Geophysicists, p. 105–270.

Gardner, F. J., and Phifer, R. L., 1953, The oil and gas fields of west Texas, part 1: Railroad Commission District 7-C: Five Star Oil Report, p. 148–198.

Garrie, D. G., 1996, DIGHEMV survey for Bureau of Economic Geology, University of Texas, Hatchel study area, Runnels County, Texas: Mississauga, Ontario, Dighem, Report 625, variously paginated.

Geonics Limited, 1992, Protem 47 operating manual: Mississauga, Ontario, Geonics Limited, variously paginated.

Jorgensen, D. G., Downey, Joe, Dutton, A. R., and Maclay, R. W., 1988, Region 16, central nonglaciated plains, *in* Back, William, Rosenshein, J. S., and Seaber, P R., eds., Hydrogeology: Geological Society of America, The Geology of North America, v. O-2, p. 141–156.

Kaufman, A. A., and Keller, G. V., 1983, Frequency and transient soundings: Amsterdam, Elsevier, Methods in Geochemistry and Geophysics, no. 16, 685 p.

Kier, R. S., Brown, L. F., Jr., and Harwood, P., 1976, Brownwood sheet: The University of Texas at Austin, Bureau of Economic Geology, Geologic Atlas of Texas, scale 1:250,000.

Lee, J. N., 1986, Shallow ground-water conditions, Tom Green County, Texas: U.S. Geological Survey, Water Resources Investigations Report 86-4177, 88 p.

McNeal, R. P., 1965, Hydrodynamics of the Permian Basin: American Association of Petroleum Geologists, Memoir 4, p. 308–326.

McNeill, J. D., 1980a, Electrical conductivity of soils and rocks: Mississauga, Ontario, Geonics Limited, Technical Note TN-5, 22 p.

_____ 1980b, Electromagnetic terrain conductivity measurement at low induction numbers: Mississauga, Ontario, Geonics Limited, Technical Note TN-6, 15 p.

_____ 1980c, EM34-3 survey interpretation techniques: Mississauga, Ontario, Geonics Limited, Technical Note TN-8, 16 p.

Paine, J. G., Dutton, A. R., Hovorka, S. D., Blüm, M. U., Mahoney, M. P., and Sullivan, E. J., 1998a, Brine in the near-surface environment: determining salinization extent, identifying sources, and estimating chloride mass using surface, borehole, and airborne EM, *in* Bell, R. S., Powers, M. H., and Larson, Timothy, eds., Proceedings, Symposium on the Application of Geophysics to Environmental and Engineering Problems: Environmental and Engineering Geophysical Society, p. 215–219.

Paine, J. G., Goldsmith, R. S., and Scanlon, B. R., 1998b, Electrical conductivity and gamma-ray response to clay, water, and chloride content in fissured sediments, Trans-Pecos, Texas: Environmental and Engineering Geoscience, v. 4, no. 2, p. 225–239.

Parasnis, D. S., 1973, Mining geophysics: Amsterdam, Elsevier, 395 p.

Rhoades, J. D., 1981, Predicting bulk soil electrical conductivity versus saturation paste extract electrical conductivity calibrations from soil properties: Soil Science Society of America Journal, v. 45, p. 42–44.

Richter, B. C., Dutton, A. R., and Kreitler, C. W., 1990, Identification of sources and mechanisms of salt-water pollution affecting ground-water quality: a case study, West Texas: The University of Texas at Austin, Bureau of Economic Geology Report of Investigations No. 191, 43 p.

Richter, B. C., and Kreitler, C. W., 1986, Geochemistry of salt water beneath the Rolling Plains, North-Central Texas: Ground Water, v. 24, no. 6, p. 735–742.

Spies, B. R., and Frischknecht, F. C., 1991, Electromagnetic sounding, *in* Nabighian, M. N., ed., Electromagnetic methods in applied geophysics—applications, part A and part B: Tulsa, Oklahoma, Society of Exploration Geophysicists, p. 285–386.

Tóth, J., 1962, A theory of groundwater motion in small drainage basins in central Alberta: Journal of Geophysical Research, v. 67, no. 11, p. 4375–4387.

West, G. F., and Macnae, J. C., 1991, Physics of the electromagnetic induction exploration method, *in* Nabighian, M. N., ed., Electromagnetic methods in applied geophysics—applications, part A and part B: Tulsa, Oklahoma, Society of Exploration Geophysicists, p. 5–45.

Wiedenfeld, C. C., Bamhill, L. J., and Novosad, C. J., 1970, Soil survey of Runnels County, Texas: U.S. Department of Agriculture, Soil Conservation Service, 60 p.

Wood, W.W., 1976, Guidelines for collection and field analysis of ground-water samples for selected unstable constituents: U.S. Geological Survey, Techniques of Water-Resources Investigations, book 1, chapter D2, 24 p.

APPENDIX A. Hatchel area geophysical sites (figs. 16 through 19). CMW sites are those where conductivity and magnetic anomalies were identified from airborne data, and there is a known well at the site; CM sites are those where airborne conductivity and magnetic anomalies are present, but there is no record of a well nearby; CW sites are those where a conductivity anomaly is present at a known well, but there is no associated magnetic anomaly; C sites are those with a conductivity anomaly but neither a known well nor a magnetic anomaly; and MW sites are those with a magnetic anomaly and a known well, but no conductivity anomaly.

CMW sites (n=69)

Site	Conductivity anomaly 56 kHz	7.2 kHz	0.9 kHz	Magnetic anomaly	RRC well[1]	Fits profile?[2]	Geophysical surveys[3]	Likely source[4]	Notes
2	Yes	No	Yes	Yes	Yes				Could be same site as 3; weak 900
3	Yes	No	No	Yes	Yes				Could be same site as 2
4	Yes	Yes	No	Yes	Yes	Yes	2MCP	Surface discharge	
5	Yes	Yes	No	Yes	Yes	Yes	1MCP	Surface discharge	Curvilinear 56,000
8	Yes	Yes	Yes	Yes	Yes	Yes	2MCP	Leaking well?	Weak 900
14	Yes	Yes	No	Yes	Yes	Yes	2P	Leaking well (plugged)	Leaking well plugged in 1991
15	Yes	Yes	No	Yes	Yes	Yes	2MCP	Leaking well (plugged)	Leaking well plugged in 1997
18	Yes	No	No	Yes	Yes		1P		
19	Yes	Yes	No	Yes	Yes	Yes	Recon	No source found	Weak 7,200; no source found
20	Yes	Yes	No	Yes	Yes	Yes	4MCP	Two leaking wells?	Weak 900; one well plugged in 1993
21	Yes	No	No	Yes	Yes				
22	Yes	Yes	Yes	Yes	Yes	Yes	2MCP	Surface discharge	Weak 7,200 and 900
26	Yes	No	No	Yes	Yes				
30	Yes	Yes	Yes	Yes	Yes	Yes	1MCP	Pit?	Weak 7,200 and 900
31	Yes	No	No	Yes	Yes				
32	Yes	No	No	Yes	Yes				
33	Yes	No	No	Yes	Yes		1P	Pit	2 wells
34	Yes	No	No	Yes	Yes		1P	No source found	Weak M
36	Yes	No	No	Yes	Yes		1MCP	Surface discharge	
39	Yes	No	No	Yes	Yes				
40	Yes	Yes	No	Yes	Yes	Yes	2MCP	Leaking well?	Weak 7,200
41	Yes	No	No	Yes	Yes				
43	Yes	No	No	Yes	Yes		1P	Leaking well?	Along stream

[1]RRC records show well at site.
[2]Site fits geophysical profile of a potentially leaking well.
[3]Types of ground-based surveys completed. P= EM34 profile at one coil separation; MCP= EM34 profiles at multiple coil separations; S=TDEM sounding.
[4]Likely salinity source interpreted from airborne and ground-based surveys.

APPENDIX A. (continued)

Site	Conductivity anomaly 56 kHz	7.2 kHz	0.9 kHz	Magnetic anomaly	RRC well[1]	Fits profile?[2]	Geophysical surveys[3]	Likely source[4]	Notes
46	Yes	No	No	Yes	Yes		1P	Surface discharge	
47	Yes	Yes	No	Yes	Yes	Yes	2MCP	Leaking well?	Part of large anomaly
48	Yes	No	No	Yes	Yes				
49	Yes	No	No	Yes	Yes				
50	Yes	No	No	Yes	Yes				Along stream
51	Yes	No	No	Yes	Yes		1P	No source found	Near Coyote Creek
52	Yes	Yes	No	Yes	Yes	Yes	2MCP	Surface discharge	
53	Yes	Yes	Yes	Yes	Yes	Yes			Weak 7,200 and 900
54	Yes	No	No	Yes	Yes				
55	Yes	No	No	Yes	Yes				
56	Yes	Yes	Yes	Yes	Yes	Yes	1P	Leaking well?	Need to locate No. 1 well
59	Yes	Yes	Yes	Yes	Yes	Yes	2P	Surface discharge	Weak 7,200 and 900
64	Yes	Yes	No	Yes	Yes	Yes			Weak 7,200
68	Yes	Yes	No	Yes	Yes	Yes	2MCP	Leak or surface spill	
69	Yes	No	No	Yes	Yes				Near high-conductivity water well
74	Yes	Yes	No	Yes	Yes	Yes	2P	Surface discharge	Weak 7,200
75	Yes	No	No	Yes	Yes		1P	Pit	C southeast of M
76	Yes	Yes	No	Yes	Yes	Yes	1P;2MCP;3S	Leaking well?	Weak 7,200
80	Yes	Yes	Yes	Yes	Yes	Yes	2MCP	Old leak or spill	Injection well; weak 56,000
88	Yes	Yes	Yes	Yes	Yes	Yes	1P; 2MCP	Leaking well?	Weak 900
89	No	Yes	Yes	Yes	Yes				
90	Yes	No	No	Yes	Yes				
93	Yes	No	No	Yes	Yes				
94	Yes	Yes	No	Yes	Yes	Yes	2P; 1MCP	Pit and leaking well?	
95	Yes	No	No	Yes	Yes		2MCP	Surface discharge	
96	Yes	No	No	Yes	Yes				
97	Yes	Yes	Yes	Yes	Yes	Yes	2MCP	Leaking well?	
98	Yes	No	No	Yes	Yes				
99	Yes	Yes	Yes	Yes	Yes	Yes	1MCP	Undetermined	
102	No	Yes	No	Yes	Yes				High 56,000
103	No	Yes	No	Yes	Yes				
105	Yes	Yes	No	Yes	Yes	Yes	2MCP	Leaking well?	Active well
106	No	Yes	No	Yes	Yes				
107	Yes	No	No	Yes	Yes				Weak 7,200
109	No	Yes	No	Yes	Yes				High 56,000

Site	Conductivity anomaly 56 kHz	7.2 kHz	0.9 kHz	Magnetic anomaly	RRC well[1]	Fits profile?[2]	Geophysical surveys[3]	Likely source[4]	Notes
110	Yes	Yes	Yes	Yes	Yes	Yes	1MCP	Leaking well?	
111	No	Yes	No	Yes	Yes				
112	No	Yes	Yes	Yes	Yes				At farmhouse and barn
113	Yes	No	No	Yes	Yes				
114	Yes	No	No	Yes	Yes				
115	Yes	No	No	Yes	Yes				
116	Yes	Yes	No	Yes	Yes	Yes	2MCP	Leaking well?	
117	Yes	No	No	Yes	Yes				
118	Yes	Yes	Yes	Yes	Yes	Yes			Weak 900
119	Yes	Yes	No	Yes	Yes	Yes			
122	Yes	No	No	Yes	Yes				

CM sites (n=15)

Site	Conductivity anomaly 56 kHz	7.2 kHz	0.9 kHz	Magnetic anomaly	RRC well[1]	Fits profile?[2]	Geophysical surveys[3]	Likely source[4]	Notes
1	Yes	No	No	Yes	No				
9	Yes	Yes	No	Yes	No	Yes	1P; 2MCP	Feedlot	Weak 7,200
17	Yes	Yes	No	Yes	No		2P;2MCP;3S	Pit	Weak 7,200
24	Yes	Yes	No	Yes	No	Yes	1P	Seep?	Well on topographic map; weak 7,200
28	Yes	No	No	Yes	No				Weak M
29	Yes	No	No	Yes	No				Along stream; weak 7,200; no access
35	Yes	No	No	Yes	No				
44	Yes	Yes	Yes	Yes	No	Yes	2MCP	Leaking well?	RRC map shows no well, but well at site
45	Yes	No	No	Yes	No				Well nearby
61	Yes	No	No	Yes	No		2P	No source found	
62	Yes	Yes	No	Yes	No	Yes		Surface discharge	Weak 7,200; irrigating with creek water
71	Yes	Yes	No	Yes	No	Yes	2P	Tanks or pit	Weak 7,200
78	Yes	No	No	Yes	No				
104	No	Yes	No	Yes	No				
121	Yes	No	No	Yes	No				

CW sites (n=12)

Site	Conductivity anomaly 56 kHz	7.2 kHz	0.9 kHz	Magnetic anomaly	RRC well[1]	Fits profile?[2]	Geophysical surveys[3]	Likely source[4]	Notes
6	Yes	No	No	No	Yes				
7	Yes	No	No	No	Yes				
10	Yes	Yes	No	No	Yes	Yes	2MCP	Leaking well (plugged)	Well replugged in 1997
12	Yes	Yes	No	No	Yes	Yes	2P	Pit	
13	Yes	No	No	No	Yes		2P	No source found	M nearby
16	Yes	Yes	No	No	Yes	Yes	2P	Leaking well (plugged)	Weak 7,200; leaking well plugged in 1997
27	Yes	No	No	No	Yes				Along stream
37	Yes	Yes	No	No	Yes	Yes	2MCP	Leaking well?	Weak 7,200
38	Yes	Yes	No	No	?	?	2MCP	No source found	Well presence and location uncertain
58	Yes	No	No	No	Yes				
72	Yes	No	No	No	Yes				
73	Yes	No	No	No	Yes		2P	Pit	

C sites (n=11)

Site	Conductivity anomaly 56 kHz	7.2 kHz	0.9 kHz	Magnetic anomaly	RRC well[1]	Fits profile?[2]	Geophysical surveys[3]	Likely source[4]	Notes
11	Yes	Yes	No	No	No		2MCP	Spill or leaking well	
25	Yes	Yes	No	No	No		3P	Pits and tanks	
42	Yes	No	No	No	No				
63	Yes	Yes	No	No	No		2MCP	Natural	Part of curvilinear 56K; weak 7,200
70	Yes	Yes	No	No	No		1P	No source found	Weak 7,200
91	Yes	No	No	No	No				
92	Yes	No	No	No	No				
100	Yes	Yes	No	No	No		2MCP	Surface discharge	
101	Yes	Yes	No	No	No		2MCP	Surface discharge	
108	Yes	Yes	No	No	No		1P	Natural	
120	Yes	Yes	No	No	No				

MW sites (n=2)

Site	Conductivity anomaly 56 kHz	7.2 kHz	0.9 kHz	Magnetic anomaly	RRC well[1]	Fits profile?[2]	Geophysical surveys[3]	Likely source[4]	Notes
65	No	No	No	Yes	Yes		1P	Leaking well	Well leaking at surface
67	No	No	No	Yes	Yes		2P	Leaking well	Well leaking at surface

Sounding only sites (n=7)

Site	Conductivity anomaly 56 kHz	7.2 kHz	0.9 kHz	Magnetic anomaly	RRC well[1]	Fits profile?[2]	Geophysical surveys[3]	Likely source[4]	Notes
81	No	No	No	No	No		1S		Sounding
82	No	No	No	No	No		1S		Sounding
83	No	No	No	No	No		1S		Sounding
84	No	No	No	No	No		1S		Sounding
85	No	No	No	Yes	Yes		1S		Sounding
86	No	No	No	No	Yes		1S		Sounding; recently plugged well
87	No	No	No	Yes	Yes		1S		Sounding

[1]RRC records show well at site.

[2]Site fits geophysical profile of a potentially leaking well.

[3]Types of ground-based surveys completed. P= EM34 profile at one coil separation; MCP= EM34 profiles at multiple coil separations; S=TDEM sounding.

[4]Likely salinity source interpreted from airborne and ground-based surveys.

APPENDIX B. Chemical composition of ground-water, surface-water, and oil-field-water samples. CRMWD data provided by the Colorado River Municipal Water District. Sample locations referenced by ID number in figure 15.

ID	Sample ID	Sample date	Well depth (ft)	Temperature (C)	Dissolved oxygen (mg/L)	PH	HCO_3 (mg/L)	Electrical conductivity (mS/m)	Cl (mg/L)	Br (mg/L)	NO_3 (mg/L)	SO_4 (mg/L)	Na (mg/L)	K (mg/L)	Mg (mg/L)	Ca (mg/L)	Ba (mg/L)	SiO_2 (mg/L)	TDS (mg/L)	Ground conductivity at 7,200 Hz (mS/m)	Ground conductivity at 56,000 Hz (mS/m)
Ground water																					
1	RUN-011	4/18/96	22.8	17.7	4	7.93	275	992	1952	nd	789	2,410	719	2.4	705	752	<0.01	15.4	7,620	290	465
2	CRMWD-12	1/17/96	66.5	20	2.8	6.73	227	374	300	1.1	dnt	1,815	114	4.9	222	595	0.03	17.3	3,295	147	325
3	CRMWD-10	1/17/96	48.8	19.4	4.9	6.9	257	354	314	1.3	dnt	1,617	158	3.6	111	653	<0.01	13.6	3,129	255	430
4	RUN-003	4/4/96	90	19.5	1.4	7.25	317	368	308	nd	212	1,350	134	2.8	151	598	0.02	22.9	3,096		
5	CRMWD-16	1/17/96	20.8	14.2	3	7.75	669	435	1,032	5.2	dnt	246	790	12	222	103	0.06	10.2	3,088	105	200
6	RUN-002	4/3/96	75	20.2	0.2	7.17	309	352	246	0.8	0.4	1,630	104	4.6	139	620	0.01	12.1	3,066	125	255
7	CRMWD-11	1/17/96	80	20.1	4.5	6.77	240	370	483	0.9	dnt	1,340	180	3.5	211	463	0.01	18.2	2,939	110	260
8	CRMWD-2	1/16/96	25.7	19	0.4	6.75	249	305	218	1.1	3.2	1,326	75	4.2	143	520	0.02	17.5	2,556	225	360
9	RUN-013	4/19/96		21	0.7	6.84	372	337	478	1.9	3.7	883	241	1.3	135	358	0.02	15.6	2,489		
10	CRMWD-5	1/16/96	40.6	19.7	3	6.7	269	323	448	2.1	dnt	1,003	123	3.5	115	464	0.04	17	2,444	222	260
11	CRMWD-3	1/16/96	45	19.7	3.6	6.85	238	369	500	2.7	13.5	806	273	4.1	98	351	0.03	19.7	2,307	185	182
12	CRMWD-19	1/29/96	51.9	20.5	3.6	6.83	264	288	234	1.1	4.5	1,003	153	5	142	343	0.02	25.5	2,175	405	235
13	CRMWD-1	1/15/96	26.4	18.9	5.8	6.73	248	259	179	0.9	dnt	990	110	4	90	390	0.01	24.9	2,036	490	135
14	CRMWD-13	1/17/96	35	18.5	nr	7.22	230	357	841	2.3	dnt	234	309	4.5	150	234	0.05	20.6	2,025	142	500
15	CRMWD-7	1/16/96	57	20.3	5.1	7.14	240	261	295	1.4	dnt	851	152	6.6	135	276	0.03	15.8	1,973	165	180
16	CRMWD-9	1/16/96	36.9	17.8	8.3	7.27	253	254	581	2.2	dnt	137	283	1.8	78	129	0.05	27.2	1,493	122	140
17	RUN-001	4/2/96	27	20	5.3	7.03	307	197	204	nd	124	363	128	3.1	65	206	0.01	19.4	1,419	360	105
18	CRMWD-4	1/16/96	64.8	20.2	3.7	6.85	249	204	232	1	4.3	334	112	2.4	92	186	0.03	19.5	1,232	175	145
19	CRMWD-6	1/16/96	69	20.8	4.7	6.95	535	164	145	0.9	dnt	102	168	<1.00	89	168	0.09	23.8	1,232	205	110
20	CRMWD-8	1/16/96		19.7	2.3	7.03	273	154	129	0.6	dnt	340	54	7.5	58	183	0.03	16.8	1,062		
21	CRMWD-17	1/17/96	36.1	19.5	nr	7.57	222	122	146	0.6	dnt	146	96	3.1	56	85	0.06	17.9	772	140	98
22	CRMWD-14	1/17/96	94.4	19.1	6.1	7.43	215	90	88	0.5	dnt	98	48	1.4	25	112	0.07	35.7	624	110	47
23	CRMWD-18	1/17/96		19.5	nr	7.18	333	80	29	0.2	dnt	35	46	<1.00	39	79	0.19	16.5	578	95	150
24	CRMWD-15	1/17/96	27	15.5	2.7	7.47	309	79	59	0.4	dnt	16	42	4.1	21	106	0.18	15.4	574	100	135
25	RUN-014	4/19/96	12.8	17.1	0.6	7.53	207	69	73	nd	31.5	23	61	3.3	20	52	0.1	9.8	481	135	155
Oil-field water																					
26	RUN-009	4/12/96		18.3	3.2	7.59	104	1,415	2,698	21.6	nd	4,130	2,378	3.4	348	553	1	1.2	10,237		
27	RUN-010	4/12/96		nm	0.1	6.5	42.7	8,924	39,190	57.7	nd	2,720	21,210	11.1	1,001	2,124	<0.01	30.6	66,387		
28	RUN-012	4/18/96		24.9	nm	6.26	30.5	8,763	38,740	60.1	nd	2,080	21,840	94.8	893	2,014	0.49	62.6	65,816		

ID	Sample ID	Sample date	Well depth (ft)	Temperature (C)	Dissolved oxygen (mg/L)	PH	HCO_3 (mg/L)	Electrical conductivity (mS/m)	Cl (mg/L)	Br (mg/L)	NO_3 (mg/L)	SO_4 (mg/L)	Na (mg/L)	K (mg/L)	Mg (mg/L)	Ca (mg/L)	Ba (mg/L)	SiO_2 (mg/L)	TDS (mg/L)
Surface water																			
29	RUN-005	4/10/96		20.4	8.3	8.1	299	335	457	2.3	nd	933	307	7.2	205	175	0.07	3.6	2,388
30	RUN-006	4/10/96		22	9.5	8.27	268	225	444	2.1	13.7	247	222	6.1	81	127	0.11	5.3	1,415
31	RUN-007	4/10/96		20.5	8.2	8.11	323	216	401	2.4	9.5	207	236	5.1	84	101	0.11	6.8	1,376
32	RUN-008	4/11/96		18.9	7.1	8.07	323	223	425	2.3	5.4	221	235	3.3	83	92	0.1	2.9	1,393
33	CRMWD-S1	1/15/96		8.01	10.8	8.14	263	248	377	1.7	1.1	277	256	3.5	79	129	0.1	8.5	1,395
34	CRMWD-S2	1/15/96		8.74	10.2	7.94	251	235	338	1.4	4.9	290	238	3	66	133	0.08	9.2	1,335
35	CRMWD-S3	1/15/96		8.77	10.1	7.87	248	232	335	1.4	4.3	272	247	3.1	64	127	0.08	9.5	1,312
36	CRMWD-S4	1/15/96		9.48	11	8.13	250	218	329	1.3	1.1	191	254	3	56	102	0.09	9.1	1,197
37	CRMWD-S5	1/15/96		8.99	10.9	8.02	308	261	419	1.9	2.6	263	248	3.5	93	136	0.11	10.8	1,487
38	CRMWD-S6	1/15/96		10.31	10.9	7.9	342	272	421	2	3.9	290	255	3.6	102	148	0.11	12.3	1,581
39	CRMWD-S7	1/15/96		11.75	12.6	8.17	241	204	333	1.2	2.2	134	198	2.8	59	114	0.09	10.3	1,096
40	CRMWD-S8	1/15/96		12.98	10.5	8.07	294	186	249	0.2	0.8	136	133	3	75	119	0.08	26.4	1,037
41	CRMWD-S9	1/16/96		10.3	9.2	7.94	289	220	363	1.3	4.4	152	204	2.7	84	128	0.06	28.2	1,256
42	CRMWD-S10	1/16/96		11.72	10	7.44	250	228	441	2	dnt	209	269	12.2	78	92	0.43	0.7	1,354
43	CRMWD-S11	1/16/96		11.9	17.8	8.02	185	1,309	3,990	9.4	dnt	484	2,143	8.4	225	338	0.15	2.4	7,385
44	CRMWD-S12	1/17/96		10.89	6.4	7.74	241	251	376	1.7	dnt	481	174	20.5	117	185	0.48	2.4	1,599
45	CRMWD-S13	1/17/96		11.08	11.2	7.78	193	410	656	3.2	dnt	1,151	378	5.9	217	294	0.04	3.5	2,901
46	CRMWD-S14	1/15/96		12.93	8.9	7.27	269	391	1,233	3.5	dnt	9	492	15.9	110	97	0.72	1.5	2,231
47	CRMWD-S15	1/16/96		10.88	9.7	8.9	519	573	1,199	5.1	dnt	870	781	13.3	353	35	0.14	1.3	3,778
48	CRMWD-S16	1/16/96		11.52	11.5	8.44	78	22	10	0.2	dnt	7	6	14.7	10	18	0.19	<0.3	144
49	CRMWD-S17	1/16/96		14.68	9.7	7.85	196	431	896	3.2	dnt	798	390	10.1	193	272	0.25	0.7	2,759
50	CRMWD-S18	1/16/96		12.49	9.4	8.49	144	37	11	0.1	dnt	1	8	11.8	14	36	0.3	<0.3	226
51	CRMWD-S19	1/16/96		15.76	8.6	8.25	137	20	67	0.3	dnt	3	29	9.4	13	51	0.3	0.4	311
52	CRMWD-S20	1/17/96		9.07	8.8	8.35	613	361	586	2.4	dnt	479	434	10	198	586	0.07	3.2	2,912
53	CRMWD-S21	1/17/96		12.13	7.9	8.52		36											

APPENDIX C. Chloride content and electrical conductivity of soils collected in this study in Runnels County. Figure 15 shows sample location referenced by ID number.

ID	Sample	Date	Ground conductivity (mS/m)	Electrical conductivity (mS/m)	Chloride (mg/kg)
54	RUN-100	4/03/96	285	283	654
55	RUN-101	4/03/96	280	492	519
56	RUN-102	4/03/96	335	28.4	4.5
57	RUN-103	4/04/96	185	26.0	1.3
58	RUN-104	4/04/96	175	34.5	7.3
59	RUN-105	4/04/96	195	26.6	2.3
60	RUN-106	4/11/96	105	21.9	2.8
61	RUN-107	4/11/96	135	30.0	14.6
62	RUN-108	4/12/96	240	30.7	6.4
63	RUN-109	4/12/96	205	24.4	6.5
64	RUN-110	4/12/96	205	47.7	57.8
65	RUN-111	4/11/96	220	29.8	13.2
66	RUN-112	4/11/96	235	14.4	1.3
67	RUN-113	4/12/96	140	1,580	5,857
68	RUN-114	4/12/96	142	39.9	2.5
69	RUN-115	4/12/96	125	31.3	4.1
70	RUN-116	4/12/96	350	132	29.9
71	RUN-117	4/12/96	135	29.7	7.1
72	RUN-118	4/12/96	145	27.7	7.6
73	RUN-119	4/19/96	282	1,078	3,846
74	RUN-120	4/19/96	285	405	144